Dynamic Relief Provision Planning for En Route Refugees in Humanitarian Logistics

by

Amirreza Pashapour

A Dissertation Submitted to the
Graduate School of Sciences and Engineering
in Partial Fulfillment of the Requirements for
the Degree of

Doctor of Philosophy

in

Industrial Engineering and Operations Management

KOÇ ÜNİVERSİTESİ

July 1, 2025

Dynamic Relief Provision Planning for En Route Refugees in Humanitarian Logistics

Koç University

Graduate School of Sciences and Engineering

This is to certify that I have examined this copy of a doctoral dissertation by

Amirreza Pashapour

and have found that it is complete and satisfactory in all respects,

and that any and all revisions required by the final

examining committee have been made.

Committee Members:

Prof. F. Sibel Salman (Advisor)

Prof. E. Lerzan Örmeci

Prof. Dilek Tüzün Aksu

Prof. Burcu Balçık

Prof. Refik Güllü

Date: ______________________________

To my parents and my sister, for their boundless love and lifelong encouragement

ABSTRACT

Dynamic Relief Provision Planning for En Route Refugees in Humanitarian Logistics
Amirreza Pashapour
Doctor of Philosophy in Industrial Engineering and Operations Management
July 1, 2025

The forced displacement crisis has become a pressing global humanitarian concern. Massive refugee movements force individuals into dire living conditions with severe inaccessibility to essential services and resources. Humanitarian organizations play a vital role in alleviating the hardships faced by refugees en route through relief aid interventions; however, the adoption of academic approaches to support these efforts remains limited. This thesis aims to optimize the periodic delivery of relief aid to geographically dispersed refugee groups en route to safe destinations, under both deterministic and stochastic migration settings.

In the deterministic setting, we introduce a Capacitated Mobile Facility Location Problem with Mobile Demand and formulate it as a mixed-integer linear program (MILP). To solve this complex problem, we develop two solution approaches: an accelerated Benders decomposition algorithm for exact optimization and a matheuristic algorithm based on an enhanced fix-and-optimize strategy. Using realistic scenarios inspired by the Honduras migration crisis, our results show that the Benders decomposition reduces computation time by 46% on average while maintaining solution quality. The matheuristic, meanwhile, produces near-optimal solutions with only a 2.4% average optimality gap and significantly reduced computational effort.

For the stochastic counterpart, we model refugee movements as a Markov decision process (MDP) with probabilistic transitions driven by migration pull factors such as safety, road conditions, and spatial proximity. To solve the MDP, we develop an approximate dynamic programming algorithm featuring customized basis functions and a novel policy replication mechanism. We further propose a state-dependent variable threshold policy that efficiently generates high-quality service plans. Applied to the Syria–Türkiye migration crisis, our approach achieves up to 25% cost savings over deterministic methods and up to 12% additional savings through coordinated planning across humanitarian organizations. The proposed methods are shown to be effective across diverse migration dynamics, including dispersed and cohesive refugee flows and multi-destination settings. Additionally, we identify service and traversal hotspots along migration routes, offering valuable guidance for tactical planning and resource pre-positioning.

In summary, this thesis contributes cost-effective, scalable, and operationally relevant solutions for humanitarian aid delivery to en route refugees and provides actionable managerial insights for addressing future displacement crises.

This doctoral research has been supported by the Scientific and Technological Research Council of Türkiye (TÜBİTAK) under Grant No. 119M229.

Keywords: humanitarian logistics, refugee crisis, refugee migration, mobile facility location, Benders decomposition, Markov decision process, approximate dynamic programming

ÖZETÇE

İnsani Lojistikte Göç Halindeki Mülteciler İçin Dinamik Yardım Sağlama Planlaması
Amirreza Pashapour
Endüstri Mühendisliği ve İşletme Yönetimi, Doktora
1 Temmuz 2025

Zorunlu yerinden edilme krizi, günümüzde küresel ölçekte acil çözüm gerektiren önemli bir insani sorun haline gelmiştir. Kitlesel mülteci hareketleri, bireyleri temel hizmet ve kaynaklara erişimin son derece kısıtlı olduğu son derece güç yaşam koşullarına sürüklemektedir. Bu süreçte insani yardım kuruluşları, göç halindeki mültecilerin karşılaştığı zorlukları hafifletmek amacıyla yardım sağlama müdahalelerinde kritik bir rol üstlenmektedir. Ancak, bu çabaların desteklenmesine yönelik akademik yaklaşımların benimsenmesi sınırlı kalmaktadır. Bu tez, güvenli bölgelere doğru hareket eden ve coğrafi olarak dağılmış mülteci gruplarına, belirli aralıklarla yardım ulaştırılmasını hem deterministik hem de stokastik göç ortamlarında optimize etmeyi amaçlamaktadır.

Deterministik ortamda, Hareketli Taleplerle Kapasiteli Mobil Tesis Yer Seçimi Problemi tanıtılarak, bu problem karma tamsayılı doğrusal programlama (MILP) modeli olarak formüle edilmiştir. Bu karmaşık problemi çözmek üzere, iki yöntem geliştirilmiştir: kesin çözüm sunan hızlandırılmış bir Benders ayrıştırması algoritması ile geliştirilmiş bir fix-and-optimize gündemine dayalı matheuristik algoritma. Honduras göç krizinden esinlenerek oluşturulan gerçekçi senaryolar üzerinden yapılan testlerde, Benders ayrıştırmasının ortalama %46 daha kısa sürede çalıştığı ve çözüm kalitesini koruduğu görülmüştür. Öte yandan, önerilen matheuristik yöntem, ortalama %2,4 optimalite açığıyla yüksek kaliteli çözümler üretmiş ve önemli ölçüde daha az hesaplama süresi gerektirmiştir.

Stokastik karşılık problemde ise, mülteci hareketleri güvenlik koşulları, yol durumu ve mekânsal yakınlık gibi dışsal göç çekim faktörlerinden etkilenen olasılıklı geçişlere sahip bir Markov karar süreci (MDP) olarak modellenmiştir. Bu modeli çözmek için, özelleştirilmiş baz fonksiyonlar ve özgün bir politika çoğaltma mekanizması içeren yaklaşık dinamik programlama algoritması geliştirilmiştir. Uygulamada anlamlı çözümler üretmek amacıyla, duruma bağlı değişken eşiklere dayalı bir politika önerilmiştir. Suriye–Türkiye göç krizine dayalı senaryolarda yapılan deneyler, stokastik çözümün deterministik yöntemlere kıyasla beklenen toplam maliyetlerde %25'e varan tasarruf sağladığını, ayrıca kurumlar arası koordineli planlama ile %12 'ye kadar ek maliyet azaltımı elde edilebileceğini ortaya koymaktadır. Önerilen yöntemlerin, hem dağınık hem de bütünleşik göç dinamiklerinde ve çoklu hedef ülke içeren senaryolarda etkili olduğu gösterilmiştir. Ayrıca, göç yolları üzerinde yüksek geçiş ve hizmet yoğunluklu noktalar belirlenmiş ve bu bulgular, taktiksel planlama ve kaynakların önceden konumlandırılması açısından önemli bilgiler sunmuştur.

Özetle, bu tez, göç halindeki mültecilere yönelik maliyet etkin, ölçeklenebilir ve operasyonel olarak uygulanabilir insani yardım dağıtım planları sunmakta; kırılgan nüfusları desteklemeye yönelik yönetsel çıkarımlar sağlamaktadır. Bulgularımız, gelecekteki yerinden edilme krizlerine yönelik yönetimsel karar süreçlerine ışık tutacak niteliktedir.

Bu doktora tez araştırması, Türkiye Bilimsel ve Teknolojik Araştırma Kurumu (TÜBİTAK) tarafından 119M229 numaralı proje kapsamında desteklenmiştir.

Anahtar Kelimeler: insani lojistik, mülteci krizi, mülteci göçü, mobil tesis yer seçimi, Benders ayrıştırması, Markov karar süreci, yaklaşık dinamik programlama

ACKNOWLEDGMENTS

Pursuing a Ph.D. has been one of the most rewarding experiences of my life. I am deeply grateful to my esteemed advisor, Prof. F. Sibel Salman, for her mentorship, intellectual guidance, and continuous encouragement throughout this journey. I have learned a great deal from her research and teaching expertise, which has significantly shaped my academic development. I am also thankful for her trust in me, which motivated me to pursue ambitious goals with confidence.

I thankfully acknowledge the members of my dissertation committee for their time, insightful feedback, and valuable suggestions, all of which greatly contributed to improving the quality and depth of this work.

I would like to express my sincere gratitude to Assoc. Prof. Dilek Günneç and Assoc. Prof. Eda Yücel, with whom I had the pleasure to collaborate as co-authors of my thesis papers. Their valuable insights, constructive feedback, and collaboration were the cornerstone in shaping the quality and depth of this research.

I remain thankful to Koç University faculty and my fellow doctoral students for their insightful discussions and for creating an inspiring academic environment.

Last but not least, I owe special thanks to my cherished family, whose unwavering support, understanding, and love accompanied me through this journey.

TABLE OF CONTENTS

LIST OF TABLES

LIST OF FIGURES

ABBREVIATIONS

Acc. BD	Accelerated Benders decomposition
ADP	Approximate dynamic programming
API	Approximate policy iteration
BD	Benders decomposition
CMFLP	Capacitated mobile facility location problem
CMFLP-MD	Capacitated mobile facility location problem with mobile demand
CM	Constructive matheuristic
CV	Coefficient of variation
EEV	Expected EV
EV	Expected value
FIFLP	Flow-interception facility location problem
FLP	Facility location problem
HL	Humanitarian logistics
HO	Humanitarian organization
IDP	Internally displaced people
IFRC	International Federation of Red Cross and Red Crescent Societies
IOM	International Organization for Migration
LB	Lower bound
LP	Linear programming
LRC	Lebanese Red Cross
MDP	Markov decision process
MILP	Mixed-integer linear programming
MF	Mobile facility
NGO	Non-governmental organization

PE	Policy evaluation
PI	Policy improvement
PR	Policy replication
RP	Recourse problem
SLR	Service level requirement
TP	Threshold policy
TRC	Turkish Red Crescent
UB	Upper bound
UNHCR	United Nations High Commissioner for Refugees
VSS	Value of stochastic solution
VTP	Variable threshold policy

Chapter 1

INTRODUCTION, MOTIVATIONS AND CONTRIBUTIONS

The world is facing an ever-increasing surge in forced displacement, driven by armed conflicts, political instability, persecution, natural disasters, and socio-economic crises. According to the United Nations High Commissioner for Refugees (UNHCR), the number of forcibly displaced people has doubled in the last decade, reaching over 122 million in 2024 (Concern worldwide US, 2023). These populations include refugees, internally displaced persons (IDPs), and asylum seekers, each facing vulnerabilities during their displacement journeys. Despite their legal distinctions, these groups often experience similar challenges and are commonly referred to as refugees in academic and policy discussions (Icduygu et al., 2001; Kotsi et al., 2022).

Humanitarian Organizations (HOs) play a critical role in delivering relief services to refugee populations, particularly those in transit. Examples of targeted relief efforts include Médecins Sans Frontières (MSF), which has set up mobile medical units along migration corridors; the Turkish Red Crescent (TRC), which established cross-border aid stations for Syrian refugees; and numerous international and local agencies that have supported Rohingya, Venezuelan, and Afghan refugees in their respective crises (MSF, 2019; Turkish Red Crescent, 2019; Kotsi et al., 2022). While much of the aid is provided at static border points, refugees often spend extended periods in transit across remote areas, making it difficult to access basic resources such as water, food, shelter, hygiene, and medical care. Consequently, the deployment of Mobile Facilities (MFs) has emerged as a promising but underutilized approach for repeated and flexible relief delivery along migration paths.

From an operational standpoint, managing relief aid distribution presents three key challenges, which motivate this thesis. First, refugee movements are inherently uncertain and shaped by volatile external conditions (Schapendonk, 2012). In addition to developing deterministic models to establish a foundational understanding of the problem, it is essential to incorporate stochastic models that can capture the dynamic and uncertain nature of refugee movements. Second, the growing scale and duration of displacement crises have outpaced available funding. this creates an urgent need for cost-efficient relief planning mechanisms (Alem, 2021; European Commission, 2022). Third, effective humanitarian operations must uphold equity by ensuring that all refugee groups receive timely aid, even under resource constraints. Evidence from field reports reveals significant disparities and unmet needs among refugee populations, especially during prolonged displacement (Rascon, 2018; Mohamed Abu Shahma, 2018).

To address these challenges, this thesis focuses on optimizing the use of MFs for delivering bundled relief services (e.g., food, water, hygiene, clothing) to en route refugee groups over time. In this thesis, we seek to answer: (i) Which refugee groups should be served in each period? and (ii) Where should MFs locate and relocate over time? We formulate two novel optimization problems to support decision-making in this context. The first is the Capacitated Mobile Facility Location Problem with Mobile Demand (CMFLP-MD), a deterministic model that minimizes fixed, operational, and relocation costs of MFs while satisfying service capacity limits and ensuring a predefined Service Level Requirement (SLR). The SLR ensures each refugee group receives service at least once every few consecutive periods during their journey. The second is a finite-horizon stochastic model formulated as a discrete-time Markov Decision Process (MDP), which incorporates uncertainty in refugee movements and soft constraints on SLR to penalize deprivation events.

In addressing the identified gaps, the foundation for supporting en route refugee groups through MFs lies in the well-established class of Capacitated Mobile Facility Location Problems (CMFLPs) (Raghavan et al., 2019). Moreover, mobility is an inherent characteristic of en route refugees due to their transient nature and the instability of their surrounding environments (Schapendonk, 2012). These two dimensions collectively motivate the formulation of the Capacitated Mobile Facility Location Problem with Mobile Demand (CMFLP-MD). Despite its practical relevance, significant gaps remain in the Humanitarian Logistics literature regarding the fulfillment of recurring demands of en route refugees under both deterministic and stochastic migration scenarios. Guided by the literature reviewed in the subsequent chapters and these research gaps, the key contributions of this thesis are summarized as follows.

First, this thesis introduces the CMFLP-MD, a novel multi-period optimization framework that enhances the modeling fidelity of humanitarian logistics (HL) settings. CMFLP-MD captures expected refugee movements, varying population sizes, service act capacities, and temporal-spatial continuity of service through SLR. The model's ability to coordinate multiple MFs across node-time pairs adds a layer of operational realism previously unexplored in the literature.

Second, we develop a mixed-integer linear programming (MILP) formulation for CMFLP-MD. Benchmark comparisons reveal that the model not only reduces computational times but also improves upon some of the best-known solutions in the literature. Two solution approaches are also proposed: an Accelerated Benders Decomposition (Acc. BD) algorithm for exact optimization, and a matheuristic algorithm based on a fix-and-optimize agenda, which consistently produces near-optimal solutions with an average optimality gap of 2.4% in our numerical experiments. These solution strategies advance earlier preliminary models and algorithms.

Third, this thesis further extends the planning horizon into stochastic environments by formulating a Markov Decision Process (MDP) model that systematizes relief provision under uncertainty. Our model captures probabilistic move-or-wait behaviors driven by external migration pull factors. To solve this problem, we develop an Approximate Dynamic Programming (ADP) approach enhanced with tailored basis functions and an innovative policy replication loop, which enables more accurate estimations of downstream costs and more robust policies.

Finally, motivated by the need for practical applicability, we propose a Value Threshold Policy (VTP) that efficiently generates high-quality service act plans. This policy not only provides computational tractability but also facilitates the derivation of actionable managerial insights. The approach demonstrates strong performance under various migration scenarios inspired by the Syria–Turkey migration context and marks, to the best of our knowledge, the first integrated exploration of MDP-based relief planning with probabilistic mobility and scalable policy generation.

Together, we believe these contributions advance the operational and methodological foundations of mobile facility planning in humanitarian logistics and offer practical decision-support tools for relief agencies. The insights and methodologies developed in this thesis aim to support HOs such as UNHCR, IOM, IFRC, and local NGOs in their mission to equitably and efficiently deliver aid to displaced populations during their migration journeys.

The structure of the thesis is organized as follows. Chapter 2 investigates relief aid provision planning under a deterministic migration environment, where refugee movements are assumed to follow known trajectories. Chapter 3 advances the study by addressing the problem within a more challenging stochastic migration environment, where refugee movements are governed by probabilistic dynamics. Finally, Chapter 4 presents concluding remarks, summarizing the key insights and contributions from the preceding chapters.

Chapter 2

RELIEF AID PROVISION PLANNING TO EN ROUTE REFUGEES UNDER A DETERMINISTIC MIGRATION ENVIRONMENT

2.1 Introduction

The world is witnessing refugee movements at its highest record over the past decade (Concern worldwide US, 2023). Triggered by the eruption of violence in Syria, a substantial migration of about 3.7 million Syrian refugees commenced towards Türkiye in 2011, with the migration continuing consistently in subsequent years (Office for the Coordination of Humanitarian Affairs (OCHA), 2023b). Recently, the outbreak of conflict in Ukraine in February 2022 resulted in over 6.2 million recorded refugees displaced from their homeland, crossing into neighboring countries in 2023, and approximately 17.6 million individuals requiring humanitarian assistance since 2023 (Agency, 2023). The tragedy of forced displacement caused by war, persecution, violence, famine, or natural disasters often pushes refugees to remain in transit for prolonged periods (Landau and Duponchel, 2011). These movements pose substantial threats to refugees' lives, create mental and somatic disorders, and hinder their access to vital resources while migrating (Seifert et al., 2018). Humanitarian organizations (HO) play a crucial role in alleviating the hardships of refugees' displacement, offering them a lifeline.

HOs have undertaken various projects globally to deliver relief aid services to refugee groups via mobile facilities (MF) (Özdamar and Ertem, 2015; Liu et al., 2021). For instance, Doctors of the World (Médecins du Monde) established a ferry project in 2015 to deliver relief aid to approximately 850,000 refugees moving toward Greece

(Shortall et al., 2017). Doctors Without Borders (Médecins Sans Frontières; MSF) has been actively providing medical assistance and treating millions of refugees since its establishment in 1971 (MSF, 2019). MSF set up MFs on the Serbia-Hungary border, where they treated nearly 100 patients daily while witnessing over 2,000 refugees crossing the border each day (Gulland, 2015). Mobile Refugee Support emerged in France in 2017 following the destruction of the Calais Jungle and La Linière camp in Grande-Synthe. They offered mobile aid, food packages, and communication services to displaced individuals in northern France (MRS, 2019). Turkish Red Crescent outlines "providing humanitarian services in cooperation with domestic and international organizations for individuals and communities suffering from population movements" as one of their primary strategic goals (Turkish Red Crescent, 2019). They conducted cross-border humanitarian aid operations to Syrian refugees from 2012 to 2019 at 14 different points near Türkiye and Syria borders (Turkish Red Crescent, 2019). These examples underscore the magnitude of relief aid delivery operations to en route refugees and the applicability of MFs in providing essential services during large-scale refugee movements.

The European Commission claims that the process of service delivery to transiting refugees has become a complex endeavor for HOs (European Commission, 2022). With a rising number of natural and man-made crises and their prolonged durations, the demand for humanitarian assistance has surged beyond the available funding allocations. This has led to a growing number of vulnerable populations with unmet needs, creating a pressing urgency to deliver timely and cost-efficient service provision plans considering HOs' limited resources (Verme and Gigliarano, 2019; European Commission, 2022). In 2018, an influx of refugees and asylum seekers from Central American nations, notably Honduras, Guatemala, El Salvador, and Nicaragua, sought sanctuary in Mexico and the United States due to poverty and violence in their homelands. The situation worsened as their home countries struggled with challenges from the COVID-19 pandemic and two powerful hurricanes in late 2020 (Office for the Coordination of Humanitarian Affairs (OCHA), 2023a). These events pushed an even greater number of individuals to embark on journeys elsewhere. Local aid efforts, spearheaded by organizations such as the Red Cross, in collaboration with humanitarian agencies like the American Friends Service Committee and the Kino Border Initiative, extended their support to these refugees. However, interviews with refugees highlighted a notable gap between the provided services and the fulfillment of everyone's needs (Rascon, 2018; Bayraktar et al., 2022).

This chapter is motivated by three challenges in humanitarian logistics (HL) research domain: (i) the complexities associated with relief aid distribution (Alegoz et al., 2024), specifically recurrent visits to en route refugees (European Commission, 2022), (ii) the need for cost-efficient service provision plans for HOs (Verme and Gigliarano, 2019), and (iii) the existing gap in addressing continual humanitarian aid operations (Kunz and Reiner, 2012). Our research seeks to optimize the logistics of capacitated MFs in delivering relief aids, including service bundles containing water, food, clothing, and medical care (Bayraktar et al., 2022), to transiting refugees. We name this optimization problem the Capacitated Mobile Facility Location Problem with Mobile Demand. In CMFLP-MD, our objective is to minimize the overall costs associated with MFs, which include fixed costs, service provision costs, and relocation costs. The problem optimally determines the number, service provision schedule, and location-relocations of MFs over a planning horizon, considering MFs' service provision capacities in terms of the number of refugees per period and refugees' populations. Additionally, we introduce a Service Level Requirement (SLR) specific to refugee groups, ensuring that the individuals of each group receive service from MFs at least once every fixed number of consecutive periods while traversing their migration path. Fig. 2.1 depicts a CMFLP-MD instance with SLR being at least once every three periods. In this figure, three refugee groups are traversing their migration paths, and two MFs provide them services until they reach terminal points.

The outline of this chapter is as follows. Section 1.2 provides a review of the relevant literature and states our contributions. Section 1.3 formally describes the CMFLP-

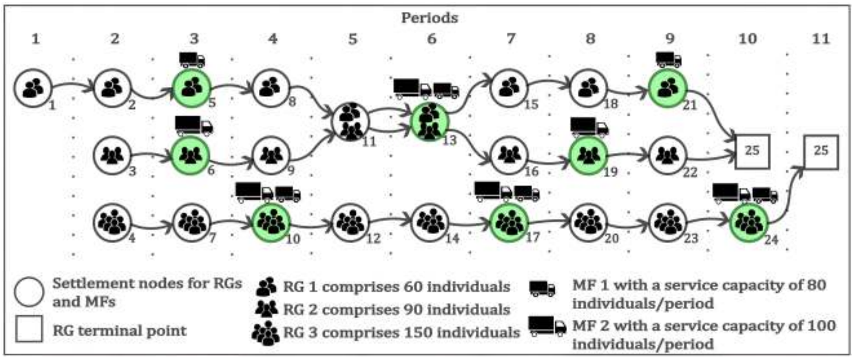

Figure 2.1: A solution to a CMFLP-MD instance with SLR being at least once every three periods. The co-location of refugee groups and MFs within the same node and period (colored nodes) indicates service provision. Node 25 serves as a terminal point for refugee groups

MD and formulates an MILP model. Section 1.4 establishes two solution methods for CMFLP-MD: an accelerated Benders decomposition approach and a constructive matheuristic. In Section 1.5, we perform computational experiments and present our results, followed by a discussion of managerial insights. Finally, Section 1.6 summarizes our concluding remarks.

2.2 Literature review

We position the CMFLP-MD with respect to six streams of relevant literature in Sections 2.2.1 to 2.2.6. Our contributions are pointed out in Section 2.2.7. Table 2.1 at the end of this Section classifies key aspects of prior studies and compares our work with relevant literature.

2.2.1 Mobile facility location problem

The *Facility Location Problem* (FLP), in a nutshell, places facilities in selected candidate locations to optimally serve clients (Farahani and Hekmatfar, 2009; Nickel and Saldanha-da Gama, 2019; Laporte et al., 2019; Turkoglu and Genevois, 2019; Dönmez et al., 2021). In principle, an FLP consists of four key components: facilities, customers or clients, a network representing their spatial arrangement, and a metric that quantifies travel costs, times, or distances between customers and facilities (Farahani and Hekmatfar, 2009). These components in our study align with MFs, refugee groups, networks of refugee paths and MF settlement places, and MFs' overall costs, respectively. The *Mobile Facility Location Problem* (MFLP) extends FLP by introducing the dynamic element of facility mobility in response to demand patterns over time (Friggstad and Salavatipour, 2011; Arabani and Farahani, 2012; Alarcon-Gerbier and Buscher, 2022). Stillström and Jackson (2007) define *mobility* as the ability to relocate between distinct geographic locations with minimal expenses. Similarly, our use of the term MF follows Bayraktar et al. (2022), wherein MFs are portable vehicles equipped with service bundles comprising food, water packs, and medical kits. MFs are capable of positioning themselves among refugees' placement nodes to deliver services in real-time.

MFs find applications in various domains, including social outreach programs (Güden and Süral, 2014; Farahani et al., 2019; Jenkins et al., 2020a; Han et al., 2021), healthcare sector (Doerner et al., 2007; Büsing et al., 2021; Yücel et al., 2020; De Vries et al., 2020; Alban et al., 2021), and HL (Nair and Miller-Hooks, 2009; Geroliminis et al., 2011; Lei et al., 2014; Bélanger et al., 2019; Li et al., 2019; Salman et al., 2021; Li et al., 2022; Bayraktar et al., 2022; Santa González et al., 2023; Avishan et al., 2023). MFs have been widely incorporated in the emergency response literature in HL (Bélanger et al., 2019), since they, in general, offer enhanced access to services compared to fixed facilities (McGowan et al., 2020). For instance, Nair and Miller-Hooks (2009) explore the benefits of proactively relocating emergency medical service vehicles to meet future demand. Their results indicate improvements of 1.30% to 6.14% in expected response times with the same number of MFs compared to static strategies. This improvement is particularly emphasized in scenarios with facility scarcity. Geroliminis et al. (2011) study the problem of locating and relocating mobile emergency response units, highlighting the importance of mobility in cases of high demand. Lei et al. (2014) address the challenge of redeploying mobile emergency units in response to traffic incidents. The authors develop a stochastic programming model to optimally reposition vehicles when some are temporarily unavailable due to service calls. Li et al. (2019) propose a robust optimization approach and a modified ant colony algorithm to determine the fleet size and location-relocation of emergency mobile units. Additionally, Li et al. (2022) establish a multi-objective model for mobile emergency material allocation model in the context of sudden disasters like floods and rainstorms. Avishan et al. (2023) propose an adjustable robust optimization approach for relief distribution in post-disaster HL operations.

Diverging from the aforementioned studies, we focus on the multi-period problem of delivering humanitarian relief aid to refugees in transit–an aspect less explored in HL literature. Among studies akin to ours, Salman et al. (2021) address health service delivery to Syrian seasonal migrant farm workers in Türkiye using mobile clinics. They optimize resource utilization and service reach by locating mobile clinics in areas with concentrated migrant populations during the harvesting season. Bayraktar et al. (2022) explore a multi-period uncapacitated MFLP to serve refugees in transit and devise an Adaptive Large Neighborhood Search (ALNS) heuristic. Santa González et al. (2023) study the planning of mobile clinic deployments for humanitarian relief distribution among villages as a multi-period location-routing problem with profits. What sets our study apart is that MFs in our problem undergo international relocations to reach out to en route refugee groups. This confines MF accessibility to only a subset of nearby nodes within a given period, considering the expansive geographical migration region. Simultaneously, we utilize the concept of MF capacity, restricting the number of refugees an MF can serve within a period. The practical applications of capacitated MFs in relief aid distribution are elaborated in Section 2.2.2. It is noteworthy that our models account for MF location-relocation decisions (Geroliminis et al., 2011; Bélanger et al., 2019; Li et al., 2019; Bayraktar et al., 2022), influenced by refugee displacements within the migration region, as opposed to MF location-routing decisions among static demands (Halper and Raghavan, 2011; Ozdamar et al., 2018; Santa González et al., 2023).

The literature on MFLP employs diverse objectives, including minimizing the distance traversed by clients and facilities (Friggstad and Salavatipour, 2011), minimizing the mean response time (Geroliminis et al., 2011), maximizing the total demand satisfaction (Halper and Raghavan, 2011; Salman et al., 2021), and minimizing combined fixed (the cost of utilized MFs) and variable costs (Güden and Süral, 2019; Bayraktar et al., 2022). Aligned with the latter group, we minimize the combined fixed and variable costs associated with the logistics of providing relief aid. Mirchandani and Francis (1990), Daskin (2011), and Kara and Rancourt (2019) review FLP, MFLP, and corresponding solution methods within the humanitarian context.

2.2.2 MF capacity restrictions

Studies on MFLP often neglect the consideration of facility capacities (Halper et al., 2015; Sterle et al., 2016; Güden and Süral, 2019; Salman et al., 2021; Bayraktar et al., 2022), although a few have explicitly addressed this aspect (Raghavan et al., 2019; Santa González et al., 2023). The introduction of capacity limitations for MFs extends MFLP to the Capacitated MFLP (CMFLP). Incorporating MF capacities aligns more closely with practical aspects of assisting en route refugee groups since MFs inherently have restrictions on commodities, equipment, and personnel, which limits the number of refugees they can serve within a period. The activity report by Turkish Red Crescent (2019) indicates that their deployed MFs along the Türkiye-Syria border could serve nearly 400-500 en route refugees daily. Raghavan et al. (2019) study a single-period CMFLP, where heterogeneous MFs reposition only once, and clients relocate to access these facilities. Santa González et al. (2023) consider a unique capacity coefficient for homogeneous mobile clinics, defining the number of patients in villages that each mobile clinic can serve in a given period. Similarly, our MF capacity is defined as the maximum number of refugees MFs can serve in every period. However, our capacity parameters are tailored for each MF, enabling the integration of both homogeneous and heterogeneous MF fleets in CMFLP-MD. Moreover, addressing capacity constraints in a multi-period setting, as in CMFLP-MD, is further complicated due to the dependence of upcoming demand levels on service provisions of previous periods.

2.2.3 *Demand mobility*

Apart from facility mobility, the literature recognizes the concept of demand mobility through the flow-interception FLP (FIFLP) (Boccia et al., 2009). FIFLP constitutes a distinct class of FLPs where customers dynamically flow between their associated origins and destinations. The FIFLP aims to identify optimal facility locations to maximize the coverage of demand flow (Gzara and Erkut, 2009). A facility can intercept a customer at any vertex on its path, aligning with the demand mobility approach proposed by Bayraktar et al. (2022). Similarly, in our problem, refugee groups are visited at the vertices of their migration paths via MFs. The single period FIFLP is rooted in seminal studies of Hodgson (1981, 1990) and Berman (1995). Berman (1997) extend FIFLP by categorizing customers into a combination of stationary and mobile classes in the network. Zeng et al. (2010) introduce a generalized formulation for various deterministic flow-interception problems. Considering refugee resettlement in the longer term, Ahani et al. (2024) study dynamic placement of refugee groups by recommending optimal locations for incoming refugee families to enhance overall employment success within the host country. Differently, our research focuses on the en route stage of refugees' migration, addressing the challenges they face in accessing essential commodities and their need for recurring service provision during this phase.

The FIFLP finds applications in urban areas where a single service provision by facilities adequately meets clients' daily demands (Sterle et al., 2016; De Vries and Duijzer, 2017). Sterle et al. (2016) study a multi-period FIFLP to optimize the locations of a set of portable variable message signs on an urban network, providing drivers with timely information during their trips. De Vries and Duijzer (2017) explore a flow refueling location problem, which optimally locates refueling or recharging stations to maximize the expected coverage of mobile vehicles in the network. Another avenue in FIFLP and demand mobility pertains to walk-in clinics that aim to accommodate patients without appointments (Zhang and Atkins, 2019; De Vries et al., 2020; Taymaz et al., 2020). Zhang and Atkins (2019) examine a medical facility network design problem, incorporating fixed facilities to capture the movement of walk-in patients in competitive and centralized environments. De Vries et al. (2020) cater to the health service demand of truck drivers as mobile entities, establishing a network of healthcare facilities along the round trips of trucks in Africa. Similarly, Taymaz et al. (2020) optimize the locations of healthcare clinics serving mobile workers who travel along routes for prolonged durations under challenging conditions. The above studies primarily address demand mobility within a single-period context, maximizing effective demand coverage. In contrast, our study focuses on serving en route refugee groups of varying population sizes, who form groups and whose recurrent demands are met in a multi-period setting.

2.2.4 Coverage and continuity of service

We adhere to the conventional Operations Research definition of coverage, signifying the accessibility of relief aids provided to refugee groups by MFs (Rancourt et al., 2015; Taymaz et al., 2020). Considering the physical barriers present in the migration region, we ascertain that a refugee group is covered only if an MF directly visits them rather than a neighboring location (Burkart et al., 2017). To this end, we introduce two crucial terms (Bayraktar et al., 2022): "node-time pairs", tuples replicating vertices across periods, and "service act", denoting the process of delivering relief aid to one or more refugee groups by an MF. A service act can only take place when both entities are situated in the same node-time pair—simultaneously occupying the same location at the same time. Formal expositions of these terms are provided in Section 2.3.

The principle of continuity of care predominantly finds applications in home healthcare routing and scheduling (Fikar and Hirsch, 2017; Barker et al., 2017; Deeny et al., 2017; Gray et al., 2018). This principle ensures ongoing care by the same healthcare practitioners for an individual, a characteristic known as relational continuity. The objective, therefore, is to minimize the number of practitioners assigned to a patient over the planning timeline (Nickel et al., 2012; Bowers et al., 2015). Continuity of care is equally crucial in our problem, as it offers several compelling advantages. It allows HOs to consistently assess the overall health status of refugees throughout their migration. It ensures timely replenishment of relief aid for refugees before depletion. Moreover, it enables HOs to establish a trusted relationship with refugees while accompanying them to safe terminal points (Robertshaw et al., 2017). Hence, we introduce the concept of "continuity of service" as a specific perspective within HL (Santa González et al., 2023), referring to the repetitive provision of follow-up relief aids to refugees. The enactment of continuity of service involves defining an SLR parameter (Bayraktar et al., 2022). In the HL literature, various demand coverage SLRs have been utilized within a time horizon, including once (Halper et al., 2015; Sterle et al., 2016; Raghavan et al., 2019), double coverage (Nair and Miller-Hooks, 2009), at least once (Zeng et al., 2010), at most once (Yücel et al., 2020; Avishan et al., 2023), exactly n times (Monemi et al., 2021), once every n periods (Savaşer, 2017; Salman et al., 2021; Santa González et al., 2023), at least once every τ periods (Bayraktar et al., 2022), and every period (Halper and Raghavan, 2011; Jena et al., 2016; Güden and Süral, 2019). Consistent with Bayraktar et al. (2022), we introduce a positive integer parameter $\tau \in \mathbb{Z}^+$, which governs the frequency of service acts performed by MFs in CMFLP-MD. Our SLR ensures that the individuals of each refugee group receive coverage at least once every τ consecutive periods.

2.2.5 *Predictability of refugee paths*

Accurate forecasting of refugee movements is crucial. It enhances the ability to safeguard refugee lives by facilitating governments and NGOs in making informed allocations of humanitarian resources (Suleimenova et al., 2017). HOs, operating independently or as a coalition, can leverage these predicted paths when supporting refugee groups (Bayraktar et al., 2022). Simulation approaches, such as Agent-based modeling (ABM) (Kniveton et al., 2011; Sokolowski et al., 2014; Sokolowski and Banks, 2014; Groen, 2016; Suleimenova et al., 2017; Güngör et al., 2022), and video games (Estrada et al., 2017) aim to capture the social interactions and network formations of en route refugees. These studies present conceptual models that consider key decision-making drivers in migration, including geographical structure, environmental risks, agents' risk attitudes, and destination preferences, to generate multiple migration scenarios, suggesting the preferred paths of migration flows. While the simulation of refugee paths is beyond the scope of the present article, we design them within the Honduras migration case study in Section 2.5.1 by mimicking actual caravan routes, adopted from the works by Woldt et al. (2019) and Bayraktar et al. (2022).

2.2.6 Benders decomposition

Achieving optimality in solving large-sized instances of CMFLP-MD, even with state-of-the-art solvers, incurs substantial computational expenses. Successful applications of Benders decomposition (BD) in the field of FLPs, such as multiple-allocation capacitated FLP (Fischetti et al., 2016), multi-period maximal covering FLP (Vatsa and Jayaswal, 2016), large-scale FLP (Fischetti et al., 2017) single-source capacitated FLP (Filippi et al., 2021), and dynamic FLP (Han et al., 2021), motivated us to develop a customized BD algorithm to solve our realistic CMFLP-MD instances. Introduced by Benders (1962), BD functions as a partition-based solution methodology for large-scale MILPs. Alongside the classic BD, different variants have emerged, including Generalized Benders Decomposition (GBD) (Geoffrion, 1972), Accelerated BD (Acc. BD) (Magnanti and Wong, 1981), the integer L-shaped method (Laporte and Louveaux, 1993), Logic-Based BD (LBBD) (Hooker and Ottosson, 2003; Guo and Zhu, 2023; Zhu et al., 2023), and Combinatorial Benders Decomposition (CBD) (Codato and Fischetti, 2006; Han et al., 2021). While BD has been widely applied in FLPs, our study pioneers the exploration of an Acc. BD in Section 2.4, tailored for the context of relief aid distribution to en route refugees in HL. For detailed implementations and comprehensive analyses of the BD method, we refer interested readers to the works of Magnanti and Wong (1981) and Rahmaniani et al. (2017).

2.2.7 Our contributions

In light of the reviewed literature, our contributions are summarized in three streams. First, we contribute to the field of HL by introducing the multi-period Capacitated Mobile Facility Location Problem with Mobile Demand. This problem optimizes the logistics of capacitated MFs utilized to deliver relief aid to en route refugees over a multi-period timeframe. The CMFLP-MD explicitly incorporates sets of refugee groups, their varying population sizes, and the service act capacities of MFs. The inclusion of these realistic factors adds a layer of complexity to CMFLP-MD as it necessitates the coordination of two or more MFs for their presence at node-time pairs while adhering to the SLR criterion. Second, despite the inherent complexity of CMFLP-MD, our MILP model demonstrates enhanced computational efficiency by reducing run times and improving upon some of the existing best-found results in the literature when benchmarked. Third, we designate two solution methodologies for CMFLP-MD: an Acc. BD algorithm, offering an exact solution approach and a matheuristic algorithm characterized by its speed and ability to yield near-optimal solutions with a 2.4% gap with the best incumbents of our numerical experiments. While earlier versions of these methods have been presented in a conference proceeding paper (Pashapour et al., 2022), our current work substantially refines and expands upon these models and solution approaches. Additionally, we provide comprehensive computational experiments, accompanied by in-depth discussions and insights, addressing the gaps in the previous study (Pashapour et al., 2022).

Table 2.1: Comparison of CMFLP-MD with prior studies (sorted chronologically)

Article	Objective	Mobility		# of	Service	Facility	Solution
		Facility	Demand	period	frequency	capacity	methods
Hodgson (1981)	min. aggregate travel times	-[1]	✓	1	Once	-	IP model
Hodgson (1990)	max. captured flow	-	✓	1	Once	-	A cannibalizing solution procedure
Berman (1995)	max. covered flow	-	✓	1	Once	-	IP model
Berman (1997)	max. covered demand	-	✓	1	Once	-	IP models
Doerner et al. (2007)	max. effectiveness of workforce employment, average accessibility, & demand coverage	✓	-	1	Once	-	Pareto-ant colony optimization, Genetic algorithm
Boccia et al. (2009)	max. intercepted flow, min. number of facilities	-	✓	1	Once	-	Heuristics
Gzara and Erkut (2009)	max. return from intercepted paths	-	✓	1	Once	-	Lagrangian relaxation
Nair and Miller-Hooks (2009)	max. double coverage, min fixed & relocation costs	✓	-	1	Double	-	Multi-objective optimization
Zeng et al. (2010)	max. covered demand	-	✓	1	At least once	✓	MIP model
Geroliminis et al. (2011)	min. mean system response time	✓	-	1	Once	-	A hypercube model, Genetic algorithm
Friggstad and Salavatipour (2011)	min. travel distance of clients & facilities	✓	✓	1	Once	-	An 8-approximation algorithm
Halper and Raghavan (2011)	max. satisfied demand	✓	-	≥ 2	Every period	✓	Heuristics
Nickel et al. (2012)	min. unscheduled tasks, patient-nurse loyalty penalty, overtime & travel costs	✓	-	≥ 2	n times	-	A two-stage constraint programming & ALNS heuristic
Güden and Süral (2014)	min. total costs	✓	-	≥ 2	Every period	✓	A preprocessing heuristic
Lei et al. (2014)	min. expected total response cost	✓	-	≥ 2	Once	-	Stochastic programming, L-shaped method
Bowers et al. (2015)	min. number of staff handover	✓	-	≥ 2	n times	-	Simulation
Halper et al. (2015)	min. total movement of facilities & clients	✓	✓	1	Once	-	Local search heuristics
Rancourt et al. (2015)	min. welfare cost of stakeholders, max. need coverage, min. number of operating centers	-	-	≥ 2	Every period	-	MIP model
Fischetti et al. (2016)	min. sum of facility opening & customer allocation costs	-	-	1	Once	✓	Benders decomposition
Jena et al. (2016)	min. capacity change, allocation & relocation cost	-	✓	≥ 2	Every period	✓	Lagrangian heuristics
Sterle et al. (2016)	max. covered demand, min. relocation cost	✓	✓	≥ 2	Once	-	A sequential integrated approach
Vatsa and Jayaswal (2016)	min. maximum uncovered demand	-	-	≥ 2	Once	-	Benders decomposition
Burkart et al. (2017)	min. fixed & travel costs	✓	-	1	Once	✓	ϵ-constraint, complete enumeration, an evolutionary algorithm
De Vries and Duijzer (2017)	max. total flow volume covered	-	✓	1	Once	-	Chance-constrained programming

[1] ✓: considered, -: not considered

(*Continued on next page*)

Table A.1 (*continued*)

Article	Objective	Mobility		# of	Service	Facility	Solution
		Facility	Demand	period	frequency	capacity	methods
Fischetti et al. (2017)	min. sum of facility opening & customer allocation costs	-	-	1	Once	-	Benders decomposition
Savaşer (2017)	min. total distance traveled by doctors	✓	-	≥ 2	Once every varying n periods	✓	Heuristics
Güden and Süral (2019)	min. sum of allocation & facility movement costs	✓	-	≥ 2	Every period	-	Branch-and-price, Heuristics
Li et al. (2019)	min. total travel, waiting time, service time costs	✓	-	≥ 2	Once	✓	Robust optimization, Any colony optimization
Raghavan et al. (2019)	min. total traveled distance	✓	✓	1	Once	✓	Branch-and-price, Heuristics
Zhang and Atkins (2019)	max. overall social welfare, max. total demand volume for a focal firm	-	✓	1	Once	✓	Probabilistic-choice & deterministic-choice models
Jenkins et al. (2020a)	max. total expected demand covered, min. maximum number of located MFs, min. MF relocations	✓	-	≥ 2	Every period	-	ϵ-constraint Method
De Vries et al. (2020)	max. patient volume served & effectiveness of health service delivery	-	✓	1	Once	-	Numerical experiments
Taymaz et al. (2020)	max. total expected weighted coverage under the Conditional-Value-at-Risk (CVaR) measure	-	✓	1	Once	-	A risk-averse stochastic optimization
Yücel et al. (2020)	max. difference between full & partial covered demand, min. total traveling cost	✓	-	≥ 2	At most once	-	Data-driven optimization
Alban et al. (2021)	max. effective adopter demand	✓	-	≥ 2	At least F times, at most T times	-	Nonlinear optimization of sigmoidal functions
Filippi et al. (2021)	min. size & incidence of high assignment & average assignment cost	-	-	1	Once	-	Benders decomposition
Han et al. (2021)	min. total service mileage	✓	-	≥ 2	Every period	✓	Benders decomposition
Monemi et al. (2021)	min. set up, transport, deployment, & penalty costs	✓	-	≥ 2	n times	✓	Branch-cut-Benders
Salman et al. (2021)	max. covered demand min. number of clinics min. travel distance	✓	✓	≥ 2	Once every varying n periods	-	An MIP model
Bayraktar et al. (2022)	min. fixed & travel costs	✓	✓	≥ 2	At least once every τ periods	-	ALNS heuristic
Li et al. (2022)	min. allocation cost & deployment time of emergency supplies	✓	-	1	Once	-	A shuffled frog leaping algorithm
Avishan et al. (2023)	max. total utility	✓	-	≥ 2	At most once	-	Adjustable robust optimization + Heuristics
Santa González et al. (2023)	max. total benefits	✓	-	≥ 2	At most once every τ periods	✓	Heuristics
Our Problem (CMFLP-MD)	min. fixed, service act, & travel costs of mobile facilities	✓	✓	≥ 2	At least once every τ periods	✓	Benders decomposition & a matheuristic

2.3 Problem definition

The CMFLP-MD is defined on a network $G = (V, E)$, consisting of two sub-graphs: $G^R = (V^R, E^R)$ corresponding to refugee groups $r \in R$ and $G^M = (V^M, E^M)$ associated with MFs $m \in M$. The node sets V^R and V^M represent the settlement locations for refugee groups and MFs, respectively. The edge set E^R comprises roads that refugee groups can traverse, typically on foot, limited by a maximum travel distance within a period (Bayraktar et al., 2022). Additionally, E^M includes pairs of nodes in V^M that are mutually accessible for MFs within half a single period, facilitating the execution of service acts in the remaining time (Bayraktar et al., 2022). Specifically, an MF located at node $i \in V^M$ can relocate to a subset of nodes denoted as J_i.

Refugees commonly travel in groups, i.e., refugee cohorts. Each refugee group $r \in R$ comprises refugees who enter the network simultaneously and follow the same path (Bayraktar et al., 2022). Building upon the discussions in Section 2.2.5, we assume refugee groups opt for a specific path. Furthermore, they move from one node to the next along their paths at each period. The set of paths is denoted as P. Each path $p \in P$ includes a sequence of consecutively connected nodes in V^R through the edges in E^R. The parameter l_p represents the number of nodes on path p, and n_{pk} denotes its k-th vertex. In particular, $n_{p,1}$ and n_{p,l_p} correspond to the origin and destination nodes of path $p \in P$ (Bayraktar et al., 2022). While multiple refugee groups may traverse the same path, they may enter the path in different periods. Let $p_r \in P$ indicate the migration path of refugee group r, and let $e_r \in T$ represent the period when refugee group r begins traversing path p_r, where $|T| = \max_{r \in R}\{l_{p_r} + e_r - 1\}$ equals the planning horizon governing the duration of relief aid distribution. Additionally, let d_r be the demand level of refugee group r, corresponding to its population size. To ensure the SLR criterion for adequate demand coverage, all d_r individuals of each refugee group $r \in R$ receive service imperatively at least once within a specified span of consecutive periods, denoted as $\tau \in \{1, 2, \cdots\}$.

Let M represent the set of available MFs. The cardinality $|M|$ serves as an upper bound on the number of deployed MFs, determined by the model according to service needs. Each MF $m \in M$ is equipped with a capacity b_m, representing the maximum number of refugees the facility can serve per period. Given that refugee group populations typically surpass MF capacities (Turkish Red Crescent, 2019; BBC News, 2021; The New York Times, 2021), it is possible for multiple MFs to visit an refugee group simultaneously. Additionally, recognizing the fact that refugee group populations typically surpass HOs' finite MF, personnel, and relief aid resources (Verme and Gigliarano, 2019; European Commission, 2022), our model accommodates demand divisibility. This allows for a partial service provision to a refugee group population in a period, avoiding costly or infeasible solutions. This assumption is compared with the case of indivisible demand in Section 2.5.4.4.

In CMFLP-MD, two fundamental concepts are the *node-time* pair and the *service act*. We define the set $\mathcal{L}_r$ of node-time pairs (i, t), indicating that refugee group r settles at node $i \in V^R$ in period $t \in T$. By definition, refugee group $r \in R$ enters path p_r from its origin node $n_{p_r,1}$ at period e_r to reach its terminal point $n_{p_r,l_{p_r}}$ at period $e_r + l_{p_r} - 1$. Mathematically, we represent the list of node-time pairs in which refugee group r can be served as $\mathcal{L}_r = \big\{(n_{(p_r,q+1)}, e_r + q) : q \in \{0, 1, \cdots, l_{p_r} - 1\}\big\}$. Furthermore, a service act refers to providing relief aid by an MF $m \in M$ at a node-time pair to an refugee group. To establish the link between refugee groups' node-time pairs and service act locations, we define $\mathcal{L} = \bigcup_{r \in R} \mathcal{L}_r$ as the union of all refugee groups' node-time pairs during which MFs can serve them. Any feasible solution to the problem offers a list of service acts assigned to deployed MFs. Each MF is allowed to appear at no more than one node per period. If an MF arrives at a node and provides relief aid, it incurs a service act cost. There is no cost associated with the idleness of MFs in a period. When idle, MFs may engage in preparatory activities such as restocking relief supplies for future service acts. It is important to note that the process of resupplying MFs belongs to a different supply chain echelon for HOs that lies beyond the scope of our study. With a focus on the last-mile distribution of relief aids, the literature consistently provides an average number of refugees that facilities are capable of serving on a daily basis (Turkish Red Crescent, 2019).

With our model, we aim to (i) determine the proportion of each refugee group's population to be served at each node-time pair; (ii) schedule the service acts to be performed by MFs; (iii) plan the location-relocations of MFs throughout the planning horizon, and (iv) decide the utilization of MFs. The objective is to minimize the total costs, including the fixed costs f_m of recruiting MF $m \in M$, service act costs o_m performed by MF m, and relocation costs c_{ij} incurred when MFs relocate within the network. Incorporating o_m into the objective function consolidates service acts to fewer node-time pairs when satisfying the SLR criterion for refugee groups. The fixed costs are incurred once for the entire planning horizon, while the service act and relocation costs are incurred on a per-period basis. Compared to the MILP presented in (Bayraktar et al., 2022), our MILP offers two key advantages: First, it ensures the SLR solely on refugee groups' settlement node-time pairs, eliminating the redundant SLR constraints developed for all node-time pairs. Second, our MILP establishes a direct link between service act and location-relocation decisions using a single constraint block, simplifying the formulation compared to the literature, which often employs several linearization constraints.

We formulate an MILP model in Section 2.3.1, and propose valid inequalities for the case of a homogeneous MF fleet in Section 2.3.2. To enhance understanding, we present an illustrative example in Section 2.3.3 to clarify the concepts.

2.3.1 Mathematical model

Our MILP elements conform to the standard notation used in Pashapour et al. (2022) for consistency and ease of readability.

Sets:

R	Set of refugee groups
M	Set of available MFs
V^R	Set of placement nodes for refugees
V^M	Set of placement nodes for MFs
P	Set of refugee paths
$\mathcal{L}_r$	Set of node-time pairs specific to refugee group $r \in R$; $\mathcal{L}_r = \big\{(n_{p_r,q+1}, e_r + q) : q \in \{0, 1, \cdots, l_{p_r} - 1\}\big\}$
$\mathcal{L}$	Set of all node-time pairs; $\mathcal{L} = \bigcup_{r \in R} \mathcal{L}_r$
J_i	Set of accessible vertices for MFs from node $i \in V^M$ in one period; $J_i \subseteq V^M$
T	Set of time periods

Parameters:

d_r	Population size of refugee group $r \in R$
p_r	Traversed path of refugee group $r \in R$; $p_r \in P$
e_r	Time period when refugee group $r \in R$ enters path $p_r \in P$; $e_r \in T$
l_p	Number of nodes on path $p \in P$
n_{pk}	k^{th} node on path $p \in P$; $k = 1, \cdots, l_p$
b_m	Service act capacity of MF $m \in M$
f_m	Fixed cost of utilizing MF $m \in M$
o_m	Service act cost for MF $m \in M$
c_{ij}	Relocation cost of MFs from node $i \in V^M$ to node $j \in J_i$
τ	Service level requirement for refugee groups; $\tau \in T$

Decision Variables:

A_{rit}	Proportion of the population of refugee group $r \in R$ planned to receive aid at node-time pair $(i,t) \in \mathcal{L}_r$
Y_{mit}	1, if MF $m \in M$ provides service at node-time pair $(i,t) \in \mathcal{L}$; 0, otherwise
X_{mijt}	1, if MF $m \in M$ relocates from node $i \in V^M$ to node $j \in J_i$ in period $t \in T$; 0, otherwise
Z_m	1, if MF $m \in M$ is utilized; 0, otherwise

Model:

$$\min \quad \sum_{m\in M} f_m Z_m + \sum_{m\in M}\sum_{(i,t)\in\mathcal{L}} o_m Y_{mit} + \sum_{m\in M}\sum_{i\in V^M}\sum_{j\in J_i}\sum_{t\in T} c_{ij} X_{mijt} \tag{2.1}$$

s.t.

$$\sum_{t=0}^{\tau-1} A_{r,(n_{p_r,q+t+1}),(e_r+q+t)} \geq 1 \qquad \forall r\in R, q=0,\cdots,l_{p_r}-\tau \tag{2.2}$$

$$\sum_{m\in M: i\in V^M} b_m Y_{mit} \geq \sum_{r\in R:(i,t)\in\mathcal{L}_r} d_r A_{rit} \qquad \forall (i,t)\in\mathcal{L} \tag{2.3}$$

$$Y_{mit} \leq \sum_{j\in V^M: i\in J_j} X_{mjit} \qquad m\in M, (i,t)\in\mathcal{L} \tag{2.4}$$

$$\sum_{j\in V^M: i\in J_j} X_{mjit} \leq \sum_{j\in J_i} X_{mij(t+1)} \qquad \forall m\in M, i\in V^M, t=1,\cdots,|T|-1 \tag{2.5}$$

$$\sum_{i\in V^M}\sum_{j\in J_i} X_{mijt} \leq Z_m \qquad \forall m\in M, t\in T \tag{2.6}$$

$$A_{rit} \geq 0 \qquad \forall r\in R, (i,t)\in\mathcal{L}_r \tag{2.7}$$

$$Y_{mit} \in \{0,1\} \qquad \forall m\in M, (i,t)\in\mathcal{L} \tag{2.8}$$

$$X_{mijt} \in \{0,1\} \qquad \forall m\in M, i\in V^M, j\in J_i, t\in T \tag{2.9}$$

$$Z_m \in \{0,1\} \qquad \forall m\in M \tag{2.10}$$

The objective function (2.1) minimizes the total costs, including fixed, service act, and relocation costs of deployed MFs. Constraints (2.2) guarantee our SLR criterion of receiving service at least once every consecutive τ periods for each refugee group. Constraints (2.3) imply capacity constraints for targeted refugee group populations at any node-time pair. Constraints (2.4) indicate that an MF can conduct an service act at a node-time pair only if it is located there. Constraints (2.5) maintain the location-relocation flow-balance of MFs inter-periods. Constraints (2.6) identify the utilization of MFs and, simultaneously, limit their presence to at most one node in every period. Finally, constraints (2.7)–(2.10) define the domains of decision variables.

The MILP (2.1)-(2.10) serves as a general framework for CMFLP-MD and can accommodate various specifications, such as the knowledge of MFs' initial placements, the presence of fixed facilities at some nodes, and network road blockages, with minimal adjustments. To address the former scenario, a constraint of the form $\sum_{j \in J_{h_m}} X_{mh_mj1} = 1;\ \forall m \in M$ ensures that MFs are initially positioned at their designated nodes $h_m \in V^M$. For the second scenario related to the existence of fixed facilities, a binary parameter $\lambda_i \in \{0,1\}; \forall i \in V^R$ can be introduced, reflecting the presence (1) or absence (0) of fixed facilities at node i. Subsequently, the left-hand side of constraints (2.2) is replaced with $\sum_{t=0}^{\tau-1} A_{r,(n_{p_r,q+t+1}),(e_r+q+t)} + \lambda_{n_{p_r,q+t+1}}$, indicating that the SLR can be relaxed for all τ-lengthed path segments that involve node i. In the latter case, where edge $(\bar{i}, \bar{j})$ is obstructed, we set $X_{m\bar{i}\bar{j}t} = 0;\ \forall m \in M, t \in T$ to represent the unavailability of the road for MFs.

2.3.2 Valid inequalities for the case of homogeneous fleet

Our proposed MILP is applicable to both heterogeneous and homogeneous MF fleets. In the latter case, we can further enhance the MILP (2.1)-(2.10) by introducing two sets of valid inequalities, where $b_m = b$ for all MF $m \in M$.

1. We employ symmetry-breaking constraints (2.11) among MFs (Bayraktar et al., 2022). This helps to utilize them in a specific order of indices and eliminate symmetric solutions.

$$Z_m \geq Z_{m+1} \qquad \forall m = 1, \cdots, |M| - 1 \tag{2.11}$$

2. We compute ρ via Equation (2.12) as a lower bound on the number of MFs required to satisfy the SLR and insert constraints (2.13) to the model. Constraints (2.13) ensure that at least ρ MFs are recruited where the cardinality of set M must be greater than ρ, i.e., $|M| > \rho$.

$$\rho = \left\lceil \frac{\sum\limits_{r \in R} d_r}{b \times \tau} \right\rceil \tag{2.12}$$

$$Z_m = 1 \qquad \forall m = 1, \cdots, \rho \tag{2.13}$$

2.3.3 An illustrative example

This section presents an illustrative example along with its optimal solution to clarify the concepts and the proposed MILP. Consider a network of $V^R = V^M = \{1, 2, \cdots, 10\}$ and edge sets E^R as depicted in Fig. 2.2 while assuming E^M connects all nodes mutually. Two refugee paths, $p_1 = \{1, 2, 4, 6, 8, 9, 10\}, p_2 = \{1, 3, 5, 7, 8, 9, 10\}$, both originating and terminating at nodes 1 and 10, are traversed by refugee groups, as shown in Fig. 2.2. Two refugee groups $R = \{1, 2\}$, with population sizes $d_1 = 20$ and $d_2 = 30$, enter paths $p_1 = 1$ and $p_2 = 2$ in periods $e_1 = 1$ and $e_2 = 2$, respectively. In a timeline of $|T| = 8$ periods, six MFs labeled as $M = \{1, \cdots, 6\}$ will conduct service acts, each having a capacity of $b_m = 15$ individuals per period. The associated costs for MFs are $f_m = 30$ and $o_m = 5$, $\forall m \in M$. Regarding the c_{ij} matrix, suppose MFs follow the shortest distance between any pair of nodes using the edges, where each edge costs one unit. For instance, $c_{17} = c_{13} + c_{35} + c_{57} = 3$. Finally, we assume an SLR of $\tau = 3$ periods.

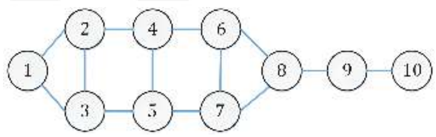

Figure 2.2: The network schematic of the illustrative example.

Table 2.2 presents the optimal solution obtained from our MILP. In this solution, only two out of six MFs are deployed to perform a total of eight service acts throughout the planning horizon, necessitating multiple relocations in the network.

The relief aid provision plan based on the optimal values of **A** and **Y** variables is visualized in Figs. 2.3 and 2.4. Specifically, Fig. 2.3 displays the proportion of the population from each refugee group receiving service at specific node-time pairs. Half of the population of refugee group 1 is served at node 2 in period 2, while the rest is served at node 4 in period 3. Subsequently, the entire refugee group 1 receives service at node 8 in period 5. Similarly, the whole population of refugee group 2 is served at node 5 in period 4 and again at node 8 in period 6. Fig. 2.4 shows the

Table 2.2: Decision variables having non-zero values in the optimal solution of the illustrative example

(r,i,t)	A_{rit}	(m,i,t)	Y_{mit}	(m,i,j,t)	X_{mijt}	(m)	Z_m
(1,2,2)	0.5	(1,2,2)	1	(1,2,4,2)	1	(1)	1
(1,4,3)	0.5	(1,4,3)	1	(1,4,5,3)	1	(2)	1
(1,8,5)	1	(1,5,4)	1	(1,5,8,4)	1		
(2,5,4)	1	(1,8,5)	1	(1,8,8,5)	1		
(2,8,6)	1	(1,8,6)	1	(1,8,8,6)	1		
		(2,5,4)	1	(1,8,8,7)	1		
		(2,8,5)	1	(1,8,8,8)	1		
		(2,8,6)	1	(2,5,8,4)	1		
				(2,8,8,5)	1		
				(2,8,8,6)	1		
				(2,8,8,7)	1		
				(2,8,8,8)	1		

node-time pair information related to eight service acts performed in the optimal solution. Among the available six MFs, only MFs 1 and 2 are deployed for service provision. MF 1 conducts service acts at nodes 2, 4, and 5 in periods 2, 3, and 4, respectively, and at node 8 in periods 5 and 6, requiring three relocations between nodes 2, 4, 5, and 8. On the other hand, MF 2 serves at node 5 in period 4 and at node 8 in periods 5 and 6, with a single relocation from node 5 to 8. The two deployed MFs incur $2 \times 30 = 60$ units of fixed and $8 \times 5 = 40$ units of service act costs. Additionally, MF 1 relocates between nodes 2, 4, 5, and 8 with a cost of $1 + 1 + 2 = 4$, and MF 2 has a single relocation from node 5 to 8 with a cost of 2, resulting in 6 units of traveling costs. Hence, the objective function value of the optimal solution is 106.

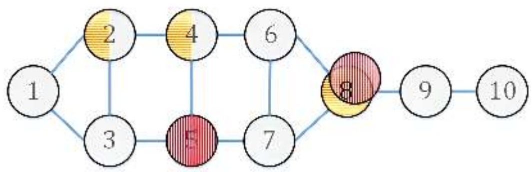

Figure 2.3: Optimal values of **A** variables for refugee groups 1 (in horizontal orange lines) and 2 (in red vertical lines)

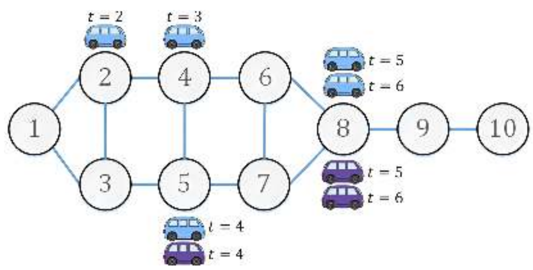

Figure 2.4: Optimal values of **Y** variables (service acts) using two MFs: 1 (in blue) and 2 (in violet)

2.4 Solution methods

Due to its complexity, in this section, we present two solution methods for solving the CMFLP-MD instances. First, we propose an Accelerated Benders decomposition (Acc. BD) algorithm as an exact solution approach in Section 2.4.1. Additionally, we design an enhanced fix-and-optimize-based constructive matheuristic (CM) approach in Section 2.4.2 to rapidly achieve high-quality solutions.

2.4.1 Benders decomposition algorithm

The CMFLP-MD includes two main decision dimensions. The first dimension concerns binary decision variables related to the execution of service acts ($\mathbf{Y}$), location-relocations ($\mathbf{X}$), and deployment of MFs ($\mathbf{Z}$). On the other hand, the second dimension involves only continuous decision variables $\mathbf{A}$, representing the proportion of refugee groups' population targeted for service provisioning. As the second dimension does not contribute to the objective function, the CMFLP-MD can be simplified by projecting variable $\mathbf{A}$ out of the model, which can be optimized in a separate subproblem. These distinctive attributes of our MILP, coupled with successful applications of BD in the context of FLPs (outlined in Section 2.2.6), motivated the development of a customized BD algorithm to effectively solve CMFLP-MD.

BD divides a problem into two distinct subproblems: a linear subproblem (LSP) and a restricted master problem (RMP). LSP is obtained by fixing the values of integer variables in the original problem, creating a linear programming formulation. In contrast, RMP incorporates constraints that involve solely integer variables. Each BD iteration consists of two steps. In the first step, RMP is solved, and its solution is fed into the dual of the LSP, referred to as the dual subproblem (DSP). In the second step, the solution of DSP induces a Benders optimality or feasibility cut, which is systematically inserted into RMP. The procedure continues until a stopping criterion is satisfied. Our LSP, DSP, and RMP models, BD cuts, and the BD stopping criterion are presented in Section 2.4.1.1. Additionally, several techniques to expedite the BD performance are explored in Section 2.4.1.2. We present an overview of the BD algorithm and the derivation of BD models in Appendix 2.A. For a comprehensive introduction to BD, readers are directed to Section 2 of the work by Rahmaniani et al. (2017).

2.4.1.1 Benders decomposition models

This section describes the general process of formulating our BD models. We begin by presenting the LSP model (2.14)-(2.17) of our BD algorithm associated with CMFLP-MD.

Linear subproblem (LSP):

$$\min \quad 0 \tag{2.14}$$

$$s.t. \sum_{t=0}^{\tau-1} A_{r,(n_{p_r,q+t+1}),(e_r+q+t)} \geq 1 \qquad \forall r \in R, q = 0, \cdots, l_{p_r} - \tau \tag{2.15}$$

$$\sum_{m \in M: i \in V^M} b_m \overline{Y}^{\theta}_{mit} \geq \sum_{r \in R:(i,t) \in \mathcal{L}_r} d_r A_{rit} \qquad \forall (i,t) \in \mathcal{L} \tag{2.16}$$

$$A_{rit} \geq 0 \qquad \forall r \in R, (i,t) \in \mathcal{L}_r \tag{2.17}$$

The LSP incorporates continuous decision variables **A** along with MILP constraints that include these variables. Since the **A** variables do not directly contribute to the objective function (2.1), the LSP objective function is basically zero. Hence, the LSP is a satisfiability problem and can be used as a feasibility check on the acquired service act plans. The term $\overline{Y}^{\theta}_{mit}$ stands for the values of **Y** integer variables obtained by RMP at iteration θ. We proceed by constructing the dual (2.18)-(2.21) of the LSP, denoted as DSP. The DSP model and its decision variables associated with constraints (2.15) and (2.16) of LSP are framed as follows.

$u_{rq} \geq 0$	$\forall r \in R,\ q \in \{0, \cdots, l_{p_r} - \tau\}$	Dual variables associated with the $(q+1)^{th}$ $\tau-$lengthed segment of path p_r traversed by refugee group $r \in R$
$v_{it} \geq 0$	$\forall (i,t) \in \mathcal{L}$	Dual variables associated with node-time pair $(i,t) \in \mathcal{L}$ as a potential pair for hosting service acts

Dual subproblem (DSP):

$$\max \quad W^{\theta}_{DSP} = \sum_{r \in R} \sum_{q=0}^{l_{p_r}-\tau} u_{rq} - \sum_{m \in M} \sum_{(i,t) \in \mathcal{L}: i \in V^M} b_m \overline{Y}^{\theta}_{mit} v_{it} \tag{2.18}$$

s.t.

$$\sum_{q=max\{0,k-\tau\}}^{min\{k-1,l_{p_r}-\tau\}} u_{rq} - d_r v_{(n_{p_r k}),(e_r+k-1)} \leq 0 \qquad \forall r \in R, k \in \{1, \cdots, l_{p_r}-1\} \tag{2.19}$$

$$u_{rq} \geq 0 \qquad \forall r \in R, q \in \{0, \cdots, l_{p_r}-\tau\} \tag{2.20}$$

$$v_{it} \geq 0 \qquad \forall (i,t) \in \mathcal{L} \tag{2.21}$$

The objective function of our DSP at iteration θ is denoted by W^{θ}_{DSP}. The dual variables $\mathbf{u}$ and $\mathbf{v}$ correspond to constraints (2.15) and (2.16) of the LSP, respectively. Ultimately, we formulate our RMP (2.22), (2.4)-(2.6), (2.8)-(2.10), and (2.23) as follows.

Restricted master problem (RMP):

$$\min \quad Z^{\theta}_{RMP} = \sum_{m \in M} f_m Z_m + \sum_{m \in M} \sum_{(i,t) \in \mathcal{L}} o_m Y_{mit} + \sum_{m \in M} \sum_{i \in V^M} \sum_{j \in J_i} \sum_{t \in T} c_{ij} X_{mijt} + \eta \tag{2.22}$$

s.t. Constraints (2.4)-(2.6), (2.8)-(2.10).

$$\eta \geq 0 \tag{2.23}$$

The objective function of the RMP at iteration θ is denoted by Z^{θ}_{RMP}. The RMP shares binary variables $\mathbf{Z}, \mathbf{Y}, \mathbf{X}$ and the constraints (2.4)-(2.6) and (2.8)-(2.10) with the MILP. Moreover, the RMP involves a non-negative variable η that serves as an upper bound on the objective function values of DSP extreme points or, equivalently, a penalty for infeasible RMP solutions.

A complete enumeration of optimality and feasibility cuts associated with the extreme points and extreme rays of the DSP, respectively, is typically impractical. Benders (1962) introduces an iterative approach for incorporating these cuts into RMP. Note that the DSP possesses a solution of $\mathbf{u} = 0$ and $\mathbf{v} = 0$. Therefore, the DSP solution space is either unbounded or feasible for any arbitrary choice of $\mathbf{Z}$, $\mathbf{Y}$, and $\mathbf{X}$. In the former case, the direction of the unboundedness must be avoided by a feasibility cut (2.25) imposed on the RMP because these extreme rays indicate that the RMP solution is MILP-infeasible. In the latter case, the DSP solution is one of its extreme points, and the addition of optimality cuts (2.24) to the RMP helps DSP to improve its objective function value among those extreme points. The parameters $\overline{u}^{\theta}_{rq}$ and $\overline{v}^{\theta}_{it}$ in Equations (2.24) and (2.25) represent the optimal values of $\mathbf{u}$ and $\mathbf{v}$ variables at iteration θ.

$$\sum_{r\in R}\sum_{q=0}^{l_{p_r}-\tau}\overline{u}^{\theta}_{rq} - \sum_{m\in M}\sum_{(i,t)\in\mathcal{L}:i\in V^M} b_m\overline{v}^{\theta}_{it}Y_{mit} \leq \eta \qquad \text{“optimality cut”} \tag{2.24}$$

$$\sum_{r\in R}\sum_{q=0}^{l_{p_r}-\tau}\overline{u}^{\theta}_{rq} - \sum_{m\in M}\sum_{(i,t)\in\mathcal{L}:i\in V^M} b_m\overline{v}^{\theta}_{it}Y_{mit} \leq 0 \qquad \text{“feasibility cut”} \tag{2.25}$$

Thus far, we have presented our BD models and the BD cuts generated during the algorithm. Prior to showing the stopping condition, we elaborate on η, which consistently equals 0 in all BD iterations, as demonstrated in Proposition 2.4.1.

Proposition 2.4.1. *The optimal value of η in all BD iterations is 0.*

Proof. Suppose x is a DSP non-zero feasible solution, satisfying constraints (2.19)-(2.21). Then, λx where $\lambda > 0$ is also a feasible DSP solution. Hence, any non-zero feasible DSP solution is an extreme ray, and the DSP solution space is a cone consisting of infinitely many extreme rays. The single extreme point of DSP is the origin solution $\mathbf{u} = 0$ and $\mathbf{v} = 0$ with the DSP objective function value of 0, which is acquired only after the RMP is enriched with sufficient feasibility cuts. Once this extreme point is attained as the DSP optimal solution for a given vector $\overline{\mathbf{Y}}^{\theta}$, the feasibility of the LSP is guaranteed. Otherwise, based on the weak duality theorem, the LSP remains infeasible due to the unboundedness of DSP. Moreover, η is an upper bound to the objective function values of DSP extreme points (Rahmaniani et al., 2017). Hence, it is an upper bound to the objective function value of the single extreme point in DSP, which equals zero. Since η is minimized in the RMP, it is optimally acquired as 0 in all BD iterations. □

Drawing upon Proposition 2.4.1, we recognize that only feasibility cuts are inserted into RMP until we pinpoint the single DSP extreme point solution in our BD. With a clear understanding of the BD cuts, we articulate the stopping criterion for our BD algorithm in Proposition 2.4.2.

Proposition 2.4.2. *Our BD algorithm terminates once it attains the single extreme point of the DSP with an objective function value of zero.*

Proof. The RMP objective function Z^{θ}_{RMP} (2.22) serves as a lower bound (LB) for the MILP objective function value. This is because the RMP is a relaxation of the MILP, encompassing its solution space. Conversely, the term $\Gamma + W^{\theta}_{DSP}$, where $\Gamma = \sum\limits_{m \in M} f_m Z_m + \sum\limits_{m \in M} \sum\limits_{(i,t) \in \mathcal{L}} o_m Y_{mit} + \sum\limits_{m \in M} \sum\limits_{i \in V^M} \sum\limits_{j \in J_i} \sum\limits_{t \in T} c_{ij} X_{mijt}$, provides an upper bound (UB) for the MILP objective function value. The BD algorithm terminates when the LB and UB coincide, i.e., $Z^{\theta}_{RMP} = \Gamma + W^{\theta}_{DSP}$. Proposition 2.4.1 indicates that η^* equals 0 in all iterations, implying $Z^{\theta}_{RMP} = \Gamma + \eta^* = \Gamma$. Consequently, the algorithm terminates, i.e., LB=UB, when W^{θ}_{DSP} equals zero at any iteration (otherwise, it is unbounded). At this point, the BD reports the single extreme point of the DSP, ensuring the feasibility of the LSP. Hence, the optimal RMP solution attains MILP-feasibility. Given that RMP solutions serve as lower bounds for the MILP, this RMP solution is deemed MILP-optimal. □

Propositions 2.4.1 and 2.4.2 provide insights into the singularity of the DSP extreme point, the optimal value of η, and the BD stopping criterion. Nevertheless, the current version of the BD exhibits quite a slow convergence. We explore several techniques to accelerate the BD algorithm in Section 2.4.1.2.

2.4.1.2 Accelerated Benders decomposition

The classical implementation of BD suffers from slow convergence, excessive computing time, and high memory requirements (Rahmaniani et al., 2017). To address these challenges and achieve faster BD convergence, several BD enhancement taxonomies have been proposed by Rahmaniani et al. (2017). As alluded to in DSP and RMP characteristics in Section 2.4.1.1, this section presents four specific refinements applied to our BD: multi-cut reformulation, two-phase approach, warm-starting the RMP, and a valid inequality in RMP, which together demonstrate a significant improvement in our BD performance. The enhanced version is referred to as "Acc. BD". In the following, we provide a detailed explanation of each technique.

1. Multi-cut reformulation: It is commonly observed that over 90% of the total BD execution time is dedicated to solving the RMP (Magnanti and Wong, 1981). On the other hand, DSP is solved efficiently due to its LP structure. Classical BD inserts a single cut into RMP at every iteration, resulting in slow convergence. Instead of generating a single cut at each iteration, the multi-cut reformulation solves the DSP multiple times, each time producing a brand-new BD cut. In particular, it aims to simultaneously detect and bound all extreme rays of the DSP for a given RMP solution, reducing the number of visits to RMP. The generation of multiple Benders cuts at each BD iteration better restricts the RMP solution space. The multi-cut reformulation approach has been proven to significantly strengthen RMP and outperform the single-cut approach (You and Grossmann, 2013; Rahmaniani et al., 2017). Algorithm 1 demonstrates the pseudo-code for the multi-cut reformulation technique. At each BD iteration, the number of executions of Algorithm 1 is bounded by $\sum_{r\in R}(l_{p_r} - \tau + 1)$.

Algorithm 1 Multi-cut reformulation

Let CUT be the BD cut set.
Add constraint block $\mathbf{C} = \{\Phi\}$ to DSP.
while true **do**:
  Solve DSP // To detect potential unboundedness directions.
  if $W^{\theta}_{DSP} = 0$ **then**:
    break // All unboundedness directions are identified. Algorithm 1 terminates.
  end if
  Update the values of $\overline{u}^{\theta}_{rq}$, $\overline{v}^{\theta}_{it}$.
  Generate the associated BD cut (2.25).
  Append the newly generated BD cut to CUT if it violates the RMP solution.
  for $r \in R$ and $q = 0, \cdots, l_{p_r} - \tau$ **do**:
    if $\overline{u}^{\theta}_{rq} > 0$ **then**:
      Add the constraint $u_{rq} = 0$ to $\mathbf{C}$.
    end if
  end for
end while
Remove the constraint block $\mathbf{C}$ from DSP.
return: CUT

2. Two-phase approach: Solving RMP to provable optimality in the initial

BD iterations is often time-consuming and unnecessary (Rahmaniani et al., 2017). A technique introduced by McDaniel and Devine (1977) allows us to derive valid Benders cuts from solutions of a Linear Relaxation of RMP (LR-RMP). We utilize LR-RMP instead of the original RMP during early BD iterations. The LR-RMP is solved until the stopping criterion is met, i.e., $W^{\theta}_{DSP} = 0$ is achieved. At this point, sufficient cuts are added to both LR-RMP and RMP. Subsequently, the LR-RMP is replaced with the original RMP while retaining the inserted Benders cuts. The BD algorithm then proceeds with RMP until the stopping condition is satisfied once again, this time with respect to RMP. By employing the two-phase approach, our RMP is enriched with high-quality BD cuts immediately.

3. Warm-start technique: When transitioning from LR-RMP to RMP, it is optional yet beneficial to initially supply RMP with a feasible solution to avoid severely inefficient root nodes. Section 2.4.2 presents a heuristic framework that offers such solutions. These feasible solutions can be utilized for warm-starting the RMP and accelerating the overall procedure.

4. A valid inequality: The SLR criterion is explicitly formulated by variables $\mathbf{A}$ and constraints (2.2) and (2.3) in the MILP model. In the RMP, however, they are projected out. Nevertheless, the SLR criterion can still be implicitly integrated into the RMP by enforcing an adequate number of service acts within each τ-length segment along the traversal paths of each refugee group independently, as expressed by Equation (2.26). These valid inequalities enhance the RMP during the initial BD iterations by preventing solutions with highly insufficient service acts.

$$\sum_{m \in M} \sum_{k=0}^{\tau-1} b_m Y_{m,(n_{p_r,q+k+1}),(e_r+q+k)} \geq d_r \qquad \forall r \in R, q \in \{0, \cdots, l_{p_r} - \tau\} \tag{2.26}$$

The pseudo-code for the proposed Acc. BD is outlined in Algorithm 2. We compared the performance of the classic BD and the Acc. BD using the illustrative example presented in Section 2.3.3. Both classic and Acc. BD approaches achieved an optimal solution with an objective value of 106. The classic BD required eight iterations, while the Acc. BD attained the optimal solution in 3 iterations. An upper limit of 300 units is considered on the DSP objective function to signal the unboundedness. Also, the valid inequalities (2.11) and (2.13) were utilized in the RMP in both approaches. Figs. 2.5 and 2.6 visualize the convergence of the lower bound (LB) and upper bound (UB) in the classic and Acc. BD iterations, respectively.

Algorithm 2 Accelerated Benders Decomposition for CMFLP-MD

$\omega \leftarrow 0$ // The master problem switch key: 0 implies solving the LR-RMP. 1 implies solving the RMP.
Initialize $\theta = 1$ // Iteration indicator.
while $True$ **do**:
    Step 1:
    if $\omega = 0$ **then**:
        Solve LR-RMP.
    else
        Solve (a warm-started) RMP. // Solution of the matheuristic (Section 2.4.2) can be used to warm start.
    end if
    $\overline{Y}^{\theta}_{mit} \leftarrow Y_{mit}$ // Updating the values of $\overline{Y}^{\theta}_{mit}$ based on LR-RMP or RMP results.
    Step 2:
    Solve DSP.
    if $W^{\theta}_{DSP} = 0$ **then**:
        if $\omega = 1$ **then**:
            break // The RMP solution is MILP-optimal, i.e., the algorithm terminates.
        else
            $\omega \leftarrow 1$
            Replace LR-RMP with RMP. // Proceed with the original RMP.
        end if
    end if
    Apply "Multi-cut reformulation" // Multiple BD cuts are generated using Algorithm 1.
    if $\omega = 0$ **then**:
        Insert the BD cuts to LR-RMP and RMP.
    else
        Insert the BD cuts to RMP.
    end if
    $\theta \leftarrow \theta + 1$ // Incrementing the iteration index.
end while
return Optimal RMP solution.

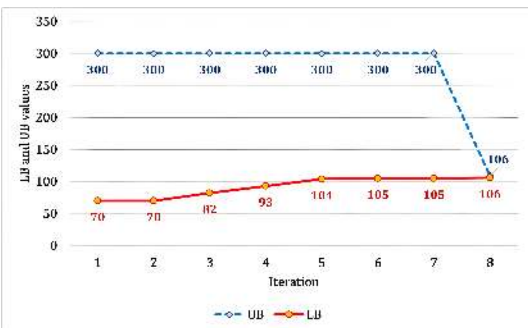

Figure 2.5: Classic BD

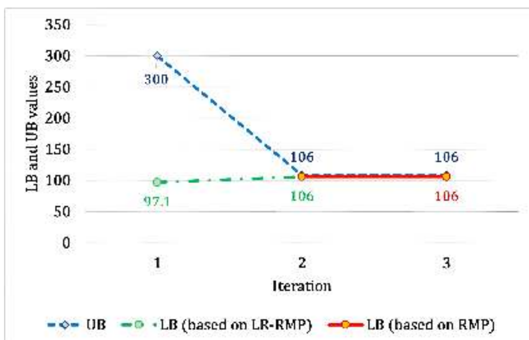

Figure 2.6: Acc. BD

2.4.2 A constructive matheuristic

In Section 2.4.1, we presented Acc. BD as an exact solution method for the CMFLP-MD. However a practical and rapid heuristic solution approach remains essential, given its practical relevance. Our MILP simultaneously meets the SLR criteria for all refugee groups, considering τ-lengthed segments along their migration paths. An alternative approach to enforcing this rule is through sequential fulfillment. This section introduces a Constructive Matheuristic (CM) that addresses the complexity of the problem by employing an intelligent fix-and-solve strategy.

The CM algorithm systematically builds a solution for the CMFLP-MD through iterations $\theta = 1, \cdots, |P|$, where $|P|$ is the number of distinct refugee paths. The algorithm tackles partial networks $\mathcal{N}^\theta$ and constructs them cumulatively; thus, $\mathcal{N}^{|P|}$ denotes the original network configuration. The CM begins by creating a partial network $\mathcal{N}^1$. It initially consists of only one path $p \in P$, along with refugee groups that trail this specific path. Next, the CM solves the associated CMFLP-MD defined on $\mathcal{N}^1$ through an MILP (2.1)-(2.6), (2.8)-(2.10), (2.27)-(2.29) to attain an service act plan for MFs considering the existing refugee groups in the partial network. The algorithm proceeds by iteratively adding one path to $\mathcal{N}^\theta$ at a time and solving the model until all paths are incorporated into the network. In every iteration $\theta + 1$, the CM fixes the values of all $\mathbf{A}$ and those $\mathbf{Y}$ decision variables that equal 1 from the solution of iteration θ. This is done to sequentially uphold the SLR for the existing refugee groups while simultaneously addressing the SLR for the newly included refugee groups. An advantageous feature of the CM is that $\mathbf{Y}$ variables that equal 0 remain flexible to change in subsequent iterations, allowing MFs the option to relocate between paths. Finally, the solution of the last CM iteration, i.e., $\theta = |P|$, provides a high-quality feasible solution for the problem. Assuming that path $p^\theta \in P$ is attached to the network $\mathcal{N}^\theta$ during iteration $\theta \in \{1, \cdots, |P|\}$ of the CM, we introduce the CM mathematical model and its new elements with respect to our proposed MILP structure below.

New Sets:

$\overline{R}^{\theta}$	Set of refugee groups associated with the newly inserted path to the network $\mathcal{N}^{\theta}$ at iteration θ, i.e., $\overline{R}^{\theta} = \{r : r \in R, p_r = p^{\theta}\}$
R^{θ}	Set of existing refugee groups in the network $\mathcal{N}^{\theta}$ up to iteration θ, by definition $R^{\theta} = R^{\theta-1} \cup \overline{R}^{\theta}$, where $R^0 = \emptyset$

New Parameters:

θ	CM iteration index, $\theta \in \{1, \cdots, \lvert P \rvert\}$
p^{θ}	The inserted path at iteration θ
$\widetilde{A}^{\theta}_{rit}$	Fixed values of A_{rit} variables until iteration θ; $\forall r \in R, (i,t) \in \mathcal{L}_r$
$\widetilde{Y}^{\theta}_{mit}$	Fixed values of Y_{mit} variable until iteration θ; $\forall m \in M, (i,t) \in \mathcal{L}$

CM Mathematical Model:

$$\min \quad \text{Eq (2.1)}$$

s.t. Constraints (2.2)-(2.6)

$$A_{rit} = \widetilde{A}^{\theta-1}_{rit} \qquad \forall r \in R^{\theta-1}, (i,t) \in \mathcal{L}_r \tag{2.27}$$

$$Y_{mit} = 1 \qquad \forall \{m \in M, (i,t) \in \mathcal{L} : \widetilde{Y}^{\theta-1}_{mit} = 1\} \tag{2.28}$$

$$A_{rit} \geq 0 \qquad r \in R^{\theta}, (i,t) \in \mathcal{L}_r \tag{2.29}$$

Constraints (2.8)-(2.10)

Constraints (2.27) and (2.28) capture the fixing aspect of the fix-and-solve-based CM model and are inserted as of the second iteration. At each iteration θ, the CM model corresponding to the partial network $\mathcal{N}^{\theta}$ is solved. Subsequently, the parameter values stored in matrices $\widetilde{A}^{\theta}_{rit}$ and $\widetilde{Y}^{\theta}_{mit}$ are updated using Equations (2.30) and (2.31), where A^*_{rit} and Y^*_{mit} denote the optimal values of **A** and **Y** decision variables at iteration θ.

$$\widetilde{A}^{\theta}_{rit} = A^*_{rit} \qquad \forall r \in \overline{R}^{\theta}, (i,t) \in \mathcal{L}_r \tag{2.30}$$

$$\widetilde{Y}^{\theta}_{mit} = Y^*_{mit} \qquad \forall m \in M, (i,t) \in \mathcal{L} \tag{2.31}$$

The order in which paths are inserted to the partial network $\mathcal{N}^{\theta}$ may impact the quality of the resulting solution. In this regard, we sort and attach the paths to $\mathcal{N}$ in a non-decreasing order of their lengths, which showed satisfactory results compared to a random insertion. Importantly, the CM algorithm allows the relocation of previously assigned MFs between paths, improving capacity utilization in subsequent iterations. By intelligently reallocating MFs, we obtain more efficient service act allocations compared to decomposing and solving the problem independently for each path, as in (Pashapour et al., 2022). The pseudo-code for the CM approach is outlined in Algorithm 3.

Algorithm 3 Constructive Matheuristic

Initialize $\theta = 1$. // Iteration indicator.
Initialize $\mathcal{N}^0 = \{\Phi\}$. // Initial empty CM network.
Initialize $\widetilde{A}_{rit}$ $\forall r \in R, (i,t) \in \mathcal{L}_R$. // A matrix to store **A** results.
Initialize $\widetilde{Y}_{mit}$ $\forall m \in M, (i,t) \in \mathcal{L}$. // A matrix to store **Y** results.
$P \leftarrow$ Sorted P in a non-decreasing order of path lengths.
for $p^\theta \in P$ **do**
    $\mathcal{N}^\theta \leftarrow \mathcal{N}^{\theta-1} + p^\theta$ // Path of interest in iteration θ is inserted to the partial network.
    Solve the CM model (2.1)-(2.6), (2.8)-(2.10), (2.27)-(2.29).
    Update $\widetilde{A}^\theta_{rit}$ and $\widetilde{Y}^\theta_{mit}$ using Equations (2.30) and (2.31).
    $\theta \leftarrow \theta + 1$
end for
return The solution of the network $\mathcal{N}^{|P|}$.

2.5 Computational analysis

In this section, we validate the proposed MILP and the two solution methods using instances based on the real-world Honduras migration crisis. Annually, tens of thousands of Central American migrants embark on a journey, forming groups colloquially referred to as "caravans" and traversing long distances primarily on foot. According to reports from the Guatemala migration office, approximately 6,000 refugees, primarily from Honduras, had set up camps near Chiquimula and along the Honduran borders. Moreover, local residents witnessed the presence of caravans comprised of up to 5,000 refugees in the vicinity. More evidence of this migration emerges as a caravan containing around 4,000 refugees is spotted within the confines of the village of Vado Hondo in Guatemala (BBC News, 2021; The New York Times, 2021). In Section 2.5.1, we describe the process of generating the necessary data for the problem instances and present our numerical results in Section 2.5.2. Section

2.5.3 compares the performance of our MILP on (Bayraktar et al., 2022)'s instances as special cases of our study for benchmarking. Finally, several sensitivity analyses and what-if scenarios are investigated in Section 2.5.4.

2.5.1 Data description

Based on the information gathered from the Honduras migration crisis, we generated 60 problem instances that are classified as small (S), medium (M), and large-sized (L), with 20 instances within each category. The selection of nodes and paths follows primary urban centers and towns, all linked by interconnected road systems, as established by Woldt et al. (2019) and Bayraktar et al. (2022). However, we opted for longer path lengths to cover a broader geographical area. We defined $V^R = V^M$, and two major Honduran cities - San Pedro Sula and Tegucigalpa - serve as the source nodes, while Mexico City stands as the single destination node. To ensure realistic travel distances, the edges along paths have been constrained to a roughly 30-mile threshold, a distance realistically traversable within a single day by walking (Bayraktar et al., 2022). A few pairs of nodes in the network were relatively distant, rendering it impossible for refugee groups to traverse them within a single period (i.e., one day). Hence, we positioned intermediate camping nodes between certain city pairs (Bayraktar et al., 2022).

Fig. 2.7 presents a representation of our migration network. A schematic of the original network for large-sized instances and subnetworks used for small and medium-sized instances, as well as the list of all cities and paths of the network, are provided in Fig. A.1 and Tables A.1 and A.2 in Appendix 2.B. The small, medium, and large-sized instances comprise 19, 28, and 48 nodes, respectively, consisting of 3, 5, and 7 distinct migration paths. General information such as the number of nodes and the number of paths is common among instances of each category, hence reported independently in Tables 2.3-2.5. For example, "N48P07", compatible with all large instances, indicates a network with 48 nodes and seven distinct paths. Additionally, the instance names indicate specific instance attributes. For example, "S01-R5M15T14" corresponds to the small instance number 01, featuring 5 refugee groups, 15 available MFs, and a time horizon of 14 periods. We describe the process of generating these specific parameters for each instance in the following.

Figure 2.7: The network associated with Honduras migration instances

refugee groups' population size is estimated based on the news reports and information regarding the crisis. We randomly selected population values from a predefined set of numbers $\{1000, 1100, 1200, \cdots, 5000\}$ (BBC News, 2021; The New York Times, 2021). Moreover, the traversed paths p_r and starting periods e_r for each $r \in R$ are randomly assigned and vary across any pair of problem instances to account for various scenarios. Each MF fleet is presumed to have a service capacity of serving 400 refugees per period, based on the activity report published by TRC in 2019 (Turkish Red Crescent, 2019). The MF fixed cost is set at $\$5,000$, representing the initial investment required for acquiring and setting up the vehicles. The operating cost is set as \$50 per period and covers expenses such as driver wages. The travel expenses of MFs are calculated based on the actual distance between pairs of nodes in the road network, the fuel consumption rate for buses, and fuel prices in Central America (Carngo website, 2022). Throughout the experiments, we set the SLR parameter to $\tau = 4$ among all case study instances. As suggested by Bayraktar et al. (2022), the values of 3 or 4 for τ serve as reasonable and operationally effective values for relief operations. In Section 2.5.4.1, we investigate the performance of different τ values in a specific instance. We note that utilizing a unique τ value yields equitable service provisions across all refugee groups.

2.5.2 Numerical results

We implement our methodologies using the Python programming environment and the Spyder Anaconda IDE platform. The instances are solved via the Pyomo optimization package and the Gurobi 11.0.0 solver factory. All computational experiments are conducted on a workstation equipped with a 64-bit operating system, a Xenon(R) 2.60 GHz CPU, and 128 GB of RAM. We imposed a time limit of 6 hours (21600s) on all instances. Moreover, to strike a balance between solution quality and computation time, a 0.02% optimality gap is set as the stopping criterion for the solver, specific to large-sized instances. Finally, both the MILP and Acc. BD. are warm-started by CM solutions amongst all instances.

Tables 2.3, 2.4, and 2.5 provide an overview of the computational results obtained for the small-, medium-, and large-sized instances, respectively. These tables include crucial metrics such as the objective function value, percentage gap w.r.t. (with respect to) the best incumbent, the number of deployed MFs, run times in seconds, and the number of iterations for the Acc. BD. The percentage gap w.r.t. the best incumbent is calculated as $100 \times (UB - \overline{Z})/\overline{Z}$, where UB represents the objective function value of the instance and $\overline{Z}$ corresponds to the best feasible solution found by either MILP, Acc. BD, or CM. As shown in Tables 2.3 and 2.4, both MILP and Acc. BD achieved optimal solutions within the specified 6-hour time limit for small and medium-sized instances. Hence, the percentage gap with the best incumbent, i.e., the optimal solution, is exclusively reported for the CM in these tables. This metric amounts to 0.82% and 2.55% for small and medium-sized instances, respectively, showcasing the near-optimal performance for CM. Furthermore, the run-time ratio of CM to MILP averages 19.4% and 11.0% for small and medium-sized instances, respectively, underscoring the run-time efficiency of the CM algorithm.

The results presented in Table 2.5 reveal that the MILP and Acc. BD methods encountered challenges in obtaining optimal solutions for 8 and 4 large-sized instances, respectively, within the 6-hour time limit, despite showing acceptable convergence towards optimality. Therefore, in addition to the previously mentioned metrics, we measure the percentage gap w.r.t. the best bound exclusively to the large-sized instances as $100 \times (UB - \underline{Z})/UB$. Here, UB represents the objective function value of the instances, and the linear relaxation lower bounds $\underline{Z}$ are reported by the solver when solving the MILP. This metric averages 1.30%, 0.63%, and 4.35% for the MILP, Acc. BD, and CM solutions, respectively. The CM and Acc. BD methods lasted 2.1% and 68.7%, respectively, of the average MILP run-time among large-sized instances. Fig. 2.8 visually compares the run time performance of the MILP and Acc. BD within the 6-hour time limit. It highlights their achievement of optimality for 12 and 16 out of 20 large-sized instances, respectively.

Table 2.6 summarizes the results from Tables 2.3, 2.4, and 2.5. Notably, the Acc. BD consistently outperformed the MILP, achieving the best incumbent solutions across all instances. Moreover, it excels the MILP with a 46% run time improvement on average by dividing their associated average run times in Table 2.6. The CM algorithm also exhibited remarkable speed and consistently maintained gaps below 9% w.r.t. both the best incumbents and best bounds. The CM achieved an average objective value gap of 2.4% compared to the best incumbent solutions across all instances. These results highlight the efficiency of the CM method, particularly for larger-scale problems where exact methods face computational challenges due to prolonged run times. Exact methods are more suitable for scenarios having relatively short displacement duration, lasting around two or three weeks, highlighting the importance of the CM method. The CM, offering high-quality relief distribution plans in reasonably short run times, emerges as a practical and effective solution for prolonged scenarios, complementing the strength of exact methods.

Table 2.3: The MILP, Acc. BD, and CM results associated with small-sized instances

Small Instances	**Objective function value**		**% Gap w.r.t. best incumbent**	**# of MFs**		**Run time (Seconds)**			**# of iters.**
($N19, P3$)	Opt.[1]	CM	CM	Opt.	CM	MILP	Acc. BD	CM	Acc. BD
S01-R5M15T14	60,128	60,630	0.83	11	11	16	22	8	3
S02-R5M15T14	60,597	60,828	0.38	11	11	19	24	9	4
S03-R5M16T14	65,630	65,988	0.55	12	12	38	36	12	4
S04-R5M16T14	66,317	66,869	0.83	12	12	24	20	11	2
S05-R6M17T14	71,413	71,846	0.61	13	13	61	42	14	4
S06-R6M17T14	71,496	71,839	0.48	13	13	44	33	12	3
S07-R6M18T14	71,570	76,919	7.47	13	14	50	40	13	4
S08-R6M18T14	76,733	77,334	0.78	14	14	30	37	14	5
S09-R7M19T14	76,644	76,938	0.38	14	14	36	24	13	3
S10-R7M19T14	83,026	83,235	0.25	15	15	125	75	23	5
S11-R7M20T15	82,419	82,758	0.41	15	15	85	61	20	5
S12-R7M20T15	87,537	87,788	0.29	16	16	117	66	21	4
S13-R8M21T15	88,058	88,463	0.46	16	16	138	94	28	5
S14-R8M21T15	88,271	88,747	0.54	16	16	171	71	20	4
S15-R8M22T15	93,806	94,324	0.55	17	17	180	82	22	5
S16-R8M22T15	93,363	93,654	0.31	17	17	164	98	21	6
S17-R9M23T16	93,782	94,151	0.39	17	17	206	86	30	5
S18-R9M23T16	99,254	99,573	0.32	18	18	195	94	37	5
S19-R9M24T16	99,104	99,411	0.31	18	18	175	105	32	5
S20-R9M24T16	104,224	104,369	0.14	19	19	214	101	34	4
Min.	60,128	60,630	0.14	11	11	16	20	8	2
Max.	104,224	104,369	7.47	19	19	214	105	37	6
Avg.	81,669	82,283	0.82	14.85	14.90	105	61	20	4.3

[1] Optimal values of the objective functions. Both MILP and Acc. BD achieved optimality.

Table 2.4: The MILP, Acc. BD, and CM results associated with medium-sized instances

Small Instances	**Objective function value**		**% Gap w.r.t. best incumbent**	**# of MFs**		**Run time (Seconds)**			**# of iters.**
($N28, P5$)	Opt.[1]	CM	CM	Opt.	CM	MILP	Acc. BD	CM	Acc. BD
M01-R5M15T19	62,941	63,673	1.16	11	11	211	119	31	3
M02-R5M15T19	69,016	69,360	0.50	12	12	207	104	32	3
M03-R5M16T19	69,118	69,712	0.86	12	12	210	83	31	4
M04-R5M16T19	69,448	70,382	1.34	12	12	161	107	40	7
M05-R6M17T19	74,604	75,519	1.23	13	13	158	173	52	6
M06-R6M17T19	74,540	75,184	0.86	13	13	219	106	36	6
M07-R6M18T19	80,130	81,174	1.30	14	14	270	131	46	7
M08-R6M18T19	80,724	81,380	0.81	14	14	188	99	39	4
M09-R7M19T20	85,570	86,125	0.65	15	15	525	244	51	6
M10-R7M19T20	86,257	92,173	6.86	15	16	561	314	54	9
M11-R7M20T20	92,372	93,545	1.27	16	16	487	193	61	4
M12-R7M20T20	93,064	98,487	5.83	16	16	606	230	56	6
M13-R8M21T21	97,405	98,787	1.42	17	17	1,022	292	93	8
M14-R8M21T21	97,686	103,873	6.33	17	18	735	329	122	7
M15-R8M22T21	102,700	103,678	0.95	18	18	1,010	255	82	7
M16-R8M22T21	103,232	109,455	6.03	18	19	973	233	90	6
M17-R9M23T21	103,683	109,733	5.84	18	19	1,162	221	95	6
M18-R9M23T21	108,443	109,610	1.08	19	19	1,210	276	100	7
M19-R9M24T21	108,929	114,803	5.39	19	20	1,463	493	92	8
M20-R9M24T21	113,993	115,352	1.19	20	20	1,636	413	128	6
Min.	62,941	63,673	0.50	11	11	158	83	31	3
Max.	113,993	115,352	6.86	20	20	1,636	493	128	9
Avg.	88,693	91,100	2.55	15.45	15.70	651	221	67	6

[1] Optimal values of the objective functions. Both MILP and Acc. BD achieved optimality.

Table 2.5: The MILP, Acc. BD, and CM results associated with large-sized instances

Large Instances ($N48, P7$)	Objective function value			% Gap w.r.t. best bound			% Gap w.r.t. best incumbent			# of MFs			Run time (seconds)			# of iters.
	MILP	Acc. BD	CM	MILP	Acc. BD	CM	MILP	Acc. BD	CM	MILP	Acc. BD	CM	MILP	Acc. BD	CM	Acc. BD
L01-R5M15T28	68,936	68,936	69,564	0.00	0.00	0.91	0.00	0.00	0.91	11	11	11	3,362	501	153	6
L02-R5M15T28	69,962	69,962	75,714	0.00	0.00	8.22	0.00	0.00	8.22	11	11	12	4,337	398	180	5
L03-R5M16T28	75,454	75,454	75,550	0.00	0.00	0.13	0.00	0.00	0.13	12	12	12	5,516	651	164	6
L04-R5M16T28	75,988	75,988	76,513	0.00	0.00	0.69	0.00	0.00	0.69	12	12	12	4,147	457	298	6
L05-R6M17T29	81,532	81,532	82,002	0.00	0.00	0.58	0.00	0.00	0.58	13	13	13	6,517	1,069	196	7
L06-R6M17T29	82,779	82,779	88,107	0.00	0.00	6.44	0.00	0.00	6.44	13	13	14	8,525	993	250	5
L07-R6M18T29	83,430	83,430	88,461	0.00	0.00	6.03	0.00	0.00	6.03	13	13	14	12,232	3,250	338	7
L08-R6M18T29	87,828	87,828	93,244	0.00	0.00	6.17	0.00	0.00	6.17	14	14	15	11,157	4,554	299	7
L09-R7M19T29	88,603	88,603	94,326	0.00	0.00	6.46	0.00	0.00	6.46	14	14	15	8,875	2,953	295	6
L10-R7M19T29	88,365	88,365	94,372	0.00	0.00	6.80	0.00	0.00	6.80	14	14	15	14,761	7,384	249	7
L11-R7M20T29	88,655	88,655	94,612	0.00	0.00	6.72	0.00	0.00	6.72	14	14	15	12,145	11,890	295	8
L12-R7M20T29	93,836	93,836	95,770	0.00	0.00	2.06	0.00	0.00	2.06	15	15	15	16,119	10,282	309	8
L13-R8M21T30	100,012	94,896	100,943	5.38	0.00	6.37	5.39	0.00	6.37	16	15	16	21,600	11,748	283	8
L14-R8M21T30	100,260	100,202	100,887	0.17	0.00	0.68	0.06	0.00	0.68	16	16	16	21,600	19,008	344	9
L15-R8M22T30	101,082	101,070	101,839	1.46	1.32	2.09	0.01	0.00	0.76	16	16	16	21,600	21,600	275	9
L16-R8M22T30	106,738	101,824	107,673	5.11	0.00	5.74	4.83	0.00	5.74	17	16	17	21,600	14,194	318	8
L17-R9M23T30	106,652	106,528	107,943	3.67	3.12	4.49	0.12	0.00	1.33	17	17	17	21,600	21,600	331	9
L18-R9M23T30	108,313	108,020	114,119	1.14	0.00	5.65	0.27	0.00	5.65	17	17	18	21,600	16,992	449	8
L19-R9M24T30	113,424	113,360	114,573	4.38	4.22	5.34	0.06	0.00	1.07	18	18	18	21,600	21,600	478	9
L20-R9M24T31	120,366	120,138	121,823	4.60	3.98	5.44	0.19	0.00	1.40	19	19	19	21,600	21,600	527	10
Min.	68,936	68,936	69,564	0.00	0.00	0.13	0.00	0.00	0.13	11	11	11	3,362	398	153	5
Max.	120,366	120,138	121,823	5.38	4.22	8.22	5.39	0.00	8.22	19	19	19	21,600	21,600	527	10
Avg.	92,111	91,570	94,902	1.30	0.63	4.35	0.55	0.00	3.71	14.60	14.50	15.00	14,025	9,636	302	7.4

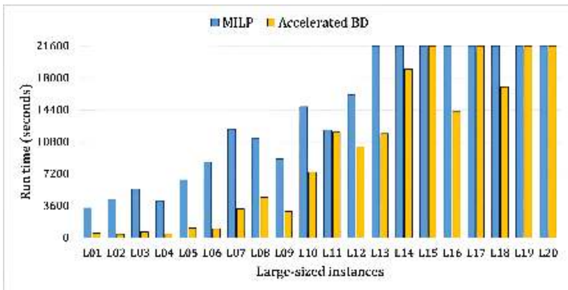

Figure 2.8: Run time comparison of the MILP and Acc. BD among 20 large-sized instances within a 6-hour time limit.

Table 2.6: The summary of results reported in Tables 2.3, 2.4, and 2.5

Instances	Avg. % gap w.r.t.						Avg. run time (seconds)		
	best bound			best incumbent					
	MILP	Acc. BD	CM	MILP	Acc. BD	CM	MILP	Acc. BD	CM
Small-sized	0.00	0.00	0.82	0.00	0.00	0.82	105	61	20
Medium-sized	0.00	0.00	2.55	0.00	0.00	2.55	651	221	67
Large-sized	1.30	0.63	4.35	0.55	0.00	3.71	14,025	9,636	302

2.5.3 Benchmarking

Bayraktar et al. (2022) address a problem similar to ours, involving relief aid provision to refugees using the identical SLR criterion to ours, albeit without capacity restrictions and specified demand levels. The authors presented a MILP formulation and an ALNS heuristic. In comparison, our study takes a more realistic approach by explicitly incorporating refugee groups' sets, their population sizes, and MF capacities. Consequently, we formulate a distinct yet refined MILP and employ different exact and matheuristic solution methods. In CMFLP-MD, the complexity arises from the possibility of requiring more than one MF to serve a refugee group fully or partially in a period. This adds a layer of intricacy to the problem, as multiple MFs need to coordinate their simultaneous presence at a specific node-time pair to provide relief aid. In contrast, the uncapacitated version assumes that a single MF can fully satisfy all SLRs at a location.

To validate our approach and enable a direct comparison, we conducted experiments on the uncapacitated instances provided by Bayraktar et al. (2022) for benchmarking through the same computational platform. Their instance titles are listed in Table 2.7. Through minor adjustments, these instances are customized to fit our formulation. Specifically, the set of refugee groups is encoded as $R = \{1, \cdots, E\}$, where E represents the number of entrances to the network in distinct node-time pairs, refugee groups' population sizes are set to 1, MF capacities are set to $|E|$, and service act costs are set to 0. Other parameters remain identical.

Our MILP outperforms both the MILP and the ALNS algorithm proposed by Bayraktar et al. (2022) in terms of runtime efficiency, as demonstrated in Table 2.7. Despite both studies achieving optimal solutions for their medium-sized instances, our MILP is solved much faster. Moreover, for their large-sized instances, our MILP not only attains optimal solutions but also improves upon some of their best incumbent solutions (highlighted in bold numbers). This performance advantage can be attributed to two key factors: First, our formulation fulfills the SLR solely on refugee groups' paths, specifically on their settlement node-time pairs. In contrast, Bayraktar et al. (2022)'s MILP includes SLR constraints within every path for all periods, resulting in redundant constraints. Second, our MILP directly links the service act ($\mathbf{Y}$) and location-relocation ($\mathbf{X}$) decision variables using a single constraint block (2.4). In contrast, Bayraktar et al. (2022) employs multiple linearization constraints for this purpose. These factors contribute to the computational efficiency of our MILP formulation, making it more suitable for solving large-scale instances.

2.5.4 Managerial insights

This section discusses how HOs can benefit from this research. We conduct sensitivity analyses on CMFLP-MD outputs in several directions to derive insights for decision-makers. Section 2.5.4.1 explores the influence of different τ values on solution attributes. Similarly, Section 2.5.4.2 investigates the effects of expanding the capacity of MFs. Section 2.5.4.3 presents the frequency and heat map of service acts across the network nodes to identify critical locations for service provision. Finally, Section 2.5.4.4 answers two what-if questions to examine the robustness of the service act plans. To conduct our sensitivity analyses, we selected the "S01-R5M15T14" instance, which comprises 19 nodes, three paths, five refugee groups, 15 MFs, and a time horizon spanning 14 periods. Given the extensive computational

Table 2.7: Performance comparison: Our MILP results vs. Bayraktar et al. (2022)'s (Ref) MILP and ALNS results

Uncapacitated instances (medium)	Optimal obj f. values[2]	Run times (seconds) (Ref) MILP	Run times (seconds) (Ref) ALNS	Run times (seconds) Our MILP	Uncapacitated instances (large)	Objective function values (Ref)	Objective function values Our MILP	Run times (seconds) (Ref) MILP	Run times (seconds) (Ref) ALNS	Run times (seconds) Our MILP
P01E01N20_1[1]	1,488	8	4	2	P01E01N30_1	2,129	2,129	183	7	3
P01E02N20_1	1,492	5	10	2	P01E02N30_1	2,133	2,133	34	32	3
P02E02N20_1	1,508	9	4	3	P02E02N30_1	2,552	2,552	5,532	15	6
P02E04N20_1	1,839	21	16	4	P02E04N30_1	2,883	2,883	10,121	119	12
P02E04N20_2	2,594	4,222	18	5	P02E04N30_2	4,098	4,098	14,400	198	10
P03E03N20_1	1,716	78	37	4	P03E03N30_1	3,003	3,003	14,400	535	13
P03E04N20_1	2,669	3,730	155	7	P03E04N30_1	4,374	4,374	14,400	2,007	24
P03E04N20_2	2,043	254	40	6	P03E04N30_2	3,965	3,965	14,400	1,618	10
P03E06N20_1	2,910	14,402	404	10	P03E06N30_1	4,613	4,613	14,400	5,919	52
P03E06N20_2	2,372	1,678	179	15	P03E06N30_2	3,667	3,667	14,400	5,196	121
P03E06N20_3	2,940	14,418	401	22	P03E06N30_3	4,642	**4,591**[3]	14,400	5,769	101
P03E06N20_4	2,837	14,412	294	12	P03E06N30_4	4,439	4,439	14,400	4,573	76
P03E06N20_5	2,614	4,370	94	8	P03E06N30_5	4,123	4,123	14,400	708	80
P04E04N20_1	2,043	305	37	6	P04E04N30_1	3.540	3,540	14,400	906	42
P04E08N20_1	2,372	1,230	209	11	P04E08N30_1	4,157	4,157	14,400	7,452	97
P04E08N20_2	2,784	11,292	431	12	P04E08N30_2	5,137	**5,100**	14,400	14,400	111
P04E08N20_3	2,940	14,402	350	17	P04E08N30_3	5,200	**5,190**	14,400	11,185	139
P04E08N20_4	3,093	14,416	453	27	P04E08N30_4	5,496	**5,397**	14,400	12,372	269
P04E08N20_5	2,940	14,402	213	17	P04E08N30_5	5,150	5,150	14,400	10,220	122
P04E10N20_1	3,264	14,407	980	31	P04E10N30_1	5,563	**5,509**	14,400	14,400	713
P04E10N20_2	2,960	13,361	857	15	P04E10N30_2	5,375	**5,250**	14,400	14,400	522
P06E10N20_1	3,215	14,415	758	90	P06E10N30_1	5,351	**5,279**	14,400	14,400	602
P06E10N20_2	3,244	14,414	647	66	P06E10N30_2	5,565	**5,478**	14,400	14,400	744
P06E10N20_3	3,311	14,409	801	57	P06E10N30_3	5,686	5,686	14,400	14,400	984
P06E13N20_1	3,217	14,403	1,704	50	P06E13N30_1	4,899	4,899	14,400	14,400	955
Min.		5	4	2	**Min.**			34	7	3
Max.		14,418	1,704	90	**Max.**			14,400	14,400	984
Avg.		7,693	364	20	**Avg.**			12,731	6,785	232

[1] P: Number of paths, E: Number of distinct entrances to the network, N: Length of the longest path, 1: ID
[2] This column represents optimal objective function values attained by both Bayraktar et al. (2022) and our MILP
[3] Numbers in bold indicate an improvement upon the best incumbent solutions by Bayraktar et al. (2022)

demands of this section and that all instances share the same network configuration and path structures, this particular instance size was chosen as a representative one.

2.5.4.1 SLR parameter analysis

To understand the impact of the value of τ on our solutions, we present a comprehensive breakdown of various metrics as reported in Table 2.8 and depicted in Figs. 2.9-2.13 while varying τ values from 2 to 9. The other parameter settings remain the same as in Section 2.5.1. The metrics include (i) objective function values, (ii) the number of deployed MFs, (iii) the number of service acts, (iv) the percent of MF workload, and (v) the percent of MF capacity utilization. A detailed explanation of each metric, along with the insights, are provided below.

Objective function values: As expected, the optimal values of the objective function decline as τ increases. A closer examination reveals that the total cost displays a heightened sensitivity to lower τ values. This implies that the overall cost of the relief operation is significantly influenced by the length of the SLR. HOs may exercise caution when selecting a small SLR parameter. In particular, they should consider both budget limitations and desired service levels, especially if they intend to perform more frequent visits.

Number of deployed MFs: The total number of MFs deployed is derived by summing the values of $\mathbf{Z}$ variables. This metric serves as a practical reference for HOs in choosing an appropriate τ value, considering their available MF fleet size and/or staff members. Similar to the trend observed in the objective function values, the number of deployed MFs exhibited a non-increasing pattern concerning τ.

Number of service acts: The number of service acts is determined by summing the values of $\mathbf{Y}$ variables. This measure offers HOs a reliable anticipation of the required quantity of service bundles. Table 2.8 reveals that the number of conducted service acts is sensitive to τ values. Opting for smaller τ values is practical only if HOs are capable of procuring abundant service bundles.

MF workload %: Besides the number of service acts, we calculate the proportion of periods during which service acts are carried out to appraise the workload of MFs. This metric is computed by dividing the total number of conducted service acts by the number of periods in which MFs operated in the network, spanning from their initial service act period until $|T|$, as captured in Equation (2.32). The optimal solutions resulted in substantial workloads for MFs, providing service acts during almost 86% of the periods.

$$\text{MF workload } \% = \frac{\sum_{m\in M}\sum_{(i,t)\in\mathcal{L}} Y_{mit}}{\sum_{m\in M} Z_m \times \left(|T| - \min\{t\in T : \sum_{i\in V^M} Y_{mit} \geq 1\} + 1\right)} \times 100 \quad (2.32)$$

MF capacity utilization %: This metric shows the extent to which MF capacities are utilized to meet the prevailing demand. It is obtained by dividing the total recurrent demands of all refugee groups along their paths based on the τ parameter by the total capacity furnished by MFs as in Equation (2.33). The results reported in Table 2.8 indicate that optimal solutions achieved a high average capacity utilization of 93.49%, indicating an efficient deployment of MFs over time.

$$\text{Capacity Utilization \%} = \frac{\sum_{r \in R} d_r \left\lfloor \frac{l_{p_r}}{\tau} \right\rfloor}{\sum_{m \in M} \sum_{(i,t) \in \mathcal{L}} b_m Y_{mit}} \times 100 \tag{2.33}$$

Table 2.8: Values of metrics associated with the instance S01-R5M15T14 under varying τ values

SLR parameter τ	Objective function value	# of deployed MFs	# of service acts	MF workload %	MF capacity utilization %
2	122,006	22	222	92.89	97.07
3	82,415	15	137	87.26	97.08
4	60,128	11	95	85.59	96.58
5	49,572	9	85	93.41	97.06
6	38,311	7	61	85.92	82.79
7	32,763	6	51	85.00	80.88
8	32,223	6	42	73.68	98.21
9	27,235	5	42	87.50	98.21
Min.	27,235	5	42	73.68	80.88
Max.	122,006	22	222	93.41	98.21
Avg.	55,582	10.1	91.9	86.41	93.49

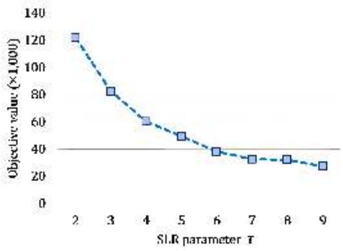

Figure 2.9: Objective function values across different SLR values

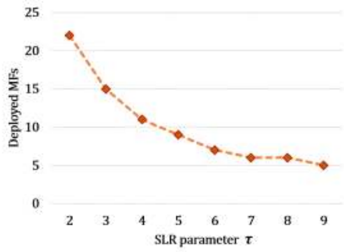

Figure 2.10: Number of deployed MFs across different SLR values

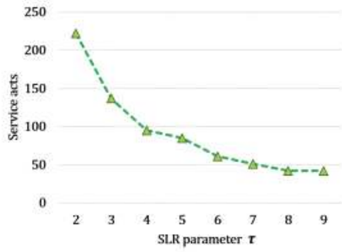

Figure 2.11: Number of service acts across different SLR values

2.5.4.2 MF capacity analysis

HOs may explore the option of expanding MF capacities to potentially reduce their overall costs or enhance their service provision quality. In our experimental setup, we let MF capacities as $b_m = 400$ for all $m \in M$ (Turkish Red Crescent, 2019). Table 2.9 reports the same metrics introduced in Section 2.5.4.1, calculated across varying MF capacities $b_m \in \{300, 350, 400, 450, 500, 550, 600\}$. The results elaborated by Figs. 2.14-2.18 show that augmenting MF capacities, even at a moderate level, leads to almost linear decreases in cost savings, the number of deployed MFs, and executed service acts while maintaining high values of MF workloads and their

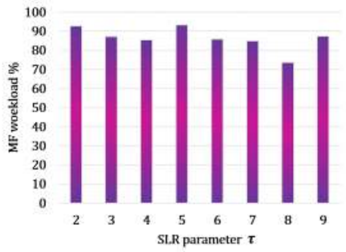

Figure 2.12: MF workload % across different SLR values

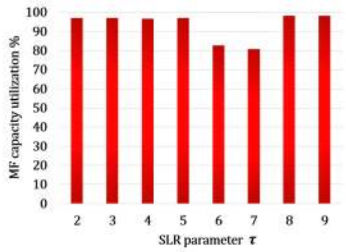

Figure 2.13: MF capacity utilization % across different SLR values

capacity utilization. This finding underscores the importance of considering the option of deploying MFs with larger capacities if economically viable.

Table 2.9: Values of metrics associated with the instance S01-R5M15T14 for $\tau = 4$ and varying MF capacity

MF capacity b_m	**Objective function value**	**# of deployed MFs**	**# of service acts**	**MF workload %**	**MF capacity utilization %**
300	76,758	14	125	88.03	97.87
350	70,873	13	109	84.50	96.20
400	60,128	11	95	85.59	96.58
450	54,753	10	88	87.13	92.68
500	49,150	9	77	85.56	95.32
550	48,928	9	73	92.95	91.41
600	43,502	8	65	83.33	94.10
Min.	43,502	8	65	83.33	91.41
Max.	76.758	14	125	92.95	97.87
Avg.	57,727	10.6	90.3	86.73	94.88

2.5.4.3 Spatial distribution of service acts

We analyzed the frequency of service acts across the network nodes by providing both a quantitative assessment and a visual illustration of the spatial service act distribution. Fig. 2.19 shows a heatmap of service acts for the “S01-R5M15T14” instance with $\tau = 4$. According to the optimal solution, nodes 7 and 17 host the most frequent service acts, each accommodating 13 service acts over 14 periods. Conversely, certain nodes do not host any service acts. Analyzing the spatial distribution of service acts enables HOs to select proper locations where they may opt to establish temporary fixed relief facilities in case of prolonged migrations instead of deploying MFs. Therefore, decision-makers can investigate the joint usage of fixed

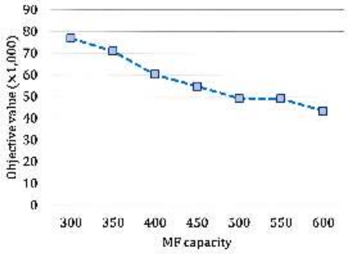

Figure 2.14: Objective function values across different MF capacities

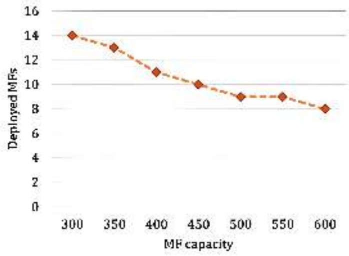

Figure 2.15: Number of deployed MFs across different MF capacities

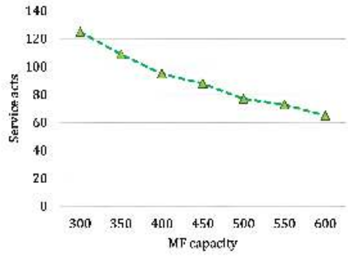

Figure 2.16: Number of service acts across different MF capacities

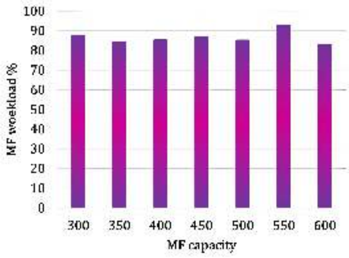

Figure 2.17: MF workload % across different MF capacities

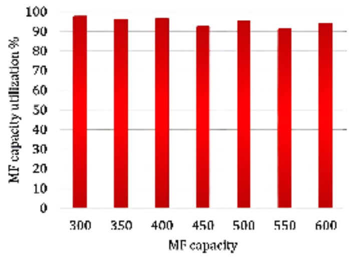

Figure 2.18: MF capacity utilization % across different MF capacities

and mobile facilities, relying on the MILP adjustments mentioned in Section 2.3.1.

2.5.4.4 What if analysis

This chapter primarily assumes the predictability of the paths traversed by refugee groups together with their consistent advancement along those paths and demand divisibility in the network. While rationales are provided in Section 2.2, we discuss two what-if scenarios and explore the implications and robustness of CMFLP-MD solutions in case these assumptions vary.

Scenario 1: A refugee group deviates from its migration path or does not advance on its path at each period.

In our models, we designated a single path for each en route refugee group, over which they progress by one node per period. This leads to specific node-time pairs for refugee groups placements over time, as explained in Section 2.3. Each service

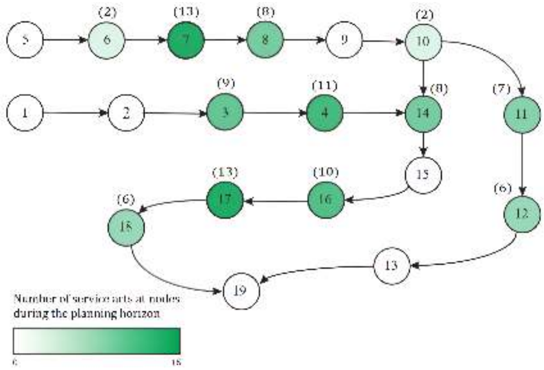

Figure 2.19: Heatmap of the frequency of service acts (shown in parentheses) for the "S01-R5M15T14" instance with $\tau = 4$

act within CMFLP-MD solutions is associated with a node-time pair. There might be situations where refugee groups diverge from their allocated node-time pairs. As a result, although the periods of the scheduled service acts remain valid, their locations (indexed as i in Y_{mit}) should be revisited. In such situations, HOs can rely on the service act plans proposed by the optimal solution, albeit with some minor adjustments. Assuming $Y_{mit} = 1$ for some MFs while their targeted refugee groups are settled at node $i' \neq i$ in period t, those MFs must conduct the same service acts at node i' instead. Although the fulfillment of the SLR is still guaranteed, additional relocation costs may be incurred. An alternative option involves re-optimizing the model based on the most up-to-date status of refugee groups and MFs to obtain new service act plans for the upcoming periods. While the latter approach entails extra computational effort, it prevents unexpected expenses arising from adherence to outdated plans. If refugee group's migration extends beyond the intended time horizon T, the latter option becomes essential.

Scenario 2: MFs are required to serve the entire population of a refugee group without the option of dividing the demand into multiple periods.

The designated MILP and solution methods offer the flexibility to achieve partial or full demand satisfaction for refugee groups over different periods, depending on the availability of MFs. Despite the simplicity of full demand satisfaction planning, it often requires deploying an increased number of MFs across the network with costly relocations before each visit, if not resulting in infeasible solutions due to resource scarcity. Technically, even if demand divisibility is not permissible, the core body of our MILP and CM approach remains applicable. The sole adjustment reverts the domain of the **A** variables from a continuous nonnegative into a binary domain.

2.5.4.5 Discussions

The outcomes of our study offer valuable insights to HOs and Non-Governmental Organizations (NGOs) striving to cost-efficiently and recurrently deliver relief aid to en route refugee groups over time. Our proposed methods generate a series of service acts designed for implementation via capacitated MFs across periods. We demonstrate the robustness of these service act plans in the face of potential alterations in refugee groups' movements. The versatility of our models allows for utilization at any stage of migration, incorporating the most recent information on refugee groups and MFs within the migration area. While our planning extends multiple days ahead, the adaptive nature of the proposed methods permits re-optimization with new data as conditions change. Hence, the designation of our CM as a rapid solution method is essential. Furthermore, considering capacity limitations and refugee populations is pivotal for obtaining an implementable solution.

Our developed models are applicable to other migration crisis scenarios, such as Syrian and Ukrainian refugee migrations. Plus, considering the relocation nature of demands, our methodologies can transcend the context of relief aid provision to en route refugee groups and are applicable to addressing any facility location problem where both facilities and demand entities are mobile. This includes problems within transportation logistics and telecommunication network design domains. Understanding the diverse challenges in migration fields—ranging from the type of crises and logistical challenges to coordination among HOs, governmental regulations, resource availability, and seasonal variations—we recognize that relief aid delivery to en route refugees in practice exhibits considerable variability. The incorporation of a tunable SLR parameter in CMFLP-MD allows HOs to adjust aid delivery frequency in the field. We note that although our results undergo theoretical validation and benchmarking, a practical implementation of the study stands as a current limitation that warrants future exploration.

2.6 Conclusion

There has been an increasing worldwide trend in the refugee movements over the past decade. The tragedy of forced displacement caused by war, persecution, violence, famine, or natural disasters often pushes refugees to remain in transit for prolonged periods. The present work is set out to assist HOs in cost-efficiently optimizing the logistics of capacitated MFs utilized to recurrently deliver relief aid to transiting refugees in a multi-period setting. This problem is introduced to the literature of HL as the Capacitated Mobile Facility Location Problem with Mobile Demands (CMFLP-MD). We envision that refugees would follow certain paths in their journey and join the convoy at different locations and times. A key characteristic of the CMFLP-MD is a periodic SLR in service provisioning. In particular, the individuals of each refugee group receive relief items at least once every fixed number of consecutive periods as they advance through their often prolonged journey.

We propose an MILP formulation for the CMFLP-MD, followed by a set of valid inequalities for the special case of a homogeneous MF fleet. Considering the complexity of the problem, we examine two solution methods to cope with large-scale problem instances: an accelerated Benders decomposition approach as an exact solution method and a matheuristic algorithm based on an enhanced fix-and-solve mechanism. We verify our MILP by benchmarking over existing instances in the literature and demonstrate its efficiency, as it speeds up the run times and improves some of the existing best-found results. We also evaluate our methodologies using realistic instances inspired by the Honduras migration crisis that commenced in 2018. Our results reveal that the accelerated BD excels with a 46% run time improvement on average and solution quality compared to the MILP. Moreover, the proposed matheuristic acquires near-optimal solutions quickly, with an average gap of 2.4% compared to best-incumbent solutions.

Our findings in Section 2.5.4 offer managerial insights with practical implications for decision-makers. First, there exists a trade-off in selecting a proper value for the SLR parameter τ. A smaller τ would enhance the effectiveness of aid to the beneficiaries by increasing the number of service acts, albeit at the expense of elevated fixed and variable costs for HOs. Essentially, the budget limitations faced by HOs (Verme and Gigliarano, 2019) necessitate a careful determination of the SLR parameter, taking into account particular resource-centric factors such as budgetary limits, availability of MFs, and relief inventory. Second, our results demonstrate suitably high values for the MF workload levels and the capacity utilizations regardless of the choice of SLR parameter, indicating that the optimal solutions achieve efficient MF fleet management. Third, our analyses highlight the feasibility of MF service capacity expansion, even in a modest proportion, as an economically viable option for HOs seeking to reduce their logistics expenditures. Fourth, by analyzing the spatial distribution of service acts, our solutions can distinguish nodes hosting more frequent relief aid provisions. These nodes serve as potential locations to establish temporary fixed facilities under prolonged migration scenarios. Lastly, while CMFLP-MD assumes that the paths followed by refugee groups can be predicted in advance, our in-depth exploration of the solution properties underscores the adaptability of our relief aid plans in the face of varying migration circumstances.

A promising avenue for future research is to address the uncertainties associated with refugee groups' displacements, which will be our goal in the next chapter. One potential approach is to develop a scenario-based model with various path-traversal possibilities. A dynamic programming formulation featuring sequential decision-making can handle refugee groups' migration patterns under imperfect information and deduce optimal service act plans. Another research direction may explore diverse types of SLRs for refugee groups based on the urgency of their needs, or multiple human, MF, and relief resource capacities, considering flexibility concepts (Akşin et al., 2015).

Chapter 3

RELIEF AID PROVISION PLANNING TO EN ROUTE REFUGEES UNDER A STOCHASTIC MIGRATION ENVIRONMENT

3.1 *Introduction*

The rise in the forced displacement crisis has become a pressing global humanitarian concern. The latest assessment by the United Nations High Commissioner for Refugees (UNHCR) reveals that the number of forcibly displaced individuals has alarmingly doubled over the past decade, reaching 122.6 million in 2024, triggered by persecution, conflict, and human rights violations (Concern worldwide US, 2023). According to the UNHCR classification (The UN Refugee Agency, 2025), forcibly displaced people are legally categorized into three groups: refugees, internally displaced persons (IDPs), and asylum seekers. Refugees are individuals who have fled their home country, crossed international borders, and are protected under international law, specifically the 1951 Refugee Convention. Asylum seekers are those who have also fled their home country and requested international protection but have not yet been granted official refugee status by the UNHCR or the host country's government. IDPs, in contrast, have fled their homes within their own country's borders. Most IDPs remain near conflict zones and do not receive the same level of international protection as refugees. Hence, they may eventually seek refuge abroad. Given that all these groups experience forced displacement, they are often collectively referred to as 'refugees' in sociological literature (Icduygu et al., 2001; Kotsi et al., 2022). In this study, we adopt the umbrella term *refugee* to refer to all forcibly displaced individuals.

Humanitarian Organizations (HOs) are pivotal in providing relief aid and services during refugee crises (Kotsi et al., 2022). For instance, during the 2011–2019 Syrian migration crisis, UNHCR, the Turkish Red Crescent (TRC), and Médecins Sans Frontières established aid stations at 14 key border crossings in Türkiye, including Afrin and Azaz. These stations provided Syrian refugees with food, medical care, and temporary shelter. After the violence in Myanmar's Rakhine State in 2017, nearly 1 million Rohingya refugees fled to Bangladesh. Organizations like the World Food Programme and the International Organization for Migration (IOM) provided food and temporary shelter along migration routes leading to Cox's Bazar. Millions of Venezuelans have escaped economic and political instability by crossing into Colombia, Ecuador, and Peru since 2015. The International Federation of Red Cross and Red Crescent Societies (IFRC), UNHCR, and local NGOs provided them with food, hygiene kits, and legal assistance. Similarly, following the 2021 Taliban takeover, many Afghans fled to neighboring countries, including Pakistan and Iran. The UNHCR, IOM, and local aid agencies have set up relief points along the borders to provide medical and emergency cash assistance to displaced people. These targeted relief efforts are vital not only for meeting basic needs but also for mitigating the psychological and social burdens experienced by displaced populations.

Refugee movements often result in extended periods of transit, where they are largely on foot (Talleraas et al., 2024). During prolonged migrations, refugees remain in a twilight zone, where their social and familial interactions are disrupted, and they are saddled with mental and somatic disorders (Miller and Rasmussen, 2017; Morina et al., 2018; Satinsky et al., 2019). Moreover, en route refugees are predominantly distanced from relief resources, including water, food, hygiene, and clothing (Oloruntoba and Banomyong, 2018). Most relief efforts for en route refugees are concentrated at static border corridors, which may fall short in addressing the intermittent and dispersed needs of mobile populations. Nevertheless, the operational potential of Mobile Facilities (MFs) has been overlooked in practice. MFs can be deployed to repeatedly deliver relief aid at multiple points along refugees' migration trajectories. However, given the physical impediments in the migration territory, MFs must directly reach the entire group to effectively deliver relief aid (Burkart et al., 2017). Hence, we define a *service act* for an MF as the protocol of dispensing relief aid to refugee groups when both entities are co-located within the same period.

From an operational viewpoint, relief aid distribution among ever-increasing flows of refugees is a challenging process for HOs. First, refugee migration routes are inherently unpredictable, and their move-or-wait decisions are shaped by unstable environmental conditions (Schapendonk, 2012). This necessitates the development of stochastic models that explicitly account for such uncertainties. Second, the rise in both the frequency and duration of crises has brought about an escalated demand for humanitarian support that surpasses existing funding resources (Alem, 2021; European Commission, 2022). This highlights the need to devise cost-efficient relief aid delivery mechanisms. Third, another major challenge is executing equitable aid distribution despite unpredictable refugee migration. Evidence from reports and interviews with Honduran and Syrian refugees revealed extortion, theft, and a notable disparity between the relief aid provided and the fulfillment of everyone's needs (Rascon, 2018; Mohamed Abu Shahma, 2018). To account for equity and prevent prolonged deprivation, our model incorporates a service level requirement (SLR) criterion, which ensures each refugee group receives relief aid at least once every consecutive timeframe. This concept allows HOs to evaluate refugee groups' health status regularly and build a trusted relationship while supplementing them (Robertshaw et al., 2017). The United Nations affirms the importance of well-being and equitable treatment of refugees through its Sustainable Development Goals (SDGs), particularly Goal #10 (Reduced Inequalities) and Goal #16 (Peace, Justice and Strong Institutions). Motivated by the aforementioned challenges and SDGs, our proposed methods provide decision support for HOs such as the UNHCR, IOM, IFRC, and local NGOs in the cost-efficient deployment of MFs to equitably serve en route refugee groups.

In this chapter, we seek to answer: (i) Which refugee groups should be served in each period? and (ii) Where should MFs locate and relocate over time? The objective is to minimize the sum of MF relocation and replenishment costs and refugees' deprivation costs in case of SLR violations. Given that HOs may encounter constraints in MF deployment or relief inventory that hinder meeting the SLR (European Commission, 2022), it is incorporated as a soft constraint in our models. Any SLR violations, interpreted as deprivation, are penalized within the objective function. The tradeoff is that delayed or insufficient service acts may result in high deprivation costs. In contrast, excessive or misallocated service acts can cause extravagant resource and capacity utilization. Our decisions are subject to (i) refugees' probabilistic displacements, (ii) MF capacity limitations for indiscriminate service acts (without demand splitting) among refugee groups, and (iii) the SLR criterion, which together can prove intricate. Notably, the number of refugees accruing relief aid between periods is not identical and depends on prior service acts, which compounds the problem. Figure 3.1 presents a schematic illustration of the problem within a single period. In principle, we tackle a finite-horizon stochastic optimization problem with uncertain horizon length, which we formulate as a discrete-time discounted Markov Decision Process (MDP) model.

The remainder of this chapter is arranged as follows. Section 2 reviews the related works and positions our study in the literature. Section 3 formulates our MDP model. In Section 4, we develop two solution methods: (i) an approximate dynamic programming (ADP) and (ii) a variable threshold policy (VTP). Section 5 presents comprehensive experiments and solution analyses on an illustrative example and instances driven by the Syrian migration crisis to assess the proposed methods and propose practical insights. Finally, Section 6 outlines concluding statements.

3.2 Literature review

We position this study with respect to four streams of related extant literature in Sections 3.2.1-3.2.3. Our contributions are stated in Section 3.2.4.

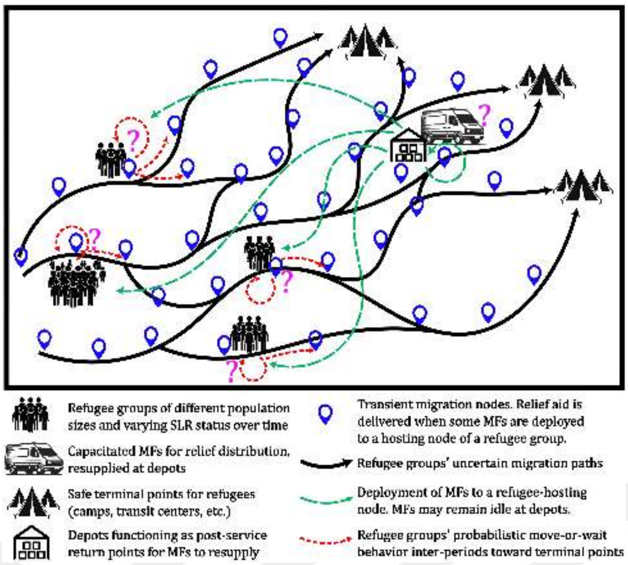

Figure 3.1: A schematic representation of the problem is shown, where the decisions to make are shown with question marks. MFs can remain idle or be deployed to provide relief aid to refugee groups. Subsequently, these groups make probabilistic move-or-wait decisions (either remain in place or migrate) along uncertain paths. Their eventual resettlement locations are realized in the subsequent period.

3.2.1 Mobile facility location problem

The backbone of supporting en route refugee groups via MFs is the well-known family of capacitated mobile facility location problems (Raghavan et al., 2019). Incorporating MF capacities aligns more closely with the practical implications of service provisioning, since MFs inherently possess limitations on personnel and equipment, thus restricting the number of individuals they can serve in each period. The activity report by Turkish Red Crescent (2019) demonstrates that their deployed MFs could serve up to 400–500 en route Syrian refugees daily. MFs find applications in disciplines such as healthcare, social outreach activities, and humanitarian logistics (HL) (Pashapour et al., 2024). Among the latter, MFs have been broadly integrated into the emergency response literature. Nair and Miller-Hooks (2009) improve expected response times of emergency medical vehicles by up to 6.14% through relocation, compared to using an equal number of static facilities to respond to future demand. Geroliminis et al. (2011) further emphasize the significance of MFs in escalated demand situations. Li et al. (2019) determine the location-relocation and fleet size of emergency mobile units via a robust optimization approach. Li et al. (2022) propose a multi-objective mobile emergency material allocation model in the aftermath of sudden-onset disasters. Avishan et al. (2023) develop a robust optimization framework to distribute relief aid during post-disaster operations in HL.

Unlike the above studies, our work is situated in multi-period relief aid provision to transiting refugees—an area less explored in the HL literature. Our decisions account for inter-period location-relocations of MFs, as in Bélanger et al. (2019); Li et al. (2019); Bayraktar et al. (2022); Pashapour et al. (2024). Among similar studies to ours, Salman et al. (2021) optimize health service delivery of mobile clinics to seasonal Syrian migrant farm workers in Türkiye. Bayraktar et al. (2022) develop an Adaptive Large Neighborhood Search to solve an uncapacitated MFLP for relief provisioning to en route refugees. Santa González et al. (2023) investigate the deployment of mobile clinics for humanitarian relief supply across villages, with profitability considerations. Pashapour et al. (2024) develop a Benders decomposition and a matheuristic to solve a capacitated variant of Bayraktar et al. (2022)'s problem. While our use of MFs is closely aligned with Pashapour et al. (2024), our location-relocations of MFs are influenced by refugee groups' probabilistic movements.

3.2.2 Uncertain mobile demand

Mobility is an intrinsic characteristic of en route refugees owing to their transient behavior and surrounding instabilities (Schapendonk, 2012). Agent-based modeling is predominantly used to develop models that explore the behavior of forcibly displaced people, identify migration patterns, and compensate for incomplete empirical information in predicting refugee movements (Frydenlund et al., 2019; Searle and van Vuuren, 2021; Güngör et al., 2024).

Refugee groups' paths have been described not as closed corridors but as open, processual phenomena (Schapendonk, 2012). Bayraktar et al. (2022) and Pashapour et al. (2024) assume refugee groups follow the shortest path from their initial location toward their nearest terminal point, advancing one node per period along these paths. Manafi and Roman (2022), however, state that refugee groups' aspirations for destination points or their migration trajectories can change over time. For example, Mallett and Hagen-Zanker (2018)'s interviews with Eritrean, Senegalese, and Syrian migrants to Europe reveal that only 24% traveled directly from their departure point to their destination by following the shortest path. The remaining 76% experienced longer journeys and spent extended periods in transit. Locational advantages—such as safety, road complexity, and proximity to destination points—are signified as pull drivers for refugee groups along their paths (Moore and Shellman, 2007; Prasad et al., 2023; Di Iasio and Wahba, 2024). Schapendonk (2012) discusses the *Moving and Waiting* behaviors as dynamics of refugees' trajectories over time, affected by the aforementioned drivers. Moving back, however, once a refugee is in transit, is typically not an option. In one of Schapendonk (2012)'s interviews, a refugee on the move emphatically stated, "*Going back? That is not possible. I cannot go back!...*". These sentiments demonstrate the challenges in accurately portraying the dynamics of refugee movements.

Among studies related to ours, Azizi et al. (2021) develop an inventory management policy to balance relief aid sharing among camp-based and urban refugee populations. In separate works, Ahani et al. (2024) and Bansak and Paulson (2024) study the dynamic placement of refugees in a host country to maximize refugees' overall expected employment success using online matching algorithms. Demir et al. (2024) improve the integration of refugee children into the host country's education system without overburdening the infrastructure, via a maximum covering problem. Diverging from these exercises, our study is centered on the transitional stage of refugee groups' migration toward the host country. Unlike Bayraktar et al. (2022) and Pashapour et al. (2024), who optimize relief distribution based on a single migration scenario, our work incorporates and justifies the role of uncertainty in refugee movements by modeling their behavior through probabilistic move-or-wait decisions. These behaviors are driven by external environmental factors, such as locational safety and proximity, as well as road barricades (Diedrichs et al., 2024), augmented with a noise term for variability.

3.2.3 DP and ADP methodologies

Since the 1950s–60s, MDPs have been used to model sequential decision-making with uncertain outcomes (Bellman, 1957). An MDP seeks the best decision policy (a strategy or contingency plan), which is a function that maps a state to an action (Puterman, 2014). For finite-horizon MDPs, backward or forward induction provides an exact solution. For infinite-horizon MDPs, value iteration or policy iteration algorithms can be employed. Linear programming is applicable for both types (Puterman, 2014). Therefore, dynamic programming is interpreted as a collection of algorithms capable of attaining optimal policies, given an environment model as a discrete MDP (Ross, 2014).

ADP emerges as an effective tool for solving large-scale stochastic optimization problems. The essence of ADP is to overcome the curse of dimensionality in DP by replacing the true value functions (or cost-to-go functions) with statistical approximations (Powell et al., 2012). Successful applications of ADP span a wide array of problems in transportation (Simao et al., 2009; Powell et al., 2012; Asadi and Nurre Pinkley, 2022; Luo et al., 2022), healthcare (He et al., 2012; Hulshof et al., 2016; Dai and Shi, 2019), dynamic fleet management (Topaloglu and Powell, 2007), scheduling (Satic et al., 2024), job shop workforce assignment (Annear et al., 2023), supply chain management (Fang et al., 2013), energy management (Wu et al., 2019), natural gas storage (Lai et al., 2010), pricing and revenue management (Nascimento and Powell, 2010; Ke et al., 2019), emergency ambulance routing (Maxwell et al., 2010), and military operations (McKenna et al., 2020; Jenkins et al., 2020b; Rempel and Cai, 2021; Jenkins et al., 2021; Liles IV et al., 2023). An ADP algorithm can utilize approximate value iteration, approximate policy iteration, or approximate linear programming regimes to estimate the value functions.

Approximate policy iteration (API) aims to learn a policy vector by estimating the coefficients of state-dependent basis functions and refining this vector through iterative updates. State-of-the-art APIs rely on temporal-difference evaluations and adjust estimates based on the immediate costs observed between state transitions (McKenna et al., 2020; Jenkins et al., 2020b, 2021; Rempel and Cai, 2021; Crumpacker et al., 2022; Liles IV et al., 2023; Gao et al., 2024). Notably, this linear approximation serves as a surrogate for the expected total future cost in the DP optimality equation. However, in many real-world settings with large and complex outcome spaces, using a single realization of state transitions may not sufficiently capture the underlying system dynamics. To mitigate this limitation, we propose a novel enhancement to the standard API, introducing a policy replication loop, resulting in what we term a three-looped API (3API). This additional loop repeatedly simulates downstream states, thus providing a richer set of observations that improves the stability and accuracy of policy vector calibration.

3.2.4 Our contributions

The primary contributions of this study are threefold. First, we systematize relief provision planning for en route refugees by developing an MDP model that incorporates probabilistic movement behaviors for refugee groups, based on external migration pull drivers. Our approach refines the applicability of the existing body of research by formulating refugees' move-or-wait behaviors and relaxing the restrictive assumption of having prior knowledge of their migration trajectories. Second, we design an ADP scheme augmented by customized basis functions and a novel policy replication loop, aimed at improving the estimation of expected costs of downstream states. Third, given the practical implications of our problem, we propose a VTP that swiftly generates high-quality service act policies and enables the derivation of extensive managerial insights. To the best of our knowledge, the present work pioneers the joint exploration of these research directions.

3.3 Problem overview

Consider refugee groups $r \in \mathcal{R} = \{1, \cdots, R\}$, each with a population $d^r \in \mathbb{Z}^+$, migrating stochastically and independently on a network $\mathcal{G}^{\mathcal{R}} = (V^{\mathcal{R}}, A^{\mathcal{R}})$ toward designated terminal points $\mathcal{H}$. HOs typically estimate refugee populations (demand levels) and their locations using satellite tracking, biometric data, real-time field assessments, or local reports. Also, consider a set of MFs $m \in \mathcal{M} = \{1, \cdots, M\}$, each endowed with a capacity $b^m \in \mathbb{Z}^+$, indicating the number of refugees they can serve per period. Our planning horizon is discretized into daily periods, consistent with operational planning cycles in the humanitarian logistics literature. The network structure ensures that each refugee group travels between two nodes within a single decision epoch, which enables a period-based representation of movement and service. This modeling choice avoids fractional movement states, facilitates macro-level service act planning, and maintains a well-defined decision structure. Figure 2 illustrates the sequence of events occurring within each period.

MFs are initially positioned at some depot sites $\mathcal{D}$ dispersed throughout the network. As argued by Bayraktar et al. (2022), refugees' trajectories are not influenced by the presence or movement of MFs. Thus, MFs relocate and intercept refugee groups on a separate network $\mathcal{G}^{\mathcal{M}} = (V^{\mathcal{M}}, A^{\mathcal{M}})$ to deliver relief aid. Let $\mathcal{J}$ denote transient stop-over nodes where refugee groups and MFs may interact for aid delivery. Therein, the sets $V^{\mathcal{R}}$ and $V^{\mathcal{M}}$ are defined as $V^{\mathcal{R}} = \mathcal{J} \cup \mathcal{H}$ and $V^{\mathcal{M}} = \mathcal{J} \cup \mathcal{D}$ for refugees and MFs, respectively. Considering the $A^{\mathcal{M}}$ structure, we assume that every pair of depots and transient nodes is mutually accessible inter-periodically for MFs. In case of inaccessibility, this can be modeled by assigning a prohibitively high relocation cost to the corresponding arcs. The arc set $A^{\mathcal{R}}$ comprises road segments connecting nodes of $V^{\mathcal{R}}$. In line with the cost-efficient relief logistics principles emphasized by European Commission (2022), and building upon the objective structure proposed in Pashapour et al. (2024), our goal is to minimize the operational costs of allocating service acts to MFs over time. Our decisions are subject to: (i) refugees' probabilistic displacements, (ii) MF capacity limitations, and (iii) an SLR criterion, due to the recurrent needs of en route refugee groups over time. The SLR requires that individuals in each refugee group be served at least once every $\tau \in \mathbb{Z}^+$ periods until the group reaches a terminal location.

The probabilistic nature of refugee movements and the uncertainty surrounding their arrival at terminal points give rise to a finite-horizon stochastic optimization problem with uncertain horizon length. We formulate this problem as an MDP model. The five fundamental components of the MDP formulation are detailed in Sections 3.3.1–3.3.5. For computational analysis purposes, a linear programming (LP) equivalent of the proposed MDP model is formulated in Appendix 3.A. Tables A.1 and A.2 in Appendix 3.B provide a glossary of notations and acronyms utilized.

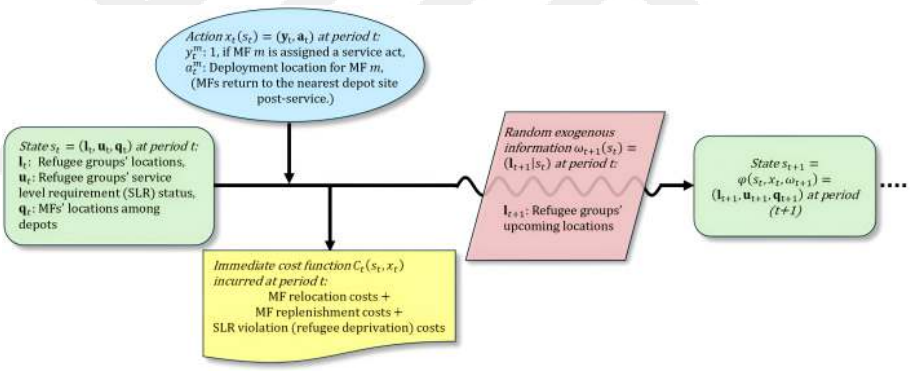

Figure 3.2: Sequence of events occurring within each period

3.3.1 State variables

At the beginning of each period $t \in \mathcal{T} = \{1, 2, \cdots\}$, the decision-maker observes three vectors: (i) the refugee groups' locations, $\mathbf{l}_t = (l_t^1, l_t^2, \cdots, l_t^R)$, where $l_t^r \in V^{\mathcal{R}}$ $\forall r \in \mathcal{R}$; (ii) the refugee groups' SLR status, $\mathbf{u}_t = (u_t^1, u_t^2, \cdots, u_t^R)$, where $u_t^r \in \{1, 2, \cdots, \tau\}$ $\forall r \in \mathcal{R}$, representing the number of remaining periods until their next relief requisition is due; and (iii) the MFs' locations, $\mathbf{q}_t = (q_t^1, q_t^2, \cdots, q_t^M)$, where $q_t^m \in \mathcal{H}$ $\forall m \in \mathcal{M}$. A refugee group's SLR status remains at τ once it reaches a terminal point. A trio of these vectors defines the state variables $s_t \in \mathcal{S}$, as expressed in Eq. (3.1). The cardinality of the state vector s_t equals $2R + M$.

$$
\begin{aligned}
s_t \in \mathcal{S} = \quad \big\{(\mathbf{l}_t, \mathbf{u}_t, \mathbf{q}_t) : \quad & l_t^r \in V^{\mathcal{R}}\ \forall r \in \mathcal{R},\ u_t^r \in \{1, \cdots, \tau\}\ \forall r \in \mathcal{R},\ q_t^m \in \mathcal{H}\ \forall m \in \mathcal{M}, \\
& u_t^r = \tau \text{ if } \exists r \in \mathcal{R} :\ l_t^r \in \mathcal{D}\big\}
\end{aligned}
\tag{3.1}
$$

3.3.2 Decision variables

Given state $s_t \in \mathcal{S}$, the decision-maker determines a vector of admissible service act allocations to MFs $m \in \mathcal{M}$, as defined in Eq. (3.2). The binary variable $y_t^m \in \{0, 1\}$ indicates whether MF m is assigned a service act. The variable $a_t^m \in \big\{\mathbf{l}_t \cap \mathcal{J}\big\} \cup \{\mathbf{q}_t\}$ denotes the deployment node for MF m in period t. If $y_t^m = 1$, then MF m must deploy to a transient hosting node for refugee groups still en route, distribute the relief aid, and return to the nearest depot $g(a_t^m) \in \mathcal{D}$. Otherwise, MF m remains at its depot.

Let $L_t = \{j \in \big\{\mathbf{l}_t \cap \mathcal{J}\big\} \mid \exists m \in \mathcal{M}, y_t^m = 1, a_t^m = j\}$ denote the set of nodes that will host service acts in period t. At every node in L_t, the capacity constraint in Eq. (3.2) guarantees adequate relief supply to recipient refugees while maintaining the indivisibility of service acts.

$$
\begin{aligned}
\mathcal{X}(s_t) \quad = \quad & \Bigg\{ \Big((y_t^1, a_t^1), (y_t^2, a_t^2), \cdots, (y_t^M, a_t^M) \Big) :\ y_t^m \in \{0,1\},\ \begin{cases} a_t^m = q_t^m & \text{if } y^m = 0 \\ a_t^m \in \big\{\mathbf{l}_t \cap \mathcal{J}\big\} & \text{if } y_t^m = 1 \end{cases}, \\
& \qquad \sum_{\substack{m \in \mathcal{M}: \\ y_t^m = 1, a_t^m = j}} b^m \geq \sum_{\substack{r \in \mathcal{R}: \\ l^r = j}} d^r \quad \forall j \in L_t \Bigg\} \quad \forall s_t \in \mathcal{S}
\end{aligned}
\tag{3.2}
$$

3.3.3 Exogenous information

After observing state $s_t \in \mathcal{S}$ and taking action $x_t \in \mathcal{X}(s_t)$, refugee groups relocate probabilistically within the network. Hence, the exogenous information in our MDP model is the set of possible refugee group relocations, denoted by $\mathcal{W}_{t+1}(s_t) = \{\mathbf{l}_{t+1} \mid s_t\}$, which should be considered when making a decision in period t, as is typical in MDP formulations. At the onset of period $t + 1$, a realization $\omega_{t+1} = (\mathbf{l}_{t+1} \mid s_t) \in$

$\mathcal{W}_{t+1}$ is revealed.

3.3.4 State transition

The state transition function $s_{t+1} = \varphi(s_t, x_t, \omega_{t+1})$ depicts how s_t evolves to s_{t+1} after an action x_t is taken and an uncertainty ω_{t+1} is revealed. In essence, the upcoming SLR status $\mathbf{u}_{t+1}$ and MF locations $\mathbf{q}_{t+1}$ are affected by the action, whereas refugee groups' movement behavior remains independent of MF service acts—since refugee groups determine their own paths and decision-makers have no control over their movements. Despite the stochastic nature of $\mathbf{l}_{t+1}$, the sets $\mathbf{u}_{t+1}$ and $\mathbf{q}_{t+1}$ evolve deterministically. Eq. (3.3) calculates the transition of SLR status $\mathbf{u}_{t+1}|s_t, x_t$. If group $r \in \mathcal{R}$ receives relief aid in period t, then u^r_{t+1} resets to the utmost SLR value τ; otherwise, it decreases by one unit until it reaches one, indicating the minimum SLR status. Fig. 3.3 provides an example of fluctuations in the SLR status of a refugee group in response to delivered service acts. In this figure, $\tau = 3$, and relief aid is delivered in periods 2, 4, and 8, while an SLR violation occurs in period 7 when the SLR status remains at one. Eq. (3.4) shows that MFs' initial placement in $t + 1$ is set to the nearest depot site $g(a^m_t)$ to their deployed location a^m_t.

$$\mathbf{u}_{t+1}|s_t, x_t = (u^1_{t+1}, u^2_{t+1}, \cdots, u^R_{t+1}) : \ u^r_{t+1} = \begin{cases} \tau & \text{if} \quad l^r_t \in L_t \\ \max\{u^r_t - 1, 1\} & \text{otherwise} \end{cases}, \quad \forall r \in \mathcal{R} \tag{3.3}$$

$$\mathbf{q}_{t+1}|x_t = \left(g\left(a^1_t\right), g\left(a^2_t\right), \cdots, g\left(a^M_t\right)\right) \tag{3.4}$$

Based on the discussion of Section 3.2.2, we characterize two inter-period refugee displacements, as illustrated in Fig. 3.4. Let $\mathcal{N}_i = \{j \in V^{\mathcal{R}} : (i, j) \in A^{\mathcal{R}}\}$ denote all adjacent nodes to node $i \in V^{\mathcal{R}}$. In the case of *moving*, a refugee group advances from $l^r_t \in V^{\mathcal{R}}$ to an adjacent node $l^r_{t+1} \in \mathcal{N}_{l^r_t}$. In contrast, in the case of *waiting*, a group remains at $l^r_{t+1} = l^r_t \in V^{\mathcal{R}}$ for an additional period. As shown in Fig. 3.4, for a group located at node 1, moving involves advancing to either node 2 or 3, while waiting implies staying at node 1. Assuming that each refugee group executes exactly one of these movement types every period, Eq. (3.5) represents the set of their upcoming placements in $t+1$.

$$\mathbf{l}_{t+1}|s_t, x_t = \left\{ \left(l^1_{t+1}, l^2_{t+1}, \cdots, l^r_{t+1}\right) \ : \ l^r_{t+1} \in \mathcal{N}_{l^r_t} \cup \{l^r_t\} \ \ \forall r \in \mathcal{R} \right\} \tag{3.5}$$

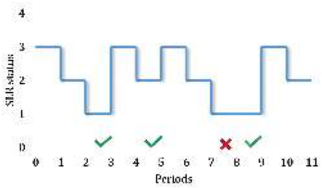

Figure 3.3: SLR status transitions for a refugee group. Relief aid is delivered in periods 2, 4, and 8 (✓) while an SLR violation has occurred in period 7 (×)

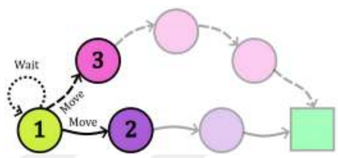

Figure 3.4: Representation of the inter-period moving and waiting behaviors

Acknowledging the challenge of measuring internal drivers of refugee migration, we model movement decisions based solely on measurable external environmental factors. These include the safety of adjacent nodes, the presence of barricades along roads, and proximity to adjacent nodes (Diedrichs et al., 2024). Following Searle and van Vuuren (2021)'s approach, Eq. (3.6) formulates move scores as a weighted sum model, augmented by a truncated normally distributed noise term bounded within the interval $[0, 1]$, with $\epsilon_{ij} \sim$ Trunc $\mathcal{N}(0.5, 1)$, to account for unforeseen internal factors and randomness in refugees' move-wait behaviors. In Eq. (3.6), the safety level of node j is denoted by $\Upsilon^{Safety}_j \in [0, 1]$, where higher values indicate safer conditions. The extent of governmental or conflict-related barricades along road ij is captured by $\Upsilon^{Openness}_{ij} \in [0, 1]$, where higher values indicate more accessible roads. Lastly, $\Upsilon^{Proximity}_{ij} \in [0, 1]$ quantifies the relative distance between nodes i and j, with higher values indicating closer proximity (Hinsch and Bijak, 2023). Proximity values are normalized such that 1 represents the shortest arc in the network, 0 the longest, and all others are determined proportionally.

$$\sigma_{ij} \ = \ w_1 \Upsilon^{Safety}_j + w_2 \Upsilon^{Openness}_{ij} + w_3 \Upsilon^{Proximity}_{ij} + w_4 \epsilon_{ij} \quad \forall i \in \mathcal{J}, j \in \mathcal{N}_i \tag{3.6}$$

Once the move scores are determined, Eq. (3.7) provides a valid probability matrix for move-wait behaviors using a softmax function. The first term in Eqs. (3.7a) and (3.7b) determines whether a refugee group chooses to move or wait. The second term in Eq. (3.7a) assigns non-negative weights to the selection of adjacent nodes. The term $\overline{\sigma_i} = \sum_{j\in\mathcal{N}_i} \sigma_{ij}/|\mathcal{N}_i|$ represents the average movement score at node i, where higher values indicate a greater likelihood of movement. The parameter $\zeta > 0$ controls the steepness of the move-wait probabilities. In this model, the weights satisfy $w_i \geq 0\ \forall i = 1, \ldots, 4$ and $\sum_{i=1}^{4} w_i = 1$. Thus, subtracting the expected move score $\mathbb{E}[\sigma_{ij}] = 0.5w_1 + 0.5w_2 + 0.5w_3 + 0.5w_4 = 0.5$ ensures the model remains unbiased. As long as each factor has a mean of 0.5 and the weights sum to 1, Eq. (3.7) is generalizable to any move score model. As an extreme case, when $w_4 = 1$, the arc scores are entirely random. Moreover, if $\zeta = 0$, the move-wait decision becomes independent of the scores and reduces to a random 50-50 choice.

$$p_{ij} = \frac{1}{1+e^{-\zeta(\overline{\sigma_i}-0.5)}} \times \frac{e^{\sigma_{ij}}}{\sum_{k\in\mathcal{N}_i} e^{\sigma_{ik}}} \quad \forall i \in \mathcal{J}, j \in \mathcal{N}_i \tag{3.7a}$$

$$p_{ii} = \frac{1}{1+e^{\zeta(\overline{\sigma_i}-0.5)}} \quad \forall i \in \mathcal{J} \tag{3.7b}$$

$$p_{ii} = 1 \quad \forall i \in \mathcal{H} \tag{3.7c}$$

$$p_{ij} = 0 \quad \text{Otherwise} \tag{3.7d}$$

Having stipulated the evolved sets of information described above, as determined by the state transition function $\varphi(s_t, x_t, \omega_{t+1})$ including Eq. (3.3), we derive the set of observable latent states $S_{t+1}|s_t, x_t$ and their associated probabilities using Eqs. (3.8) and (3.9), respectively.

$$s_{t+1} \in S_{t+1}|s_t, x_t = \left\{(\mathbf{l}_{t+1}|s_t, x_t\ ,\ \mathbf{u}_{t+1}|s_t, x_t\ ,\ \mathbf{q}_{t+1}|s_t, x_t)\right\} \tag{3.8}$$

$$P(s_{t+1}|s_t, x_t) = \prod_{r\in\mathcal{R}} p_{l_t^r, l_{t+1}^r} \tag{3.9}$$

3.3.5 Objective function

Task allocation to MFs yields an immediate cost $\mathcal{C}(s_t, x_t)$, as defined in Eq. (3.10), comprising three terms: MF relocation costs, MF resupply costs, and refugees' deprivation costs under SLR violations. At each period, an action $(0, a_t^m)$ indicates the idleness of MF m and incurs no relocation cost. However, an action $(1, a_t^m)$ incurs a relocation cost for MF m that includes traveling from its current depot to the service act location, followed by a return trip to the nearest depot. Regarding the second term, Bayraktar et al. (2022) overlooked resupply costs, while Pashapour et al. (2024) modeled them linearly with the number of service acts. Instead, we model resupply at a per-kit cost o to restock MFs for upcoming service acts. Lastly, violating the SLR by not visiting a refugee group with $u_t^r = 1$ incurs a cost of γd^r, where γ denotes the per-refugee, per-period deprivation cost.

$$\mathcal{C}(s_t, x_t) = \sum_{\substack{m \in \mathcal{M}: \\ y_t^m = 1}} \left(c^m_{q_t^m, a_t^m} + c^m_{a_t^m, g(a_t^m)} \right) + \sum_{\substack{r \in \mathcal{R}: \\ l_t^r \in L_t}} o.d^r + \sum_{\substack{r \in \mathcal{R}: \\ u_t^r = 1, l_t^r \notin L_t}} \gamma.d^r \tag{3.10}$$

In light of the MDP elements described in Sections 3.3.1–3.3.5, our objective is to determine an optimal service act allocation policy through the Bellman Eq. (3.11), where $\mathcal{V}(.)$ is a non-negative real-valued value function. This equation minimizes the expected total discounted cost while balancing immediate and future costs. Here, $\beta \in [0, 1)$ is the discount factor, and the expectation $\mathbb{E}$ is induced by the transition probability distribution in Eq. (3.9).

$$\mathcal{V}(s_t) = \min_{x_t \in \mathcal{X}(s_t)} \Big(\mathcal{C}(s_t, x_t) + \beta \mathbb{E}\big[\mathcal{V}(s_{t+1}) | s_t, x_t\big] \Big) \tag{3.11}$$

The dynamic program in Eq. (3.11) can be solved using classical DP algorithms, such as Value Iteration and Policy Iteration, or a linear programming equivalent (see Appendix 3.A). Nevertheless, obtaining an optimal solution via classical DP methods is intractable even for moderate problem sizes. The state space cardinality is characterized by $|\mathcal{S}| = \mathcal{O}\big(|V^{\mathcal{R}}|^R \times \tau^R \times |\mathcal{H}|^M\big)$. The action space follows $|\mathcal{X}| = \mathcal{O}\big((R+1)^M\big)$, since each MF either remains idle or relocates to a hosting node of refugee groups. Similarly, considering refugees' movement types, the exogenous information space grows as $|\mathcal{W}| = \mathcal{O}(2^R)$. Consequently, the sets $\mathcal{S}$, $\mathcal{X}$, and $\mathcal{W}$ exhibit exponential growth with respect to problem inputs R and M. In Section 3.4, we propose frameworks to approximately solve Eq. (3.11).

3.4 General framework

In this section, we present the concepts underlying our solution methods. Sections 3.4.1 and 3.4.2 establish our ADP and VTP algorithms.

3.4.1 Approximate dynamic programming

We design an ADP algorithm to obtain efficient service act policies based on value function approximations. We begin by recasting the optimality equation (3.11) into an altered version in Eq. (3.13), which adopts a *post-decision state* (or *post-state*) variable convention. A post-state $s_t^x = \varphi^x(s_t, x_t)$ captures the state of the network after observing s_t and taking action x_t, but before the uncertainty ω_{t+1} is revealed. In our context, $s_t^x = (\mathbf{l}_t, \mathbf{u}_{t+1}, \mathbf{q}_{t+1})$ refers to the situation where MFs have completed their service acts, but refugee resettlements are pending. Eq. (3.12) implies that $\mathcal{V}(s_t^x)$ represents the expected value function over all possible downstream states in Eq. (3.11). Post-state variables offer computational advantages by eliminating the embedded expectation in the Bellman equation and mitigating the curse of dimensionality associated with the outcome space (Ruszczyński, 2010).

$$\mathcal{V}(s_t^x) \triangleq \mathbb{E}\Big[\mathcal{V}(s_{t+1})|s_t^x\Big] \tag{3.12}$$

$$\mathcal{V}(s_t) = \min_{x_t \in \mathcal{X}(s_t)} \Big(\mathcal{C}(s_t, x_t) + \beta \mathcal{V}(s_t^x)\Big) \tag{3.13}$$

To efficiently compute $\mathcal{V}(s_t^x)$, we define a set of basis functions to approximate the value functions of post-states as $\overline{\mathcal{V}}(s_t^x)$. Let $\phi(s_t^x) \coloneqq \big(\phi_f(s_t^x)\big)_{f\in\mathcal{F}}$ denote a vector of basis functions, where each $f \in \mathcal{F}$ corresponds to a post-state-dependent feature. Well-designed features can capture nonlinearities in the value function, and their affine combination can serve as a precise approximation architecture (Bertsekas, 2011). Eq. (3.14) defines this affine approximation:

$$\overline{\mathcal{V}}(s_t^x|\theta) \triangleq \theta^\top \phi(s_t^x) = \sum_{f \in \mathcal{F}} \theta_f \phi_f(s_t^x) \tag{3.14}$$

where θ is a vector of weights corresponding to the basis functions. Given a properly calibrated θ and an appropriate feature set, Eq. (3.13) becomes Eq. (3.15), and the best action for any state is approximated via Eq. (3.16). This equation is typically solved either exactly or using an ϵ-greedy policy in the literature (Jenkins et al., 2021; McKenna et al., 2020; Liles IV et al., 2023). However, solving it optimally for large-scale migration instances is impractical due to the extensive action space. Therefore, we employ a Genetic Algorithm (GA) to solve Eq. (3.16). GA hyperparameters are tested in subsection 3.5.3.9.

$$\mathcal{V}(s_t|\theta) \approx \min_{x_t \in \mathcal{X}(s_t)} \Big(\mathcal{C}(s_t, x_t) + \beta\theta^\top \phi(s_t^x)\Big) \tag{3.15}$$

$$x_t^*(s_t|\theta) \approx \arg\min_{x_t \in \mathcal{X}(s_t)} \Big(\mathcal{C}(s_t, x_t) + \beta\theta^\top \phi(s_t^x)\Big) \tag{3.16}$$

Hereafter, we introduce our basis functions and endeavor to calibrate the policy vector θ. The first basis function (3.17) estimates the amount of relief aid required by a refugee group before reaching a terminal point. Specifically, $\chi_i = 1+\sum_{j\in\mathcal{N}_i} \chi_j/|\mathcal{N}_i|$ denotes the expected number of periods needed to reach an accessible terminal node from node i, assuming refugees always move. Here, $\chi_j = 0$ for terminal nodes $j \in \mathcal{H}$. To make $\chi_{l_t^r}$ unbiased, we scale it by the average move score across the network, $\overline{\overline{\sigma}} = \sum_{(i,j)\in A^{\mathcal{R}}} \sigma_{ij}/|A^{\mathcal{R}}|$, and subtract the group's SLR status to account for their initial supplies. This expression estimates the number of periods an individual remains in need. The entire term is multiplied by group size and divided by τ. The maximization ensures non-negativity. Overall, Eq. (3.17) reflects that larger groups, farther from terminal points, with lower initial supplies and situated on networks with lower mobility, impose proportionally higher costs (Bayraktar et al., 2022).

The second basis function (3.18) estimates the potential shortfall in MF capacity for refugee groups whose service urgency is highest (i.e., those with SLR status = 1). Specifically, $L_t^1 = \{j \in \{\mathbf{l}_t \cap \mathcal{J}\} \mid \exists r \in \mathcal{R}, u_{t+1}^r = 1, l_t^r = j\}$ identifies the nodes hosting groups with SLR status equal to one. The average MF capacity is $\overline{b} = \sum_{m \in \mathcal{M}} b^m / M$. Dividing the total demand at each node of L_t^1 by $\overline{b}$ and rounding up yields the minimum number of MFs required. Subtracting the available fleet size M and taking the maximum with zero gives an estimate of the MF shortfall.

Improving approximation quality may require designing more basis functions. As solving Eq. (3.16) is repeated throughout the ADP iterations, choosing compact yet expressive basis functions is essential for computational tractability. Our preliminary tests show that these two first-order basis functions (together with size $R+1$), are sufficient to approximate the value function with high accuracy across instances. We therefore chose not to include more complex combinations, which would introduce unnecessary computational burden without significant performance gains. Our experiments in Section 3.5 confirm the accuracy and sufficiency of the two proposed basis functions.

$$\phi_1^r(s_t^x) = \max\left\{\frac{d^r}{\tau}\left(\frac{\chi_{l_t^r}}{\overline{\overline{\sigma}}} - u_{t+1}^r\right), 0\right\} \quad \forall r \in \mathcal{R} \tag{3.17}$$

$$\phi_2(s_t^x) = \max\left\{-M + \sum_{j \in L_t^1} \left\lceil \sum_{r \in \mathcal{R}: l_t^r = j} \frac{d^r}{\overline{b}} \right\rceil, 0\right\} \tag{3.18}$$

Our proposed ADP utilizes an API framework inspired by the works of McKenna et al. (2020); Jenkins et al. (2020b); Liles IV et al. (2023). API begins with a base policy θ and produces a sequence of improved policies through two nested loops: an outer loop for policy improvement (PI) and an inner loop for policy evaluation (PE). In this study, we embody a novel policy replication (PR) loop within PE. Accordingly, we reorganize the loops as: outer (PI), middle (PE), and inner (PR).

We now describe these nested loops and motivate the inclusion of PR.

Given a θ vector from the outer loop, each middle loop $z = 1, \dots, Z$ randomly samples a post-state $s^x_{t-1,z}$ and records its basis function $\phi(s^x_{t-1,z})$. Refugee resettlements are then simulated one step forward using the probability matrix in Eq. (3.7), resulting in a new state $s_{t,z}$. The best action for this state is determined via Eq. (3.16), and the immediate cost $\mathcal{C}(s_{t,z}, x_{t,z} \mid \theta)$ is recorded. Finally, $s_{t,z}$ transitions to the post-state $s^x_{t,z}$, and its basis function $\phi(s^x_{t,z})$ is also recorded.

Traditional APIs apply policy evaluation to each sampled post-state $s^x_{t-1,z}$ only once. However, due to the vast outcome space, relying on a single realization may underexploit post-state information and fail to adequately capture the expected value functions of downstream states (see Eq. (3.12)). To address this and balance the exploration–exploitation trade-off, we introduce a novel inner loop $i = 1, \dots, I$ for each sampled post-state $z \in Z$, which repeatedly simulates downstream states and collects statistics. While refugee locations and SLR statuses are held fixed within the inner loop, MF locations can be resampled in each z-iteration. This enhances the exploration of post-states and eliminates the need to include MF locations in the basis functions. Importantly, limiting the number of inner iterations I helps mitigate overfitting. We analyze the impact of different I values on PR performance in Section 3.5.3.10.

Once the middle loop completes, statistics from $Z \cdot I$ observations are recorded in the basis function evaluation matrices Ω_{t-1} and Ω_t of dimension $(Z \cdot I) \times (R + 1)$, and a vector of immediate costs $\hat{C}_t$ of size $(Z \cdot I) \times 1$, as shown in Eq. (3.19). To calibrate the θ vector, the outer loop begins by computing $\hat{\theta}$, an estimate of θ, using a Least-Squares Temporal Difference (LSTD) learning process. LSTD is an efficient algorithm for estimating the adjustable θ vector when approximating value functions using a linear basis function architecture (Bradtke and Barto, 1996). It performs a least-squares regression to minimize the squared temporal difference errors:

$$\Omega_{t-1} \triangleq \begin{bmatrix} \phi(s^x_{t-1,1,1}) \\ \phi(s^x_{t-1,1,2}) \\ \vdots \\ \phi(s^x_{t-1,Z.I}) \end{bmatrix}_{Z.I\times(R+1)}, \quad \Omega_t \triangleq \begin{bmatrix} \phi(s^x_{t,1,1}) \\ \phi(s^x_{t,1,2}) \\ \vdots \\ \phi(s^x_{t,Z.I}) \end{bmatrix}_{Z.I\times(R+1)}, \quad \hat{C}_t \triangleq \begin{bmatrix} \mathcal{C}(s_{t,1,1}, x_{t,1,1}) \\ \mathcal{C}(s_{t,1,2}, x_{t,1,2}) \\ \vdots \\ \mathcal{C}(s_{t,Z.I}, x_{t,Z.I}) \end{bmatrix}_{Z.I\times 1} \tag{3.19}$$

McKenna et al. (2020) examine two formulas for estimating $\hat{\theta}$: the conventional normal equation from linear regression, and the instrumental variables method (Eqs. (3.20a) and (3.20b), respectively). The latter method uses instruments that are correlated with the regressors but uncorrelated with the regression errors (Söderström and Stoica, 2002). Accordingly, we adopt the instrumental variables method in our experiments. To prevent matrix singularity and improve generalization, we incorporate a regularization term $\mu\mathbf{I}$, where $\mu \geq 0$ and $\mathbf{I}$ is a $(R+1)\times(R+1)$ identity matrix scaled by μ.

$$\hat{\theta} = \left[(\Omega_{t-1} - \beta\Omega_t)^\top (\Omega_{t-1} - \beta\Omega_t) + \mu\mathbf{I}\right]^{-1} (\Omega_{t-1} - \beta\Omega_t)^\top \hat{C}_t \quad \text{Normal equation method} \tag{3.20a}$$

$$\hat{\theta} = \left[(\Omega_{t-1})^\top (\Omega_{t-1} - \beta\Omega_t) + \mu\mathbf{I}\right]^{-1} (\Omega_{t-1})^\top \hat{C}_t \quad \text{Instrumental variables method} \tag{3.20b}$$

Finally, once $\hat{\theta}$ is computed, the outer loop updates the policy vector using the harmonic step-size rule: $\theta \leftarrow (1-\alpha_n)\theta + \alpha_n\hat{\theta}$. On the right-hand side, θ denotes the cumulative estimate from prior outer loop iterations, while $\hat{\theta}$ is the most recent estimate. The coefficient $\alpha_n = 1/n^\delta$ is a polynomial smoothing step-size rule with $\delta \in (0.5, 1]$. As n increases, more weight is given to accumulated past estimates. We refer to the proposed ADP as *3API*, as outlined in Algorithm 4. Upon termination, it yields a calibrated θ vector that generates a high-quality service act policy via Eq. (3.16). The tunable algorithmic parameters of 3API include N, Z, and I (the number of PI, PE, and PR iterations, respectively), μ (regularization parameter), and δ (step-size exponent).

Algorithm 4 3API Algorithm

Initialize the θ-vector, i.e., $\theta \leftarrow \overrightarrow{\mathbf{1}}$
for $n = 1$ to N **do**: // Policy improvement loop
  for $z = 1$ to Z **do**: // Policy evaluation loop
    Pick a random post-state $s^x_{t-1,z} = \varphi^x(s_{t-1}, x_{t-1})$
    Record the basis function evaluation $\phi(s^x_{t-1,z})$
    for $i = 1$ to I **do**: // Policy replication loop
      Simulate a transition from $s^x_{t-1,z}$ to the next state $s_{t,z,i}$
      Obtain the best decision x_t
      Record the cost contribution $\mathcal{C}(s_{t,z,i}, x_t)$
      Transit to the post-state $s^x_{t,z,i} | s_{t,z,i}, x_t$
      Record the basis function evaluation $\phi(s^x_{t,z,i})$
      Resample MF locations within $s^x_{t-1,z}$
    end for
  end for
  Apply LSTD: Compute $\hat{\theta}$
  Update θ
end for
return θ and $\overline{\mathcal{V}}(.|\theta)$

Algorithm 5 Genetic Algorithm (GA) embedded in the 3API

Input: State s_t; N_{GA}: Number of iterations; *pop*: Initial population; n_c: Number of offspring; p'_m: Mutation probability
Each chromosome $x_t \in \mathcal{X}(s_t)$ represents an action
Fitness function: $\mathcal{C}(s_t, x_t) + \beta\theta^\top \phi(s^x_t)$ plus a penalty for infeasibility
Initialize *pop* with random chromosomes
Evaluate fitness for each chromosome
for $i = 1$ to N_{GA} **do**
  Select parents from *pop* based on fitness (Roulette Wheel Selection)
  Generate n_c offspring via single-point crossover between parent pairs
  Apply mutation to each offspring (random MF decision modification) with probability p'_m
  Evaluate offspring fitness
  Combine parents and offspring; select the best *pop* chromosomes to form the new population
end for
Return: Fitness of the best chromosome; Best chromosome as the decision output

3.4.2 Variable threshold policy

While ADP offers a static, offline solution by determining the best action for each state in a single run, real-world deployments demand a more responsive approach. Specifically, there is a critical need for an online policy that can dynamically adapt to evolving problem inputs. A purely myopic rule, focusing solely on minimizing immediate service act allocation costs without accounting for future consequences, performs poorly under our SLR criterion. To address this, we propose a VTP that incorporates a τ-stage-look-ahead mechanism, based on a structural result presented in Proposition 3.4.1. Leveraging this proposition, the VTP is designed as a state-dependent policy that balances short-term costs with long-term service equity. The overall structure of the VTP is illustrated in Figure 3.5.

Proposition 3.4.1. ***A structural property:*** *Let $\eta \in \{1, \ldots, \tau\}$ be a variable threshold parameter used to identify a candidate set of refugee groups $\hat{\mathcal{R}}$ whose SLR status is less than or equal to η. At each period t, there exists an optimal threshold η_t^*—the smallest value below which an SLR violation is inevitable in future periods.*

Proof. Proof By definition, η implies that, starting from period t, at least η consecutive periods, $\{t, t+1, \ldots, t+\eta-1\}$, are required to visit all candidate refugee groups in $\hat{\mathcal{R}}$ at least once. Therefore, any group with $u_t^r > \eta$ can be safely excluded from $\hat{\mathcal{R}}$, as their service act can be postponed to period $t + \eta$ or later without violating their SLR status. This exclusion reduces costs, since $|\hat{\mathcal{R}}|$ is non-decreasing in η, and relocation and resupply costs increase with $|\hat{\mathcal{R}}|$. To ensure service act feasibility—i.e., to prevent any SLR violations over the next τ periods—the initial candidate set $\hat{\mathcal{R}}$ includes all en route refugee groups. Notably, η and $|\hat{\mathcal{R}}|$ exhibit diminishing returns over the iterations of the VTP loop due to the iterative refugee group exclusions. Upon termination, the optimal η_t^* is the smallest feasible value, below which an SLR violation is inevitable. Reducing η_t^* by even one unit would delay the service act for refugee groups with $u_t^r = \eta$, who must be served by $t+\eta-1$, causing SLR violations for some of them. ■ □

Using the property in Proposition 3.4.1, the VTP operates as follows. Initially, the set $\hat{\mathcal{R}}$ includes all en route refugee groups. The threshold η_t represents the minimum time window required to ensure each group in $\hat{\mathcal{R}}$ is visited at least once. In each iteration, η_t is computed by solving the binary optimization problem 'Model 1', which structurally resembles the classic Bin Packing Problem, where the number of bins equals η_t. Notably, any group with an SLR status greater than η_t (denoted $\mathcal{R}'$)

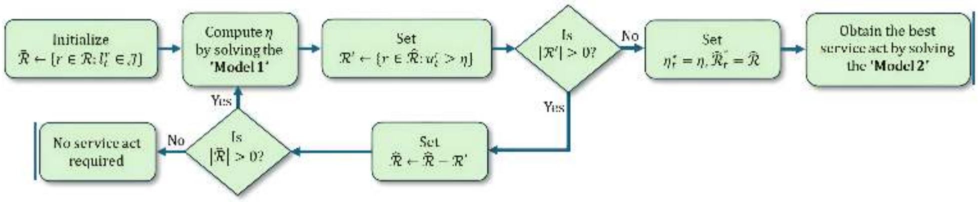

Figure 3.5: VTP flowchart: Model 1 computes the SLR threshold to determine candidate refugee groups for service. If one or more candidates are identified, Model 2 selects the optimal service action; otherwise, no service is performed in that period.

can be safely excluded from $\hat{\mathcal{R}}$, as their SLR levels will remain adequate even if they are not visited within this time window. If such exclusions occur (i.e., $|\mathcal{R}'| > 0$), the set of candidate refugee groups $\hat{\mathcal{R}}$ is updated and η_t is recalculated by resolving 'Model 1'. If the updated set becomes empty, i.e., $\hat{\mathcal{R}} = \emptyset$, no service act is required in the current period, and the VTP terminates with zero cost. If no exclusions occur (i.e., $|\mathcal{R}'| = 0$), the iteration terminates, and the current values η_t and $\hat{\mathcal{R}}$ are finalized as η_t^* and $\hat{\mathcal{R}}_t^*$, respectively. These results are passed to 'Model 2', a binary optimization problem based on the classic Mobile Facility Location Problem with priority considerations, which determines cost-efficient service act locations and MF locations. Importantly, the finalized set $\hat{\mathcal{R}}_t^*$ always includes all urgent refugee groups (with $u_t^r = 1$) present in $\hat{\mathcal{R}}$. The number of VTP iterations is at most τ.

VTP: 'Model 1'

Sets:

$\hat{\mathcal{R}}$ Set of candidate refugee groups $\hat{\mathcal{R}} \in \mathcal{R}$

$\mathcal{M}$ Set of MFs

Parameters:

d^r Population size of refugee group $r \in \hat{\mathcal{R}}$

b^m Service act capacity of MF $m \in \mathcal{M}$

t Current period

Decision Variables:

E_j	1, if period $j \in \{t, \cdots, t+\tau-1\}$ is used for service acts; 0, otherwise
F_{mrj}	1, if MF $m \in \mathcal{M}$ visits refugee group $r \in \hat{\mathcal{R}}$ in period $j \in \{t, \cdots, t+\tau-1\}$; 0, otherwise

$$\min \quad \eta = \sum_{j=t}^{t+\tau-1} E_j \tag{3.21a}$$

$$\text{s.t.} \quad \sum_{r \in \hat{\mathcal{R}}} F_{mrj} \leq E_j \qquad \forall m \in \mathcal{M}, j \in \{t, \cdots, t+\tau-1\} \tag{3.21b}$$

$$\sum_{m \in \mathcal{M}} \sum_{j=t}^{t+\tau-1} b^m F_{mrj} \geq d^r \qquad \forall r \in \hat{\mathcal{R}} \tag{3.21c}$$

$$E_j \geq E_{j+1} \qquad \forall j \in \{t, \cdots, t+\tau-2\} \tag{3.21d}$$

$$F_{mrj}, E_j \in \{0,1\} \qquad \forall m \in \mathcal{M}, r \in \hat{\mathcal{R}}, j \in \{t, \cdots, t+\tau-1\} \tag{3.21e}$$

The objective function (3.21a) minimizes η as the minimum time window needed to visit all refugee groups $\hat{\mathcal{R}}$ at least once. Constraints (3.21b) limit the service act delivery by each MF in each period to at most one candidate refugee group. Constraints (3.21c) ensure demand satisfaction for all $\hat{\mathcal{R}}$ within the η onward periods. Constraints (3.21d) serve as symmetry-breaking constraints among the τ onward periods by prioritizing the earlier ones. Finally, constraints (3.21e) declare domains of the decision variables.

VTP: 'Model 2' ($\eta_t^*, \hat{\mathcal{R}}_t^*$)

Sets:

$\hat{\mathcal{R}}_t^*$	Set of candidate refugee groups $\hat{\mathcal{R}}_t^* \subseteq \mathcal{R}$
$\hat{\mathrm{I}}$	Set of locations corresponding to the candidate refugee groups in $\hat{\mathcal{R}}_t^*$
$\mathcal{M}$	Set of available MFs
V^M	Set of MF placement locations
Ξ_j	Set of locations $i \in \hat{\mathrm{I}}$ with minimum SLR status $\underline{u}_i = j$, $\forall j \in \{1, ..., \eta_t^*\}$

Parameters:

l^r	Location of candidate refugee group $r \in \hat{\mathcal{R}}_t^*$
q^m	Location of MF $m \in \mathcal{M}$
$\underline{u}_i$	Minimum u_t^r level among refugee group(s) $r \in \hat{\mathcal{R}}_t^*$ located at $i \in \hat{\mathbf{I}}$
d^r	Population size of refugee group $r \in \hat{\mathcal{R}}$
b^m	Service act capacity of MF $m \in \mathcal{M}$
o	Per-kit resupply cost of MFs
c_{ij}^m	Relocation cost of MF $m \in \mathcal{M}$ from node $i \in V^M$ to $j \in V^M$
g_i	Nearest depot site to location $i \in V^{\mathcal{M}}$
η_t^*	Optimal threshold parameter

Decision Variables:

G_{mi}	1, if MF $m \in \mathcal{M}$ provides a service act at location $i \in \hat{\mathbf{I}}$; 0, otherwise
Y_i	1, if location $i \in \hat{\mathbf{I}}$ hosts service act(s); 0, otherwise

$$\min \quad \sum_{m\in\mathcal{M}} \sum_{i\in\hat{\mathbf{I}}} (c_{l^m,i}^m + c_{i,g_i}^m) G_{mi} + \sum_{i\in\hat{\mathbf{I}}} \sum_{r\in\hat{\mathcal{R}}:l^r=i} od^r Y_i - \sum_{i\in\hat{\mathbf{I}}} \sum_{r\in\hat{\mathcal{R}}:l^r=i} \gamma d^r Y_i \tag{3.22a}$$

$$\text{s.t.} \quad \sum_{i\in\hat{\mathbf{I}}} G_{mi} \leq 1 \qquad \forall m \in \mathcal{M} \tag{3.22b}$$

$$\sum_{m\in\mathcal{M}} b^m G_{mi} \geq \sum_{r\in\hat{\mathcal{R}}:l^r=i} d^r Y_i \qquad \forall i \in \hat{\mathbf{I}} \tag{3.22c}$$

$$Y_i \geq Y_{i'} \qquad \forall i \in \Xi_j, i' \in \Xi_{j'}, j \in \{1, \cdots, \eta_t^* - 1\}, j' \in \{j+1, \cdots, \eta_t^*\} \tag{3.22d}$$

$$G_{mi}, Y_i \in \{0,1\} \qquad \forall m \in \mathcal{M}, i \in \hat{\mathbf{I}} \tag{3.22e}$$

The objective function (3.22a) minimizes the relocation and resupply costs of the MFs. Since the VTP framework prohibits any deprivation, the final term in the objective function serves as an incentive to trigger service acts by the MFs—without it, no services would be initiated. This structure enables the efficient allocation of available MF capacity among the visited candidate refugee groups. Constraints

(3.22b) restrict each MF to performing a service act at no more than one node per period. Constraints (3.22c) ensure that the total demand at each node is met by the available MF capacity. Constraints (3.22d) prioritize nodes i with lower $\underline{u}_i$ values to favor service to refugee groups with lower SLR status. Finally, constraints (3.22e) define the decision variable domains. It is worth noting that the VTP costs ultimately correspond to the time-discounted sum of the first two terms in the objective function (3.22a).

Algorithm 6 VTP Structure

Initialize $\hat{\mathcal{R}} \leftarrow \{r \in \mathcal{R} : l_t^r \in \mathcal{J}\}$
while True **do**
    Compute η by solving **Model 1**
    Set $\mathcal{R}' \leftarrow \{r \in \hat{\mathcal{R}} : u_t^r > \eta\}$ // Excluded refugee groups
    if $|\mathcal{R}'| > 0$ **then**
        Update $\hat{\mathcal{R}} \leftarrow \hat{\mathcal{R}} - \mathcal{R}'$
        if $|\hat{\mathcal{R}}| = 0$ **then** // No service act required
            Return 0-cost solution
        end if
    else
        Set $\eta_t^* \leftarrow \eta$, $\hat{\mathcal{R}}_t^* \leftarrow \hat{\mathcal{R}}$
        Break
    end if
end while
Return: Obtain the best service act by solving **Model 2** with η_t^* and $\hat{\mathcal{R}}_t^*$

3.5 Computational experiments

In this section, we design migration instances to demonstrate the applicability of our proposed MDP model and solution approaches. Section 3.5.1 presents an illustrative example and provides its optimal and approximate results for comparison. In Section 3.5.2, we conduct computational experiments on 25 instances inspired by the Syrian migration crisis. Extensive sensitivity analyses are performed in Section 3.5.3 to examine the impact of key parameters and assumptions on the service act policies and to discuss the resulting managerial insights. All solution methods are implemented in Python, with mathematical models formulated in Pyomo and solved using Gurobi 12.0.1. Experiments are conducted on a 64-bit Intel(R) Xeon(R) system with a 3 GHz CPU and 128 GB RAM. Table A.6 in Appendix 3.C summarizes the baseline experimental settings used throughout Section 3.5.

3.5.1 An illustrative example

Consider $\mathcal{G}^{\mathcal{R}} = (V^{\mathcal{R}}, A^{\mathcal{R}})$ with $V^{\mathcal{R}} = \{1, 2, \ldots, 19\}$ and $A^{\mathcal{R}}$ comprising all directed arcs, as shown in Fig. 3.6. Additionally, let $\mathcal{G}^{\mathcal{M}}$ be a complete directed graph with node set $V^{\mathcal{M}} = \{1, \ldots, 18\}$. Suppose two refugee groups, $\mathcal{R} = \{1, 2\}$, with $d^1 = 150$ and $d^2 = 250$ refugees, are relocating through transient nodes $\mathcal{J} = \{1, \ldots, 18\}$ toward the terminal point $\mathcal{H} = \{19\}$. A single MF, $\mathcal{M} = \{1\}$, with the capacity to serve $b^1 = 400$ refugees per period, can be initially located at one of the depot sites at nodes $\mathcal{H} = \{5, 16\}$. The SLR parameter is set to $\tau = 3$. The MF resupply cost is $o = 1$, and the unit deprivation cost is $\gamma = 5$. All remaining parameter settings are provided in Appendix 3.C.

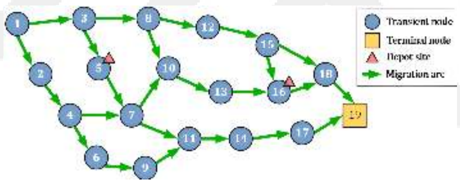

Figure 3.6: Network configuration of the illustrative example

To assess the impact of state characteristics on outputs, we analyze six representative states listed in Table 3.1. Given the manageable state space size ($|\mathcal{S}| =$ 6,050), we use both LP and VI approaches to validate the optimal value functions. We then compare our proposed 3API with the classic API based on the converged approximate value functions. For VTP, we report the average (Avg.), standard deviation (Std.), and coefficient of variation ($CV\% = 100 \times$ Std./Avg.) over $N' = 100$ migration simulations per state. Since ADP and VTP approximations deviate from the optimal value functions, we calculate percentage deviations as %dev. $= 100 \times \left|\left(\overline{\mathcal{V}}(s) - \mathcal{V}^*(s)\right)\right| / \mathcal{V}^*(s)$, where lower values are preferable. Table 3.1 shows that as refugee groups move closer to the terminal point, value functions decline, while worsening SLR statuses increase them. In particular, the last state's unavoidable SLR violation raises its value function due to deprivation costs. Among

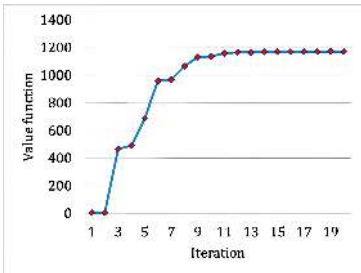

Figure 3.7: Value function convergences for the state with ID=3 analyzed in Table 3.1 using VI

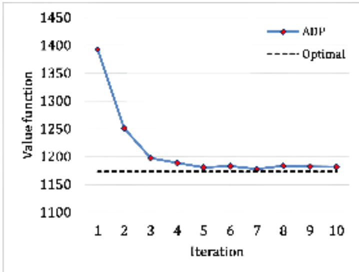

Figure 3.8: Value function convergence for the state with ID=3 analyzed in Table 3.1 using ADP

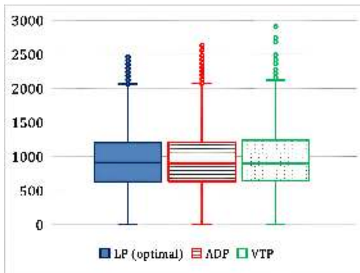

Figure 3.9: Box plot comparison of the LP (optimal), ADP, and VTP solutions applied to all states

the six states, 3API exhibits better convergence with lower %dev.. Extending the analysis to all states, API and 3API achieved average deviations of 5.43% and 5.18%, respectively, under identical computational effort ($Z.I = 5{,}000$).

Table 3.1: Optimal and approximate value functions for six different states of the illustrative example

		$\mathcal{V}^*(s_1)$	$\overline{\mathcal{V}}(s_1)$							
	State (s_1)		ADP				VTP			
ID	$\left((l_1^1, l_1^2), (u_1^1, u_1^2), (q_1^1)\right)$	DP	3API†	%dev.	API††	%dev.	Avg.	Std.	%CV	%dev.
1	((1,5),(3,3),(5))	1322	1307	1.13	1301	1.59	1339	232	17.33	1.29
2	((2,3),(3,3),(16))	1333	1320	0.98	1318	1.13	1346	236	17.53	0.98
3	((3,4),(3,3),(5))	1172	1184	1.02	1191	1.62	1176	219	18.62	0.34
4	((3,4),(1,3),(16))	1316	1342	1.98	1349	2.51	1364	225	16.50	3.65
5	((4,8),(3,2),(5))	1090	1101	1.01	1108	1.65	1094	167	15.27	0.37
6	((4,8),(1,1),(16))	1985	2033	2.42	2040	2.77	2016	212	10.52	1.56
	Computation time (seconds)	LP: 5 VI: 14	7		7		5 †††			

†: $Z = 2500$ & $I = 2$ ††: $Z = 5,000$ & $I = 1$ †††: Per each state & simulation

Regarding DP methods, the LP model achieved optimal value functions in 5 seconds, while the VI method converged to the optimal value functions with an absolute precision of $\Delta = 0.01$ in 14 seconds. Both ADP methods reached convergence in 7 seconds, and each VTP simulation per state took approximately 5 seconds. Figure 3.7 illustrates the VI convergence for a representative state (ID = 3), while Figure 3.8 depicts the ADP convergence toward its optimal value function. Additionally, Figure 3.9 presents boxplots of value functions across all states and demonstrates the accuracy of the proposed methods relative to the optimal value functions.

3.5.2 Test case description

The Syrian Civil War (2011–2019) triggered a severe humanitarian crisis, displacing millions and reshaping geopolitical dynamics across the Middle East. Given its shared border with Syria, Türkiye became a primary destination for displaced populations. Motivated by this crisis, we designed a migration network encompassing key affected regions in Syria and Türkiye, based on official reports (Migration Policy Centre (MPC), 2013; ORSAM, 2014; AIDA: Asylum Information Database, 2022). The network comprises 80 major cities and villages hosting refugees, with arcs representing real-world road connections. Appendix 3.C provides full details on this test case, where we generated 25 instances with varying input sizes. Instances include identifiers (IDs) and titles, along with the number of refugee groups (R) and MFs (M). The initial placements of refugees and MFs vary to capture a broad range of scenarios. MF capacities are selected from $\{400, 500\}$, as outlined in Turkish Red Crescent (2019). Refugee group sizes range from $\{100, 200, \ldots, 1000\}$ to reflect diverse demand levels. The SLR parameter is set to $\tau = 3$ periods, with initial refugee SLR statuses set to $u_1^r = \tau$.

We classify node safety and road openness factors into three levels: 0.5 (risky), 0.7 (less risky), and 0.9 (almost safe), based on the aforementioned reports and media sources such as The Guardian (2025). The proximity factor is normalized on a scale from 0 (longest road) to 1 (shortest road), with all intermediate values linearly interpolated. Real-world road distances are obtained from the *OpenRouteService* tool. By incorporating fuel consumption rates and fuel prices, following Pashapour et al. (2024), the relocation cost (in \$ monetary units) is set to 15% of the road distance. According to World Relief (2024), a relief kit costs approximately \$25, which we adopt as the unit resupply cost. While various values have been considered for the deprivation coefficient (Foster, 2007), we set the per-individual, per-period deprivation cost to \$50—roughly twice the unit relief kit cost.

The hyperparameters for ADP and GA are selected based on prior studies (McKenna et al., 2020; Jenkins et al., 2021; Younas et al., 2018). To balance convergence and computational efficiency, additional experiments are conducted in subsection 3.5.3.9 to fine-tune the GA iteration count and population size. The weights in the movement score are determined based on the criticality and practical relevance of each factor. Node safety ($w_1 = 0.4$) is given the highest weight, as refugees prioritize reaching safer areas to avoid conflict zones. Road openness ($w_2 = 0.3$) is the second important factor, as even safe destinations may be inaccessible due to barricades, checkpoints, or military activity. Proximity ($w_3 = 0.2$) is assigned a lower weight, as shorter travel distances help reduce exposure to danger but are secondary to safety and accessibility. Finally, the noise factor is set to $w_4 = 0.1$. These weights may be refined in practice via field-based expert consultation or Delphi methods.

Table 3.2 presents results from the ADP (with 3API) and VTP methods. The ADP column shows the converged approximate value functions, while VTP results are based on 100 migration scenarios. The CV% (coefficient of variation) is computed as $100 \times$ Std./Avg., and the Diff% column reports the percentage difference between VTP average costs and ADP-converged results, calculated as $100 \times |(ADP - VTP)| / VTP$.

We emphasize that the key consideration is the proximity of the approximated value functions to the true (but unknown) optimal value functions, which are intractable due to the curse of dimensionality in DP. Since the true value function is intractable in large-scale settings, we rely on sampled estimates. Both ADP and VTP may converge to approximations that are slightly above or below the true value function - this is a natural outcome of sample-based learning and does not indicate infeasibility. Instead, smaller bias indicates a more accurate and higher-quality policy. Our test case results confirm that both methods are computationally efficient and produce closely aligned outcomes, with VTP achieving faster performance. Hence, we rely on VTP to conduct the remaining analyses in Section 5.3.

Table 3.2: ADP (with 3API) and VTP numerical results for the test case instances. The initial states of the instances are reported in Tables A.8 and A.9 in Appendix 3.C.

Instance		Expected total discounted costs					Run time (second)	
		ADP	VTP			Diff%	ADP	VTP
ID	**Title**		**Avg.**	**Std.**	**CV%**			
1	R2M2	55240	57421	11052	19.25	3.80	285	9.16
2	R2M3	101595	102131	14914	14.60	0.52	472	9.80
3	R3M3	107717	109104	14027	12.86	1.27	787	10.49
4	R3M4	181711	181082	29334	16.20	0.35	1134	10.13
5	R4M3	103668	111361	14700	13.20	6.91	1306	14.42
6	R4M4	155248	155360	22823	14.69	0.07	1698	10.81
7	R4M5	212303	199162	31239	15.69	6.60	2233	10.47
8	R5M5	170468	174026	20263	11.64	2.04	3123	11.38
9	R5M6	201230	197925	24307	12.28	1.67	3950	11.23
10	R5M7	247581	250074	32283	12.91	1.00	4736	11.11
11	R6M7	212071	213763	27041	12.65	0.79	6490	11.68
12	R6M8	284439	288921	31969	11.06	1.55	7558	11.81
13	R6M9	372198	352796	43047	12.20	5.50	7510	11.58
14	R7M9	272400	268716	29859	11.11	1.37	9667	12.19
15	R7M10	378935	353070	35531	10.06	7.33	11233	12.34
16	R7M11	506911	473609	50275	10.62	7.03	12648	12.46
17	R8M11	381835	371372	40401	10.88	2.82	16668	13.24
18	R8M12	463349	430473	41809	9.71	7.64	18478	13.03
19	R8M13	557457	510010	53258	10.44	9.30	20858	13.42
20	R9M13	478142	444706	40312	9.06	7.52	27383	14.91
21	R9M14	613002	547602	51730	9.45	11.94	30441	15.23
22	R9M15	704205	658926	54779	8.31	6.87	33167	15.64
23	R10M16	602120	545166	49258	9.04	10.45	37566	19.79
24	R10M17	623141	594288	52427	8.82	4.86	47109	20.34
25	R10M18	696456	650817	53128	8.16	7.01	50806	20.83
	Min.	55240	57420	11052	8.16	0.07	285	9.16
	Max.	704205	658926	54779	19.25	11.94	50806	20.83
	Avg.	347337	329675	34791	11.80	4.65	14292	13.10

3.5.3 Scenario analysis and insights

This section presents a series of analyses based on different assumptions and parameter settings derived from the test case instances. Unless otherwise stated, we use instance IDs 5, 10, 15, 20, and 25 as our representative test cases.

3.5.3.1 The value of the stochastic solution and cost bounds for migration scenarios

In this section, we quantify the Value of the Stochastic Solution (VSS), which measures the benefit of employing a policy derived from the stochastic model over a policy obtained from a deterministic approximation. Recently, Pashapour et al. (2024) investigated deterministic optimization of relief aid distribution in a single migration scenario, where each refugee group $r \in \mathcal{R}$ follows the shortest path $\mathcal{P}_{l_1^r}$ from its initial location l_1^r to the nearest terminal point, advancing one node per period without inter-period delays. To replicate this deterministic setting, we extract the shortest paths $\mathcal{P}_i$ from each transient node $i \in \mathcal{J}$ in our test case network. We also adjust transition probabilities in Eq. (3.7) by setting $p_{ij} = 1$ for $(i, j) \in \mathcal{P}_i$, $p_{ii} = 1$ for all $i \in \mathcal{H}$, and 0 otherwise. Using this single scenario, we execute the VTP to obtain a deterministic service act policy π_d whose total cost constitutes the Expected Value (EV). Letting RP (Recourse Problem) denote the expected total cost of the stochastic model, Proposition 3.5.1 establishes that EV serves as a lower bound (LB) for RP.

Proposition 3.5.1. *Solving the VTP on the deterministic variant of the problem, where each refugee group follows the shortest path from its initial location to the nearest terminal point and advances one node per period, provides a lower bound on the RP total costs.*

Proof. Proof Bayraktar et al. (2022) show in their analysis of service act frequency that, in a deterministic migration scenario, a refugee group r traversing path p^r must be served at least $\lfloor |p^r|/\tau \rfloor$ times. Consider two migration scenarios, $\mathcal{I}_d$ (deterministic) and $\mathcal{I}_s$ (stochastic), with identical refugee group characteristics and MF information. The only difference lies in the migration dynamics: in $\mathcal{I}_d$, all refugee groups follow the shortest paths from their initial locations to the nearest terminal points, advancing deterministically by one node per period. In contrast, in $\mathcal{I}_s$, refugee groups migrate stochastically by exhibiting move-wait behavior along dynamically changing paths. As a result, the effective path length for each group in the stochastic scenario satisfies $|p^r(\mathcal{I}_s)| \geq |p^r(\mathcal{I}_d)|$, because stochastic migration introduces additional delays or detours. Consequently, the minimum number of required service acts also satisfies $\lfloor |p^r(\mathcal{I}_s)|/\tau \rfloor \geq \lfloor |p^r(\mathcal{I}_d)|/\tau \rfloor$. This implies that the deterministic variant of any migration scenario assumes the least service frequency among all feasible stochastic realizations. Given the identical characteristics of $\mathcal{I}_d$ and $\mathcal{I}_s$ instances, this implies that the total demand level in need of relief aid over time and accordingly the required MF relocations in $\mathcal{I}_s$ are at least as great as those in $\mathcal{I}_d$. Since these quantities directly contribute to the total cost through their multiplication with cost coefficients in the first two terms of the minimization objective function of Model 2 in the VTP framework, it follows that the total cost computed under the deterministic setting constitutes a lower bound on the expected total cost in the stochastic migration scenario. ■ □

Moreover, let EEV (Expected result of the EV solution) denote the average performance of the deterministic policy when simulated in the stochastic environment. To compute EEV, we apply π_d to 100 stochastic migration scenarios and use the What-if Analysis procedure from Pashapour et al. (2024) to adjust service act locations (without changing the periods) to accommodate deviations in refugee locations. If migrations extend beyond the π_d timeline, we reoptimize for the refugee groups still en route. Simultaneously, we apply VTP at each period of these scenarios to compute RP. Proposition 3.5.2 shows that the resulting EEV serves as an upper bound (UB) for RP.

Proposition 3.5.2. *Applying the service acts of π_d to stochastic migration scenarios results in an upper bound on the RP.*

Proof. Proof Let π_d denote the service act policy derived from the deterministic migration scenario $\mathcal{I}_d$, and π_s be the policy for the stochastic setting. Suppose both policies are evaluated in the stochastic environment $\mathcal{I}_s$ at period t, where the system state is s_t. Here, π_s selects service actions $x_t^{\pi_s}$ based on the realized state s_t, i.e., the true and observed filtration of the system. In contrast, π_d selects actions $x_t^{\pi_d}$ based on a projected or expected state s'_t, which reflects a deterministic approximation by assuming all refugee groups follow shortest paths without stochastic delays. If $s_t = s'_t$, the actions and resulting costs coincide, i.e., $\mathcal{C}(s_t, x_t^{\pi_s}) = \mathcal{C}(s'_t, x_t^{\pi_d})$ However, in general, $s_t \neq s'_t$ due to inherent randomness in refugee movement. Since s_t is the true system state at time t, and since π_s is optimized given s_t, it yields the lowest possible cost achievable under that realization. Thus, we have $\mathcal{C}(s_t, x_t^{\pi_s}) \leq \mathcal{C}(s_t, x_t^{\pi_d})$. There are several sources of cost inflation when applying π_d in a stochastic setting. The deterministic policy may anticipate that certain refugee groups will have arrived at terminal camps by time t, while in reality they are delayed. As a result, planned MF withdrawals may leave en route groups undersupported, leading to SLR violations and associated deprivation costs. Moreover, policies designed under an expected path may overcommit, underutilize, or deploy MFs inefficiently at certain time steps. These inefficiencies, stemming from policy-state mismatch, accumulate over time and lead to higher total costs when executing π_d in $\mathcal{I}_s$. Therefore, the EEV serves as a potential upper bound to the true stochastic recourse cost RP. ■ □

Empirical illustrations of the LB and UB are presented in Figure 3.10. Letting the relative VSS be defined as $VSS = 100 \times (EEV - RP)/EEV$, our findings across all instances indicate a 25% reduction in expected total costs when using the stochastic model compared to deterministic solutions. Furthermore, the significant gap between the LB and UB from the deterministic model raises concerns regarding its reliability for HOs in planning operations. Beyond cost savings, the stochastic model also enhances service effectiveness. The average SLR status of en route refugees—indicating the level of relief received—increased from 2.00 to 2.07, representing a 3.5% improvement. More importantly, average SLR violations across all instances dropped from 4.91 to 0.

Insight 1. *The stochastic model not only achieves a significant reduction in expected total costs but also enhances service quality by improving average SLR status over time and completely eliminating SLR violations. These findings demonstrate the advantages of stochastic planning and suggest that deterministic approaches, despite being computationally simpler, may significantly underestimate operational costs and lead to SLR violations in complex relief aid distribution operations in HL.*

3.5.3.2 Refugee group dynamics: dispersion vs. cohesion

The existing literature often assumes that refugee groups remain intact during migration. In this section, we explore how group dispersion and group cohesion affect the expected total costs. Under dispersion, a single group is split into two subgroups that take different migration paths, with their combined population and SLR status equal to the original group. In contrast, cohesion involves merging two groups into a single larger group that follows a unified trajectory.

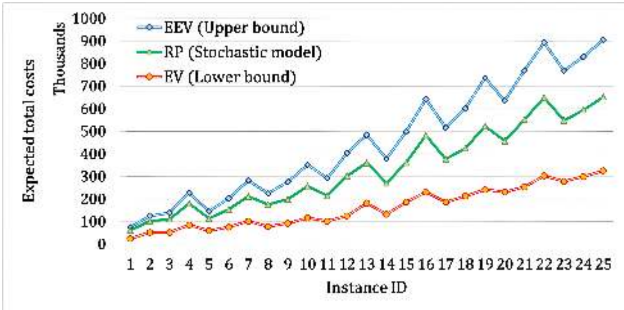

Figure 3.10: Comparison of EV (LB), RP, and EEV (UB) across 25 test case instances.

To examine the effects of group dynamics, we introduce three dispersion and cohesion rates, $\kappa \in \{0.25, 0.5, 0.75\}$. In a dispersion scenario with rate κ, $\lfloor \kappa R \rfloor$ refugee groups (out of R) are randomly selected for splitting. Each selected group is divided into two subgroups with randomly assigned populations, preserving the original group's total size and SLR status. As a result, the total number of groups increases to $R + \lfloor \kappa R \rfloor$, while the aggregate refugee population remains unchanged. In a cohesion scenario with rate κ, $\lfloor \kappa R \rfloor$ groups are randomly chosen and merged with other groups at their respective locations, inheriting their SLR status. This process reduces the number of groups to $R - \lfloor \kappa R \rfloor$, again without altering the total refugee population.

The impact of these group dynamics on the expected total cost, averaged over 100 migration scenarios and five test instances, is illustrated in Figure 3.11. The percentage change is calculated as the difference between the new and original expected total costs, divided by the original value and expressed as a percentage. The results show that dispersion leads to a greater increase in expected total costs than the cost reduction achieved through cohesion. This can be attributed to the fact that dispersion increases the number of en-route refugee groups, perturbs migration dynamics, and prolongs the planning horizon. Moreover, higher levels of dispersion, especially when the number of MFs is fixed, can lead to additional deprivation costs.

Insight 2. *Our proposed VTP framework can effectively handle refugee group dynamics such as dispersion and cohesion. HOs can use VTP to make informed, timely decisions and avoid unexpected costs during relief distribution planning.*

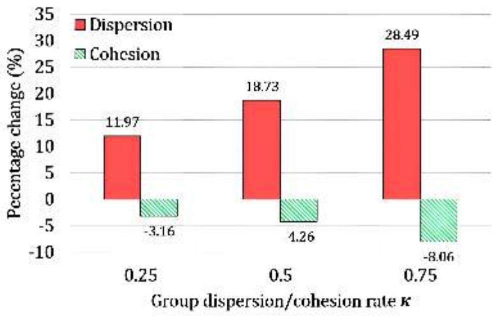

Figure 3.11: Average percentage change with respect to the original expected total costs among the five test instances under dispersion and cohesion scenarios

3.5.3.3 Tactical planning of key parameters

Arslan et al. (2021) study refugee camp network design aimed at minimizing the cost of opening camps and routing service providers. Beyond its real-time operational use, the VTP can also serve as a simulation tool to support HOs in similar tactical planning. These applications include: (i) identifying high-need hotspots along likely refugee trajectories for fixed facility placement, (ii) locating depots near areas with frequent mobile facility (MF) visits, and (iii) selecting a budget-aware, refugee-centered value for the τ parameter. To illustrate these capabilities, we analyze results from 100 VTP simulations across all test case instances. Figures 3.12 and 3.13 show the locations with the highest frequency of relief distributions and MF visits, respectively. Figure 3.14 visualizes the intensity of aid distribution across the network. Additionally, by simulating the VTP under various τ values, HOs can determine a budget-aware and refugee-centered τ using Eq. 3.23. As discussed in Section 3.5.3.1, RP denotes the expected total cost of the stochastic recourse problem. It can be estimated by applying VTP to migration simulations. Pashapour et al. (2024) show that total costs in a migration setting are nonincreasing in τ.

$$\tau^* = \min_{\tau \in \mathbb{N}} \{RP \leq \text{Budget}\} \tag{3.23}$$

Insight 3. *Simulation results from the VTP framework support tactical planning by* *(i) suggesting potential sites for fixed facilities based on recurring refugee presence, (ii) informing depot placement near high-frequency MF nodes to enhance responsiveness, and (iii) enabling budget-aware selection of the most refugee-centered SLR parameter.*

3.5.3.4 Refugees migrating to multiple neighboring countries

Migration models often assume that all refugee flows head toward a single host country. However, in practice, refugees may seek safety across multiple neighboring countries, each supported by its own HO. Recognizing this, we can extend our framework to accommodate multi-destination scenarios with minimal structural adjustments. These include clustering refugee groups and MFs by their corresponding HO, expanding the network to allow each transient node to maintain distinct sets of adjacent nodes for each possible destination, and introducing additional camps and connecting roads into the migration network. Once integrated, the planning problem can be addressed either in a decentralized manner, where each HO manages its own set of refugee groups and MFs, or centrally, where all refugee groups and MF resources are pooled and jointly optimized.

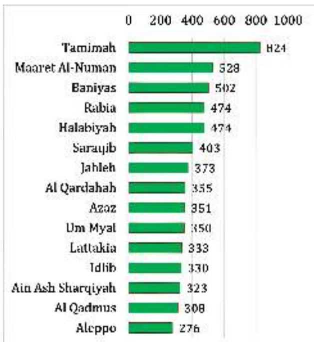

Figure 3.12: List of locations with the highest frequency of relief aid distribution averaged across all test case instances

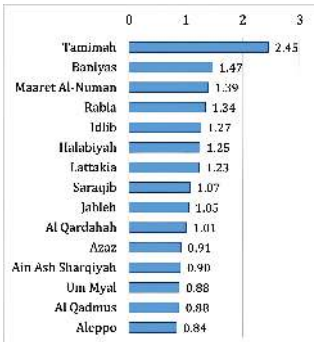

Figure 3.13: List of locations with the highest MF visits averaged across all test case instances

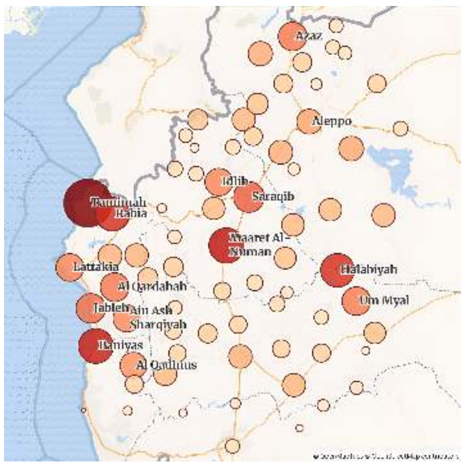

Figure 3.14: Average spatial distribution heatmap of relief aid across all test case instances

To this end, we model a setting that involves two destination countries: Türkiye and Lebanon. Here, the TRC and the Lebanese Red Cross (LRC) represent the HOs. The migration network is expanded to include two additional camp locations within Lebanon, and new adjacent node sets are defined for all transient nodes. For each test instance, we generate 100 migration scenarios, randomly assigning refugee groups and MF fleets to the two HOs. The initial locations of these groups and MFs among depot sites are also distributed randomly across the network. We analyze two operational configurations: one where the two HOs manage their respective refugee groups independently, and another cooperative configuration in which all refugee and MF fleets are jointly managed. Crucially, refugee group movements are kept identical across these two settings to clearly observe the benefits of MF sharing and cooperation, as discussed by Balcik et al. (2010); Adsanver et al. (2024). The results, shown in Figure 3.15, indicate that the cooperative configuration leads to a 12% reduction in expected total costs.

Insight 4. *In cross-border migration scenarios where refugee groups are dispersed across multiple neighboring countries with distinct trajectories, cooperation among HOs can lead to around 12% cost savings and more efficient utilization of MF fleets. By pooling resources and jointly planning relief efforts, HOs can better coordinate service delivery and improve adaptability in relief operations.*

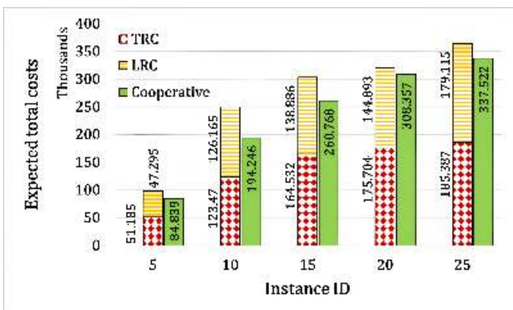

Figure 3.15: Expected total cost comparison of disjoint vs. cooperative relief aid strategies by two HOs

3.5.3.5 Analysis of the MF fleet size

In this section, we propose a lower bound $LB_{\mathcal{M}}$ on the number of MFs in Equation (3.24), based on available information regarding the number of refugee groups, their population sizes, and a given SLR parameter τ. Any MF fleet size below $LB_{\mathcal{M}}$ inevitably violates the SLR criterion. The bound $LB_{\mathcal{M}}$ is derived as the smallest MF fleet capable of meeting the needs of all individuals within τ periods. Furthermore, the product of fleet size and the SLR parameter must be no less than the number of refugee groups to ensure adequate coverage of their geographical dispersion.

$$LB_{\mathcal{M}} \quad = \quad \min\left\{\mathcal{M}' \subseteq \mathcal{M} : \sum_{m \in \mathcal{M}'} b_m \cdot \tau \geq \sum_{r \in \mathcal{R}} d_r \ , \ |\mathcal{M}'| \cdot \tau \geq R\right\} \tag{3.24}$$

We analyze the outcomes of our largest instance (ID=25) under varying MF fleet sizes, with the SLR parameter set to $\tau = 3$. This instance consists of 10 refugee groups with a total population of 6,400 individuals. Additionally, nine MFs have a capacity of 500, and another nine have a capacity of 400. Accordingly, the MF fleet size M is analyzed with respect to the lower bound $LB_{\mathcal{M}} = 5$, as shown in Figure 3.16. The results are presented as the percentage increase in expected total costs relative to the original VTP cost of this instance (reported in Table 3.2), divided by that cost.

Insight 5. *Increasing the MF fleet size leads to a non-increasing trend in the expected total costs of relief distribution operations. When fleet maintenance costs are also considered, HOs can determine the optimal fleet size that balances cost and service level, as long as the final fleet size remains above the specified lower bound. This trade-off analysis is dynamic and applicable to scenarios in which refugee group information evolves over time.*

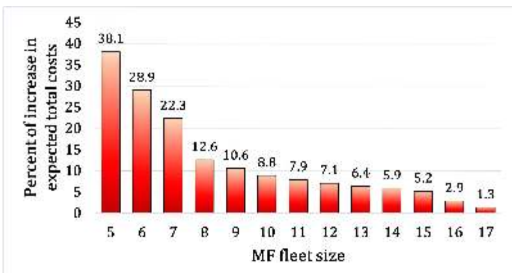

Figure 3.16: Percentage increase in expected total costs for the instance with ID=25 when the MF fleet size is below the reference level

3.5.3.6 Analysis on the number of policy replication inner iterations

In Section 4.1, we introduced a novel policy replication (PR) loop within the ADP algorithm and initially set $I = 2$ as the number of PR iterations. To ensure a fair comparison, we maintained the total number of middle and inner iterations, $Z \times I$, constant across each outer loop N in our computational experiments. In this section, we analyze the effect of varying I on the convergence of ADP. For this purpose, we use the illustrative example where optimal value functions are known and can serve as benchmarks. We evaluate values of $I \in \{1, 2, \ldots, 10\}$, and for each, we compute the ten replications of absolute percent deviation of the converged value function from the optimal value functions across all states, as shown in Figure 3.17. To ensure divisibility by all I values, we fix the total number of iterations at $Z \times I = 2520$, where $Z = 2520/I$, and set $N = 10$. Figure 3.17 illustrates that while differences are minor for small values of I, lower I values, particularly around 1, yield slightly smaller deviations from the optimal. Larger values of I, which emphasize exploitation over exploration, tend to underperform and are not recommended. Thus, Inner PR loop iteration numbers of $I = 2$ or $I = 3$ are recommended when 3API is utilized within the ADP algorithm.

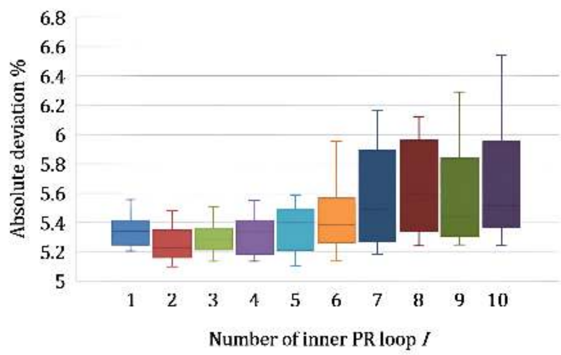

Figure 3.17: Box plots for the average absolute percent deviation of the converged value functions from the optimal values across all states of the illustrative example, for each policy replication parameter $I \in \{1, 2, \ldots, 10\}$ while $Z \times I = 2520$ is fixed

3.5.3.7 Comparison of the variable threshold policy with fixed threshold policies

In this section, we evaluate the performance of the VTP against simpler Fixed Threshold Policies (TPs). The fixed TP approach is structurally more straightforward, as it bypasses the need for iteratively solving Model 1. Instead, it selects candidate refugee groups directly based on a predefined threshold parameter, η. This reduces the algorithm to solving a classic Capacitated Mobile Facility Location Problem (CMFLP) with priority considerations as formulated in 'Model 2' for each fixed TP. Motivated by this simplicity, we investigate whether introducing variability in threshold selection (via VTP) can yield performance improvements. To assess this, we conduct 100 simulation runs for the VTP and for fixed TPs using $\eta \in 1, 2, 3$, a range consistent with the SLR parameter setting of $\tau = 3$. These policies are applied to the largest test instance (ID = 25), with MF fleet sizes of 4, 5, and 6, each MF having a capacity of 500 individuals per period.

The results are presented as box plots in Figure 3.18. We observe that VTP provides cost advantages, especially under tight MF fleet capacities. Specifically, when the fleet size is more limited, the adaptive behavior of VTP becomes more valuable in selectively prioritizing service to refugee groups. The average η values observed in VTP across fleet sizes 4, 5, and 6 are 2.25, 2.10, and 1.96, respectively. This indicates a non-increasing trend in η as fleet capacity increases. Further testing with larger fleet sizes revealed that the average η approaches 1. This suggests that in scenarios with sufficient or abundant MF capacity, the optimal service policy converges to a simple threshold rule where refugee groups are served as soon as their SLR status reaches 1. In such cases, a fixed TP with $\eta = 1$ performs comparably to VTP, and thus can be used as a practical substitute.

3.5.3.8 Benchmarking ADP with existing instances from the literature

To evaluate the effectiveness of the ADP algorithm, we test its performance on 20 large-scale benchmark migration instances developed by Pashapour et al. (2024), which are inspired by the Honduras migration crisis. These instances simulate five to nine refugee groups migrating from Honduras and Guatemala to a terminal des-

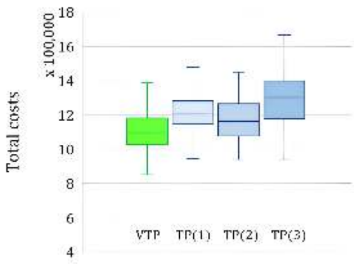

MF size = 4

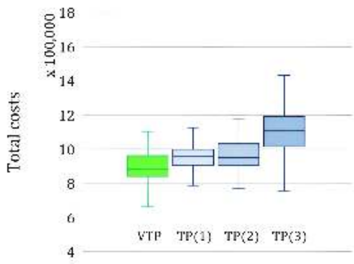

MF size = 5

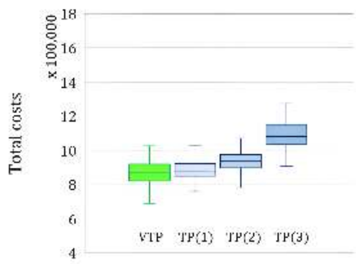

MF size = 6

Figure 3.18: VTP and TP results when applied to the largest instance with ID=25, under varying MF fleet sizes

tination in Mexico City. The scenarios involve a capacitated MF fleet with sizes ranging from 15 to 24 units.

To adapt these instances to the ADP framework, we extract the relevant parameters required for the ADP basis functions. Among these, only two parameters, χ_i and $\overline{\overline{\sigma}}$, require specific adjustments. Since Pashapour et al. (2024) assign shortest paths to each refugee group, we extend χ_i to χ_{ir} for each group r, computing it as $\chi_{ir} = \chi_{jr}+1$, where $j = \mathcal{N}_i$ along path $\mathcal{P}_i$ and $\chi_{hr} = 0$ for $h \in \mathcal{H}$ for all groups. We set $\overline{\overline{\sigma}} = 1$, as their model does not consider refugee waiting behavior. All other parameters, including refugee population sizes, MF fleet size and capacity, τ values, initial SLR statuses, and average MF capacities, are adopted directly from the original instances.

A feature of the benchmark instances is that refugee settlements are known in advance across the time horizon. To reflect this in the ADP, we sample refugee settlements from a randomly selected period, with corresponding SLR statuses chosen randomly. Furthermore, since the benchmark model assumes that MFs remain idle at their current nodes, we model this behavior by assuming the existence of depot sites at each node, allowing MFs to stay in place post-service. The ADP implementation uses the classic API framework with the default algorithmic settings introduced in Section 5. This choice is justified by the determinism of refugee resettlement realizations, which causes the 3API method to yield results identical to API, rendering a separate implementation unnecessary.

One important adjustment for a fair comparison is that Pashapour et al. (2024) incorporate a fixed deployment cost for each MF. To isolate and compare operational performance, we exclude these fixed costs from their reported results. The outcomes of both the ADP and benchmark studies are summarized in Table 3.3. In this Table, each instance ID corresponds to one of the 20 large-scale cases from Pashapour et al. (2024). The reported total costs include MF fixed costs, while the operational costs are computed as:

$$\text{Operational Costs} = \text{Total Costs} - 5000 \times \text{MFs Utilized}$$

and the percentage differences are calculated as:

$$\%\text{Diff.} = 100 \times \frac{|\text{Operational Costs} - \text{ADP}|}{\text{Operational Costs}}$$

These values are also visualized in Figure 3.19. On average, the ADP exhibits an absolute cost deviation of approximately 3.68% from the benchmark results, with the maximum difference remaining below 7%. These findings support the suitability and convergence of the ADP in replicating performance on a pre-established migration scenario testbed.

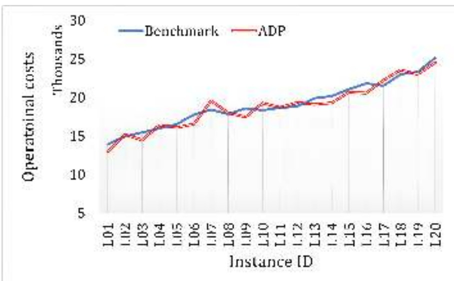

Figure 3.19: Relative performance of the ADP algorithm versus the benchmark operational costs from Pashapour et al. (2024) across all 20 large-scale instances. Each bar represents the absolute percentage difference between the ADP and benchmark solutions.

Table 3.3: Comparison of ADP operational costs with the benchmark results across 20 large-scale migration instances from Pashapour et al. (2024). Operational costs are obtained by excluding fixed MF deployment costs (5000 per unit) from the total costs reported in the benchmark. The percentage difference shows the relative deviation of the ADP results from the benchmark operational costs.

Instance ID	Benchmark			ADP	% Diff.
	Total costs	MFs utilized	Operational costs		
L01-R5M15T28	68936	11	13936	12983	6.84
L02-R5M15T28	69962	11	14962	15208	1.64
L03-R5M16T28	75454	12	15454	14493	6.22
L04-R5M16T28	75988	12	15988	16430	2.76
L05-R6M17T29	81532	13	16532	16116	2.52
L06-R6M17T29	82779	13	17779	16542	6.96
L07-R6M18T29	83430	13	18430	19566	6.16
L08-R6M18T29	87828	14	17828	17990	0.91
L09-R7M19T29	88603	14	18603	17490	5.98
L10-R7M19T29	88365	14	18365	19271	4.93
L11-R7M20T29	88655	14	18655	18717	0.33
L12-R7M20T29	93836	15	18836	19345	2.70
L13-R8M21T30	94896	15	19896	19085	4.08
L14-R8M21T30	100202	16	20202	19316	4.39
L15-R8M22T30	101070	16	21070	20678	1.86
L16-R8M22T30	101824	16	21824	20591	5.65
L17-R9M23T30	106528	17	21528	22243	3.32
L18-R9M23T30	108020	17	23020	23582	2.44
L19-R9M24T30	113360	18	23360	23036	1.39
L20-R9M24T31	120138	19	25138	24525	2.44

3.5.3.9 *Analysis of the GA population size and GA iteration count within ADP*

We investigate how different scaling factors of $(R+M)$, when used as GA population size and GA iteration count, influence the GA performance embedded within the ADP and thus the convergence behavior of the ADP algorithm. This analysis is conducted on three test case instances with IDs 6, 12, and 18. The results in Figure 3.20 indicate that setting the GA population size to $5(R+M)$ and the iteration count to $4(R+M)$ offers a suitable trade-off between convergence quality and computational efficiency.

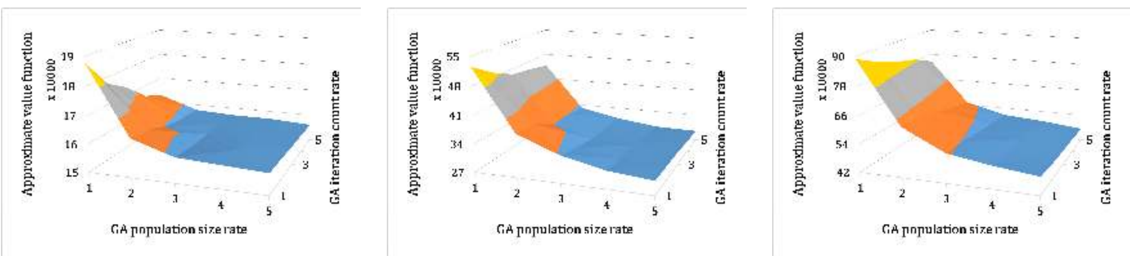

I06-R4M4 I12-R6M8 I18-R8M12

Figure 3.20: Analyzing the GA population size and GA iteration count

3.5.3.10 Operational flexibility

While most forcibly displaced individuals migrate on foot, alternative modes of transportation—such as buses, trucks, or other ground vehicles—are occasionally employed to facilitate refugee movements along certain segments of their journey. Our models can naturally accommodate such variations by expanding the adjacent node sets $\mathcal{N}_i$ of transient nodes. This reflects an increased access radius due to faster or longer-range mobility. Such a modification allows the framework to represent broader movement possibilities without altering the core mechanics of the model or compromising its tractability. Moreover, the proposed VTP is also applicable to maritime migration scenarios in which ground-based operations are not possible. For instance, when refugee groups travel via boats or remain aboard ships for extended durations, the same VTP framework can be applied by considering a fleet of ships as service vessels and by estimating the approximate location of refugee boats at sea, based on direct distances between these entities.

3.6 Conclusion

Relief aid distribution among en route forcibly displaced groups presents an increasingly complex challenge for HOs. Recent displacement patterns are becoming more dynamic, the global demand for humanitarian assistance continues to outpace available resources, and the situation is further strained by the rising frequency and duration of crises. This study equips humanitarian actors with decision support to cost-efficiently and equitably serve en route refugee groups over time, especially when resources are scarce. Our model ensures that individuals in each group are served at least once during every consecutive timeframe. The objective is to minimize the expected total costs of MF relocations, replenishments, and the severe penalties associated with unmet service needs. Delayed or insufficient service may lead to large deprivation costs, which trade off against excessive or poorly allocated service that results in inefficient resource use. Our service decisions account for (i) the probabilistic movement of refugee groups, (ii) MF capacity limits that prohibit demand splitting, and (iii) the SLR criterion, which is affected by interdependent refugee needs that evolve based on previous service.

We model this complex problem as a finite-horizon MDP with an uncertain horizon length. To solve it, we employ an ADP framework with customized basis functions and a novel policy replication loop. This framework incorporates an LSTD learning method to accurately estimate the policy vector associated with the basis functions. For practical relevance, we also introduce an online VTP for the efficient deployment of MFs under field conditions. Both methods are observed to be within computational reach and are validated through synthetic and realistic scenarios inspired by the Syria migration crisis of 2011–2019.

Our experiments reveal that stochastic planning reduces expected total costs by 25% compared to deterministic baselines. Additionally, it improves aid delivery quality by 3.5% in terms of refugees' average SLR status over time, with SLR violations dropping to zero. We show that the existing deterministic policy provides lower-bound estimates and upper-bound performance baselines for the total costs of any migration scenario. We also find that refugee group cohesion can lower logistical costs, whereas dispersed group behaviors exacerbate cost and complexity. In multi-destination settings, coordinated planning between HOs across host countries can lead to up to 12% in cost savings. Moreover, our simulations identify high-frequency refugee and MF visits that allow HOs to preemptively allocate infrastructure and storage resources to critical points along migration routes.

The broader applicability of our approach extends to other mobile service delivery domains, such as mobile healthcare units, temporary infrastructure for transient populations, or emergency telecommunications, where dynamic, equitable, and cost-efficient planning remains paramount (see Sterle et al. (2016); Zhang and Atkins (2019); De Vries et al. (2020); Taymaz et al. (2020)). A methodological challenge of the present work involves the precise design of the migration network and the unforeseen migration drivers. We addressed these challenges in our test case by extracting network data from existing reports and focusing on measurable external environmental drivers with a noise term. Notably, our proposed VTP overcomes these limitations because it is implemented in an online manner. While factors such as refugees' demographics, feedback loops, and interdependencies can be easily integrated into the move score equation, their measurement and validation, and the corresponding value of information in this context (Güllü, 1996) warrant further exploration. In addition, on-site validation of our results remains a limitation of this chapter. Regarding service prioritization, HOs may use distinct SLR parameters for each refugee group. Furthermore, although practically complex, accounting for communication between refugee groups in navigating their migration flows is worth investigation.

Chapter 4

CONCLUDING REMARKS

This thesis addresses the critical operational challenges faced by humanitarian organizations in distributing relief aid to forcibly displaced populations during prolonged migration journeys. With the global surge in displacement driven by conflict, natural disasters, and socio-political instability, delivering timely and equitable assistance to en route refugees has become a complex and resource-constrained task.

To support HOs in this context, we studied two interconnected optimization problems involving the operational deployment of capacitated mobile facilities for multi-period service provision. In the deterministic setting, we introduced the Capacitated Mobile Facility Location Problem with Mobile Demands, where refugee groups follow known migration paths, and each group must be served at least once in every fixed number of consecutive periods, governed by a service-level requirement (SLR). We developed a mixed-integer linear programming formulation, along with exact and heuristic solution methods, and validated the model using realistic instances inspired by the Honduras migration crisis. Our results confirmed the model's practical relevance, highlighting cost trade-offs in SLR planning and opportunities for MF capacity optimization and infrastructure prepositioning.

To capture the stochastic and evolving nature of displacement, we further extended the CMFLP-MD into a dynamic decision-making framework modeled as a finite-horizon Markov Decision Process with uncertain migration patterns. This stochastic formulation, inspired by the Syrian refugee crisis, incorporates refugees' move-or-wait behaviors along uncertain migration trajectories, both affected by external migration pull factors, such as safety conditions, road openness, and spatial proximity. We proposed an Approximate Dynamic Programming (ADP) solution method based on tailored basis functions and Least-Squares Temporal Difference (LSTD) learning. Additionally, we developed an online Value-Triggered Policy (VTP) to enable real-time field deployment under uncertain conditions. Our experiments reveal that stochastic planning reduces expected total costs by 25% compared to deterministic baselines. Additionally, it improves aid delivery quality by 3.5% in terms of refugees' average SLR status over time, with SLR violations dropping to zero. We show that the existing deterministic policy provides lower-bound estimates and upper-bound performance baselines for the total costs of any migration scenario. We also find that refugee group cohesion can lower logistical costs, whereas dispersed group behaviors exacerbate cost and complexity. In multi-destination settings, coordinated planning between HOs across host countries can lead to up to 12% in cost savings. Moreover, our simulations identify high-frequency refugee and MF visits that allow HOs to preemptively allocate infrastructure and storage resources to critical points along migration routes.

Collectively, the thesis provides robust decision support tools for optimizing mobile service delivery under both deterministic and uncertain refugee migration scenarios. Beyond humanitarian logistics, the methods developed here apply to other dynamic mobile service systems such as mobile healthcare, emergency infrastructure deployment, and public service provision to transient populations.

Future research can extend this work by incorporating more detailed behavioral and demographic attributes of refugee groups, integrating communication and feedback mechanisms, and testing the methods through field data. Exploring different SLR schemes, coordinating multi-actor service delivery across countries, and refining the stochastic modeling of unforeseen migration drivers are also promising directions. Ultimately, this research contributes to the advancement of operations research methodologies tailored to address urgent global humanitarian challenges.

BIBLIOGRAPHY

Adsanver, B., Balcik, B., Bélanger, V., and Rancourt, M.-È. (2024). Operations research approaches for improving coordination, cooperation, and collaboration in humanitarian relief chains: A framework and literature review. *European Journal of Operational Research*, 319(2):384–398.

Agency, U. R. (2023). Ukraine emergency. https://www.unrefugees.org/emergencies/ukraine/. (last accessed: June 2024).

Ahani, N., Gölz, P., Procaccia, A. D., Teytelboym, A., and Trapp, A. C. (2024). Dynamic placement in refugee resettlement. *Operations Research*, 72(3):1087–1104.

AIDA: Asylum Information Database (2022). Country report: Türkiye. https://asylumineurope.org/wp-content/uploads/2023/07/AIDA-TR_2022-Update.pdf, last accessed 10.30.2024.

Akşin, O. Z., Cakan, N., Karaesmen, F., and Örmeci, E. L. (2015). Flexibility structure and capacity design with human resource considerations. *Production and Operations Management*, 24(7):1086–1100.

Alarcon-Gerbier, E. and Buscher, U. (2022). Modular and mobile facility location problems: A systematic review. *Computers & Industrial Engineering*, page 108734.

Alban, A., Blaettchen, P., De Vries, H., and Van Wassenhove, L. N. (2021). Resource allocation with sigmoidal demands: Mobile healthcare units and service adoption. *Manufacturing & Service Operations Management*, Articles in Advance:1–18.

Alegoz, M., Acar, M., and Salman, F. S. (2024). Value of sorting and recovery in post-disaster relief aid distribution. *Omega*, 122:102946.

Alem, D. (2021). Insights from vulnerability-driven optimisation for humanitarian logistics. *Journal of the British Academy*, 9(s8):23–53.

Annear, L. M., Akhavan-Tabatabaei, R., and Schmid, V. (2023). Dynamic assignment of a multi-skilled workforce in job shops: An approximate dynamic programming approach. *European Journal of Operational Research*, 306(3):1109–1125.

Arabani, A. B. and Farahani, R. Z. (2012). Facility location dynamics: An overview of classifications and applications. *Computers & Industrial Engineering*, 62(1):408–420.

Arslan, O., Kumcu, G. Ç., Kara, B. Y., and Laporte, G. (2021). The location and location-routing problem for the refugee camp network design. *Transportation Research Part B: Methodological*, 143:201–220.

Asadi, A. and Nurre Pinkley, S. (2022). A monotone approximate dynamic programming approach for the stochastic scheduling, allocation, and inventory replenishment problem: Applications to drone and electric vehicle battery swap stations. *Transportation Science*, 56(4):1085–1110.

Avishan, F., Elyasi, M., Yanıkoğlu, İ., Ekici, A., and Özener, O. Ö. (2023). Humanitarian relief distribution problem: an adjustable robust optimization approach. *Transportation Science*, 57(4):1096–1114.

Azizi, S., Bozkir, C. D. C., Trapp, A. C., Kundakcioglu, O. E., and Kurbanzade, A. K. (2021). Aid allocation for camp-based and urban refugees with uncertain demand and replenishments. *Production and Operations Management*, 30(12):4455–4474.

Balcik, B., Beamon, B. M., Krejci, C. C., Muramatsu, K. M., and Ramirez, M. (2010). Coordination in humanitarian relief chains: Practices, challenges and opportunities. *International Journal of production economics*, 126(1):22–34.

Bansak, K. and Paulson, E. (2024). Outcome-driven dynamic refugee assignment with allocation balancing. *Operations Research*, 72(6):2375–2390.

Barker, I., Steventon, A., and Deeny, S. R. (2017). Association between continuity of care in general practice and hospital admissions for ambulatory care sensitive conditions: Cross sectional study of routinely collected, person level data. *BMJ Open: British Medical Journal*, 356.

Bayraktar, O. B., Günneç, D., Salman, F. S., and Yücel, E. (2022). Relief aid provision to en route refugees: Multi-period mobile facility location with mobile demand. *European Journal of Operational Research*, 301(2):708–725.

BBC News (2021). Migrant caravan: Mexico presses US to reform immigration policies. https://www.bbc.com/news/world-latin-america-55714865. (last accessed: June 2024).

Bélanger, V., Ruiz, A., and Soriano, P. (2019). Recent optimization models and trends in location, relocation, and dispatching of emergency medical vehicles. *European Journal of Operational Research*, 272(1):1–23.

Bellman, R. (1957). A markovian decision process. *Journal of Mathematics and Mechanics*, pages 679–684.

Benders, J. F. (1962). Partitioning procedures for solving mixed-variables programming problems. *Numerische Mathematik*, 4(1):238–252.

Berman, O. (1995). Flow-interception problems. *Facility Location: A Survey of Applications and Methods*, pages 389–426.

Berman, O. (1997). Deterministic flow-demand location problems. *Journal of the Operational Research Society*, 48(1):75–81.

Bertsekas, D. P. (2011). Approximate policy iteration: A survey and some new methods. *Journal of Control Theory and Applications*, 9(3):310–335.

Boccia, M., Sforza, A., and Sterle, C. (2009). Flow intercepting facility location: Problems, models and heuristics. *Journal of Mathematical Modelling and Algorithms*, 8:35–79.

Bowers, J., Cheyne, H., Mould, G., and Page, M. (2015). Continuity of care in community midwifery. *Health Care Management Science*, 18:195–204.

Bradtke, S. J. and Barto, A. G. (1996). Linear least-squares algorithms for temporal difference learning. *Machine Learning*, 22:33–57.

Burkart, C., Nolz, P. C., and Gutjahr, W. J. (2017). Modelling beneficiaries' choice in disaster relief logistics. *Annals of Operations Research*, 256:41–61.

Büsing, C., Comis, M., Schmidt, E., and Streicher, M. (2021). Robust strategic planning for mobile medical units with steerable and unsteerable demands. *European Journal of Operational Research*, 295(1):34–50.

Carngo website (2022). Van rental in Tegucigalpa. https://www.carngo.com/car-rental/honduras-tegucigalpa-van. (last accessed: June 2024).

Codato, G. and Fischetti, M. (2006). Combinatorial Benders' cuts for mixed-integer linear programming. *Operations Research*, 54(4):756–766.

Concern worldwide US (2023). The 10 largest refugee crises to know in 2025. https://concernusa.org/news/largest-refugee-crises/, last accessed 05.24.2025.

Crumpacker, J. B., Robbins, M. J., and Jenkins, P. R. (2022). An approximate dynamic programming approach for solving an air combat maneuvering problem. *Expert Systems* *with Applications*, 203:117448.

Dai, J. G. and Shi, P. (2019). Inpatient overflow: An approximate dynamic programming approach. *Manufacturing & Service Operations Management*, 21(4):894–911.

Daskin, M. S. (2011). *Network and discrete location: models, algorithms, and applications*. John Wiley & Sons.

De Vries, H. and Duijzer, E. (2017). Incorporating driving range variability in network design for refueling facilities. *Omega*, 69:102–114.

De Vries, H., Van de Klundert, J., and Wagelmans, A. P. (2020). The roadside healthcare facility location problem a managerial network design challenge. *Production and Operations Management*, 29(5):1165–1187.

Deeny, S., Gardner, T., Al-Zaidy, S., Barker, I., and Steventon, A. (2017). Briefing: Reducing hospital admissions by improving continuity of care in general practice. *London: The Health Foundation*, pages 1–9.

Demir, S. M., Sahinyazan, F. G., Kara, B. Y., and Buluc, E. (2024). No country for young refugees: Barriers and opportunities for inclusive refugee education practices. *Production and Operations Management*, pages 1–15.

Di Iasio, V. and Wahba, J. (2024). The determinants of refugees' destinations: Where do refugees locate within the EU? *World Development*, 177:106533.

Diedrichs, D. R., Hill, A., Li, Y., and Miller Schubert, A. (2024). Dynamical simulation of the Syrian refugee crisis: quantifying the driving factors of forced migration. *SIMULATION*, 100(2):157–170.

Doerner, K., Focke, A., and Gutjahr, W. J. (2007). Multicriteria tour planning for mobile healthcare facilities in a developing country. *European Journal of Operational Research*, 179(3):1078–1096.

Dönmez, Z., Kara, B. Y., Karsu, Ö., and Saldanha-da Gama, F. (2021). Humanitarian facility location under uncertainty: Critical review and future prospects. *Omega*, 102:102393.

Estrada, L. E. P., Groen, D., and Ramirez-Marquez, J. E. (2017). A serious video game to support decision making on refugee aid deployment policy. *Procedia Computer Science*, 108:205–214.

European Commission (2022). Humanitarian Logistics Policy. https://ec.europa.eu/

echo/index_en, last accessed 10.30.2024.

Fang, J., Zhao, L., Fransoo, J. C., and Van Woensel, T. (2013). Sourcing strategies in supply risk management: An approximate dynamic programming approach. *Computers & Operations Research*, 40(5):1371–1382.

Farahani, R. Z., Fallah, S., Ruiz, R., Hosseini, S., and Asgari, N. (2019). OR models in urban service facility location: A critical review of applications and future developments. *European Journal of Operational Research*, 276(1):1–27.

Farahani, R. Z. and Hekmatfar, M. (2009). *Facility location: Concepts, models, algorithms and case studies*. Springer Science & Business Media.

Fikar, C. and Hirsch, P. (2017). Home health care routing and scheduling: A review. *Computers & Operations Research*, 77:86–95.

Filippi, C., Guastaroba, G., and Speranza, M. G. (2021). On single-source capacitated facility location with cost and fairness objectives. *European Journal of Operational Research*, 289(3):959–974.

Fischetti, M., Ljubić, I., and Sinnl, M. (2016). Benders decomposition without separability: A computational study for capacitated facility location problems. *European Journal of Operational Research*, 253(3):557–569.

Fischetti, M., Ljubić, I., and Sinnl, M. (2017). Redesigning Benders decomposition for large-scale facility location. *Management Science*, 63(7):2146–2162.

Foster, M. (2007). *International refugee law and socio-economic rights: refuge from deprivation*. Number 51. Cambridge University Press.

Friggstad, Z. and Salavatipour, M. R. (2011). Minimizing movement in mobile facility location problems. *ACM Transactions on Algorithms (TALG)*, 7(3):1–22.

Frydenlund, E., Jones, E. C., and Padilla, J. J. (2019). Mobility in crisis: An agent-based model of refugees' flight to safety. *Human Simulation: Perspectives, Insights, and Applications*, pages 191–208.

Gao, X., Kong, N., and Griffin, P. (2024). Shortening emergency medical response time with joint operations of uncrewed aerial vehicles with ambulances. *Manufacturing & Service Operations Management*, 26(2):447–464.

Geoffrion, A. M. (1972). Generalized Benders decomposition. *Journal of Optimization Theory and Applications*, 10:237–260.

Geroliminis, N., Kepaptsoglou, K., and Karlaftis, M. G. (2011). A hybrid hypercube–genetic algorithm approach for deploying many emergency response mobile units in an urban network. *European Journal of Operational Research*, 210(2):287–300.

Gray, D. J. P., Sidaway-Lee, K., White, E., Thorne, A., and Evans, P. H. (2018). Continuity of care with doctors—a matter of life and death? A systematic review of continuity of care and mortality. *BMJ Open: British Medical Journal*, 8(6):e021161.

Groen, D. (2016). Simulating refugee movements: Where would you go? *Procedia Computer Science*, 80:2251–2255.

Güden, H. and Süral, H. (2014). Locating mobile facilities in railway construction management. *Omega*, 45:71–79.

Güden, H. and Süral, H. (2019). The dynamic p-median problem with mobile facilities. *Computers & Industrial Engineering*, 135:615–627.

Gulland, A. (2015). The refugee crisis: What care is needed and how can doctors help? *BMJ Open: British Medical Journal*, 351.

Güllü, R. (1996). On the value of information in dynamic production/inventory problems under forecast evolution. *Naval Research Logistics (NRL)*, 43(2):289–303.

Güngör, Ö., Günneç, D., Salman, F. S., and Yücel, E. (2022). Prediction of migration paths using agent-based simulation modeling: The case of Syria. *Proceedings of the International Conference on Industrial Engineering and Operations Management*, pages 1050–1061.

Güngör, Ö., Günneç, D., Salman, S., and Yücel, E. (2024). Simulation of migration paths using agent-based modeling: The case of Syrian refugees en route to Turkey. *Socio-Economic Planning Sciences*, page 102089.

Guo, P. and Zhu, J. (2023). Capacity reservation for humanitarian relief: A logic-based benders decomposition method with subgradient cut. *European Journal of Operational Research*, pages 942–970.

Gzara, F. and Erkut, E. (2009). A lagrangian relaxation approach to large-scale flow interception problems. *European Journal of Operational Research*, 198(2):405–411.

Halper, R. and Raghavan, S. (2011). The mobile facility routing problem. *Transportation Science*, 45(3):413–434.

Halper, R., Raghavan, S., and Sahin, M. (2015). Local search heuristics for the mobile facility location problem. *Computers & Operations Research*, 62:210–223.

Han, J., Zhang, J., Zeng, B., and Mao, M. (2021). Optimizing dynamic facility location-allocation for agricultural machinery maintenance using Benders decomposition. *Omega*, 105:102498.

He, M., Zhao, L., and Powell, W. B. (2012). Approximate dynamic programming algorithms for optimal dosage decisions in controlled ovarian hyperstimulation. *European Journal of Operational Research*, 222(2):328–340.

Hinsch, M. and Bijak, J. (2023). The effects of information on the formation of migration routes and the dynamics of migration. *Artificial Life*, 29(1):3–20.

Hodgson, M. J. (1981). The location of public facilities intermediate to the journey to work. *European Journal of Operational Research*, 6(2):199–204.

Hodgson, M. J. (1990). A flow-capturing location-allocation model. *Geographical Analysis*, 22(3):270–279.

Hooker, J. N. and Ottosson, G. (2003). Logic-based Benders decomposition. *Mathematical Programming*, 96(1):33–60.

Hulshof, P. J., Mes, M. R., Boucherie, R. J., and Hans, E. W. (2016). Patient admission planning using approximate dynamic programming. *Flexible Services and Manufacturing Journal*, 28(1):30–61.

Icduygu, A., Sirkeci, I., and Muradoglu, G. (2001). Socio-economic development and international migration: a turkish study. *International Migration*, 39(4):39–61.

Jena, S. D., Cordeau, J.-F., and Gendron, B. (2016). Solving a dynamic facility location problem with partial closing and reopening. *Computers & Operations Research*, 67:143–154.

Jenkins, P. R., Lunday, B. J., and Robbins, M. J. (2020a). Robust, multi-objective optimization for the military medical evacuation location-allocation problem. *Omega*, 97:102088.

Jenkins, P. R., Robbins, M. J., and Lunday, B. J. (2020b). Approximate dynamic programming for military medical evacuation dispatching policies. *INFORMS Journal on Computing*, 33(1):2–26.

Jenkins, P. R., Robbins, M. J., and Lunday, B. J. (2021). Approximate dynamic programming for the military aeromedical evacuation dispatching, preemption-rerouting, and redeployment problem. *European Journal of Operational Research*, 290(1):132–143.

Kara, B. Y. and Rancourt, M.-È. (2019). Location problems in humanitarian supply chains. *Location Science*, pages 611–629.

Ke, J., Zhang, D., and Zheng, H. (2019). An approximate dynamic programming approach to dynamic pricing for network revenue management. *Production and Operations Management*, 28(11):2719–2737.

Kniveton, D., Smith, C., and Wood, S. (2011). Agent-based model simulations of future changes in migration flows for Burkina Faso. *Global Environmental Change*, 21:S34–S40.

Kotsi, T. O., Wu, O. Q., and Pedraza-Martinez, A. J. (2022). Donations for refugee crises: In-kind vs. cash assistance. *Manufacturing & Service Operations Management*, 24(6):3001–3018.

Kunz, N. and Reiner, G. (2012). A meta-analysis of humanitarian logistics research. *Journal of Humanitarian Logistics and Supply Chain Management*, 2(2):116–147.

Lai, G., Margot, F., and Secomandi, N. (2010). An approximate dynamic programming approach to benchmark practice-based heuristics for natural gas storage valuation. *Operations Research*, 58(3):564–582.

Landau, L. B. and Duponchel, M. (2011). Laws, policies, or social position? Capabilities and the determinants of effective protection in four African cities. *Journal of Refugee Studies*, 24(1):1–22.

Laporte, G. and Louveaux, F. V. (1993). The integer L-shaped method for stochastic integer programs with complete recourse. *Operations Research Letters*, 13(3):133–142.

Laporte, G., Nickel, S., and Saldanha-da Gama, F. (2019). Introduction to location science. In *Location Science*, pages 1–21. Springer.

Lei, C., Lin, W.-H., and Miao, L. (2014). A stochastic emergency vehicle redeployment model for an effective response to traffic incidents. *IEEE Transactions on Intelligent Transportation Systems*, 16(2):898–909.

Li, J., Fu, H., Lai, K. K., and Ram, B. (2022). Optimization of multi-objective mobile emergency material allocation for sudden disasters. *Frontiers in Public Health*, 10:927241.

Li, J., Lai, K. K., and Lin, Q. (2019). Robust optimization solution to emergency mobile facility fleet size and location. *Mathematical Problems in Engineering*, 2019:1–11.

Liles IV, J. M., Robbins, M. J., and Lunday, B. J. (2023). Improving defensive air battle management by solving a stochastic dynamic assignment problem via approximate dynamic programming. *European Journal of Operational Research*, 305(3):1435–1449.

Liu, K., Zhang, H., and Zhang, Z.-H. (2021). The efficiency, equity and effectiveness of location strategies in humanitarian logistics: A robust chance-constrained approach. *Transportation Research Part E: Logistics and Transportation Review*, 156:102521.

Luo, X., Li, L., Zhao, L., and Lin, J. (2022). Dynamic intra-cell repositioning in free-floating bike-sharing systems using approximate dynamic programming. *Transportation Science*, 56(4):799–826.

Magnanti, T. L. and Wong, R. T. (1981). Accelerating Benders decomposition: Algorithmic enhancement and model selection criteria. *Operations Research*, 29(3):464–484.

Mallett, R. and Hagen-Zanker, J. (2018). Forced migration trajectories: An analysis of journey- and decision-making among Eritrean and Syrian arrivals to Europe. *Migration and Development*, 7(3):341–351.

Manafi, I. and Roman, M. (2022). A way to Europe: New refugees' migration patterns revealed. *Sustainability*, 14(2):748.

Maxwell, M. S., Restrepo, M., Henderson, S. G., and Topaloglu, H. (2010). Approximate dynamic programming for ambulance redeployment. *INFORMS Journal on Computing*, 22(2):266–281.

McDaniel, D. and Devine, M. (1977). A modified Benders' partitioning algorithm for mixed integer programming. *Management Science*, 24(3):312–319.

McGowan, C. R., Baxter, L., Deola, C., Gayford, M., Marston, C., Cummings, R., and Checchi, F. (2020). Mobile clinics in humanitarian emergencies: a systematic review. *Conflict and Health*, 14(1):1–10.

McKenna, R. S., Robbins, M. J., Lunday, B. J., and McCormack, I. M. (2020). Approximate dynamic programming for the military inventory routing problem. *Annals of Operations Research*, 288(1):391–416.

Migration Policy Centre (MPC) (2013). Syrian refugees in turkey. https://labs.ozyegin.edu.tr/ozumigs/files/2015/05/Syrian-Refugees-in-Turkey.pdf, last accessed 10.30.2024.

Miller, K. E. and Rasmussen, A. (2017). The mental health of civilians displaced by armed conflict: An ecological model of refugee distress. *Epidemiology and Psychiatric Sciences*, 26(2):129–138.

Mirchandani, P. B. and Francis, R. L. (1990). *Discrete location theory*. Wiley, New York, ©1990.

Mohamed Abu Shahma (2018). Report: Gaza Aid Workers Are Forcing Displaced Families To Pay For Food. https://worldcrunch.com/focus/israel-palestine-war/unrwa-gaza-aid-scandal/. (last accessed: May 2025).

Monemi, R. N., Gelareh, S., Nagih, A., Maculan, N., and Danach, K. (2021). Multi-period hub location problem with serial demands: A case study of humanitarian aids distribution in Lebanon. *Transportation Research Part E: Logistics and Transportation Review*, 149:102201.

Moore, W. H. and Shellman, S. M. (2007). Whither will they go? a global study of refugees' destinations, 1965–1995. *International Studies Quarterly*, 51(4):811–834.

Morina, N., Akhtar, A., Barth, J., and Schnyder, U. (2018). Psychiatric disorders in refugees and internally displaced persons after forced displacement: a systematic review. *Frontiers in Psychiatry*, 9:433.

MRS (2019). Mobile support for refugees stranded in foreign countries. https://www.mobilerefugeesupport.org/about-us. (last accessed: June 2024).

MSF (2019). Medecins Sans Frontieres - Doctors Without Borders. https://www.doctorswithoutborders.org/who-we-are, last accessed 10.30.2024.

Nair, R. and Miller-Hooks, E. (2009). Evaluation of relocation strategies for emergency medical service vehicles. *Transportation Research Record*, 2137(1):63–73.

Nascimento, J. and Powell, W. (2010). Dynamic programming models and algorithms for the mutual fund cash balance problem. *Management Science*, 56(5):801–815.

Nickel, S. and Saldanha-da Gama, F. (2019). Multi-period facility location. *Location Science*, pages 303–326.

Nickel, S., Schröder, M., and Steeg, J. (2012). Mid-term and short-term planning support for home health care services. *European Journal of Operational Research*, 219(3):574–587.

Office for the Coordination of Humanitarian Affairs (OCHA) (2023a). Need for humanitarian assistance grows as migration in Central America reaches new highs. https://reliefweb.int/report/honduras/need-humanitarian-assistance-grows-migration-central-america-reaches-new-highs. (last accessed: June 2024).

Office for the Coordination of Humanitarian Affairs (OCHA) (2023b). UNHCR Türkiye operational update. https://reliefweb.int/report/turkiye/unhcr-turkiye-operational-update-june-2023-entr. (last accessed: June 2024).

Oloruntoba, R. and Banomyong, R. (2018). Humanitarian logistics research for the care of refugees and internally displaced persons: A new area of research and a research agenda. *Journal of Humanitarian Logistics and Supply Chain Management*, 8(3):282–294.

ORSAM (2014). The Situation of Syrian Refugees in the Neighboring Countries: Findings, Conclusions and Recommendations - Report No: 189. https://orsam.org.tr/d_hbanaliz/Analiz_189_eng.pdf, last accessed 10.30.2024.

Ozdamar, L., Aksu, D. T., Yasa, E., and Ergunes, B. (2018). Disaster relief routing in limited capacity road networks with heterogeneous flows. *Journal of Industrial and Management Optimization*, 14(4):1367–1380.

Özdamar, L. and Ertem, M. A. (2015). Models, solutions and enabling technologies in humanitarian logistics. *European Journal of Operational Research*, 244(1):55–65.

Pashapour, A., Günneç, D., Salman, F. S., and Yücel, E. (2022). A capacitated mobile facility location problem with mobile demand: Recurrent service provision to en route refugees. In *International Network Optimization Conference (INOC)*, pages 1–6.

Pashapour, A., Günneç, D., Salman, F. S., and Yücel, E. (2024). Capacitated mobile facility location problem with mobile demand: Efficient relief aid provision to en route refugees. *Omega*, page 103138.

Powell, W. B., Simao, H. P., and Bouzaiene-Ayari, B. (2012). Approximate dynamic programming in transportation and logistics: a unified framework. *EURO Journal on Transportation and Logistics*, 1(3):237–284.

Prasad, S., Borra, H., Woldt, J., Altay, N., and Tata, J. (2023). Migrant flows: Humanitarian operational aspects of people in transit. *Production and Operations Management*, 32(10):3311–3327.

Puterman, M. L. (2014). *Markov decision processes: discrete stochastic dynamic programming*. John Wiley & Sons.

Raghavan, S., Sahin, M., and Salman, F. S. (2019). The capacitated mobile facility location problem. *European Journal of Operational Research*, 277(2):507–520.

Rahmaniani, R., Crainic, T. G., Gendreau, M., and Rei, W. (2017). The Benders decomposition algorithm: A literature review. *European Journal of Operational Research*, 259(3):801–817.

Rancourt, M.-È., Cordeau, J.-F., Laporte, G., and Watkins, B. (2015). Tactical network planning for food aid distribution in Kenya. *Computers & Operations Research*, 56:68–83.

Rascon, J. (2018). Migrant caravan: KPRC2's Jacob Rascon reports in Mexico. https://www.click2houston.com/news/2018/11/01/migrant-caravan-kprc2s-jacob-rascon-reports-in-mexico/. (last accessed: June 2024).

Rempel, M. and Cai, J. (2021). A review of approximate dynamic programming applications within military operations research. *Operations Research Perspectives*, 8:100204.

Robertshaw, L., Dhesi, S., and Jones, L. L. (2017). Challenges and facilitators for health professionals providing primary healthcare for refugees and asylum seekers in high-income countries: a systematic review and thematic synthesis of qualitative research. *BMJ open*, 7(8).

Ross, S. M. (2014). *Introduction to stochastic dynamic programming*. Academic Press.

Ruszczyński, A. (2010). Commentary—post-decision states and separable approximations are powerful tools of approximate dynamic programming. *INFORMS Journal on Computing*, 22(1):20–22.

Salman, F. S., Yücel, E., Kayı, İ., Turper-Alışık, S., and Coşkun, A. (2021). Modeling mobile health service delivery to Syrian migrant farm workers using call record data. *Socio-Economic Planning Sciences*, 77:101005.

Santa González, R., Cherkesly, M., Crainic, T. G., and Rancourt, M.-È. (2023). Multi-period location routing: An application to the planning of mobile clinic operations in Iraq. *Computers & Operations Research*, page 106288.

Satic, U., Jacko, P., and Kirkbride, C. (2024). A simulation-based approximate dynamic programming approach to dynamic and stochastic resource-constrained multi-project scheduling problem. *European Journal of Operational Research*, 315(2):454–469.

Satinsky, E., Fuhr, D. C., Woodward, A., Sondorp, E., and Roberts, B. (2019). Mental health care utilisation and access among refugees and asylum seekers in Europe: A systematic review. *Health Policy*, 123(9):851–863.

Savaşer, S. (2017). *Periodic location routing problem: an application of mobile health services in rural area*. PhD thesis, Bilkent University.

Schapendonk, J. (2012). Turbulent trajectories: African migrants on their way to the European Union. *Societies*, 2(2):27–41.

Searle, C. and van Vuuren, J. H. (2021). Modelling forced migration: A framework for conflict-induced forced migration modelling according to an agent-based approach. *Computers, Environment and Urban Systems*, 85:101568.

Seifert, L., Kunz, N., and Gold, S. (2018). Humanitarian supply chain management responding to refugees: A literature review. *Journal of Humanitarian Logistics and Supply Chain Management*, 8(3):398–426.

Shortall, C. K., Glazik, R., Sornum, A., and Pritchard, C. (2017). On the ferries: The unmet health care needs of transiting refugees in Greece. *International Health*, 9(5):272–280.

Simao, H. P., Day, J., George, A. P., Gifford, T., Nienow, J., and Powell, W. B. (2009). An approximate dynamic programming algorithm for large-scale fleet management: A case application. *Transportation Science*, 43(2):178–197.

Söderström, T. and Stoica, P. (2002). Instrumental variable methods for system identification. *Circuits, Systems and Signal Processing*, 21(1):1–9.

Sokolowski, J. A. and Banks, C. M. (2014). A methodology for environment and agent development to model population displacement. In *Proceedings of the 2014 Symposium on Agent Directed Simulation*, pages 1–11.

Sokolowski, J. A., Banks, C. M., and Hayes, R. L. (2014). Modeling population displacement in the Syrian city of Aleppo. In *Proceedings of the Winter Simulation Conference 2014*, pages 252–263. IEEE.

Sterle, C., Sforza, A., and Amideo, A. E. (2016). Multi-period location of flow intercepting portable facilities of an intelligent transportation system. *Socio-Economic Planning Sciences*, 53:4–13.

Stillström, C. and Jackson, M. (2007). The concept of mobile manufacturing. *Journal of*

Manufacturing Systems, 26(3-4):188–193.

Suleimenova, D., Bell, D., and Groen, D. (2017). A generalized simulation development approach for predicting refugee destinations. *Scientific Reports*, 7(1):1–13.

Talleraas, C., Erdal, M. B., Larssen, M. F., and Tollefsen, A. F. (2024). Refugee journey infrastructures: Exploring migration trajectories from south sudan to uganda. *Population, Space and Place*, page e2842.

Taymaz, S., Iyigun, C., Bayindir, Z., and Dellaert, N. (2020). A healthcare facility location problem for a multi-disease, multi-service environment under risk aversion. *Socio-Economic Planning Sciences*, 71:100755.

The Guardian (2025). The reluctant collaborator: surviving Syria's brutal civil war – and its aftermath. https://www.theguardian.com/news/2025/mar/13/the-reluctant-collaborator-surviving-syrias-brutal-civil-war-and-its-aftermath, last accessed 04.02.2025.

The New York Times (2021). Migrant caravan, now in Guatemala, tests regional resolve to control migration. https://www.nytimes.com/2021/01/17/world/americas/migrant-caravan-us-biden-guatemala-immigration.html. (last accessed: June 2024).

The UN Refugee Agency (2025). Refugee Data Finder. https://www.unhcr.org/refugee-statistics, last accessed 10.30.2024.

Topaloglu, H. and Powell, W. B. (2007). Sensitivity analysis of a dynamic fleet management model using approximate dynamic programming. *Operations Research*, 55(2):319–331.

Turkish Red Crescent (2019). Turkish Red Crescent 2019 Activity Report. https://www.Kizilay.org.tr/ms/reports/Turkish-Red-Crescent-2019-Annual-Report-min.pdf, last accessed 10.30.2024.

Turkoglu, D. C. and Genevois, M. E. (2019). A comparative survey of service facility location problems. *Annals of Operations Research*, pages 1–70.

Vatsa, A. K. and Jayaswal, S. (2016). A new formulation and Benders decomposition for the multi-period maximal covering facility location problem with server uncertainty. *European Journal of Operational Research*, 251(2):404–418.

Verme, P. and Gigliarano, C. (2019). Optimal targeting under budget constraints in a humanitarian context. *World Development*, 119:224–233.

Woldt, J. J., Prasad, S., and Tata, J. (2019). Supply chain management, national culture, and refugee network performance. *Journal of Humanitarian Logistics and Supply Chain Management*, 9:109–130.

World Relief (2024). Kits for refugees. https://worldrelief.org/welcome-refugees-in-America/, last accessed 10.30.2024.

Wu, Y., Ravey, A., Chrenko, D., and Miraoui, A. (2019). Demand side energy management of EV charging stations by approximate dynamic programming. *Energy Conversion and Management*, 196:878–890.

You, F. and Grossmann, I. E. (2013). Multicut Benders decomposition algorithm for process supply chain planning under uncertainty. *Annals of Operations Research*, 210(1):191–211.

Younas, I., Kamrani, F., Bashir, M., and Schubert, J. (2018). Efficient genetic algorithms for optimal assignment of tasks to teams of agents. *Neurocomputing*, 314:409–428.

Yücel, E., Salman, F. S., Bozkaya, B., and Gökalp, C. (2020). A data-driven optimization framework for routing mobile medical facilities. *Annals of Operations Research*, 291:1077–1102.

Zeng, W., Castillo, I., and Hodgson, M. J. (2010). A generalized model for locating facilities on a network with flow-based demand. *Networks and Spatial Economics*, 10(4):579–611.

Zhang, Y. and Atkins, D. (2019). Medical facility network design: User-choice and system-optimal models. *European Journal of Operational Research*, 273(1):305–319.

Zhu, X., Son, J., Zhang, X., and Wu, J. (2023). Constraint programming and logic-based benders decomposition for the integrated process planning and scheduling problem. *Omega*, 117:102823.

Appendix 2.A. Classical Benders Decomposition (Rahmaniani et al., 2017)

Consider an MILP of the form (A.1)-(A.5).

$$\min f^T y + c^T x \tag{A.1}$$

$$s.t. \quad By + Dx = d \tag{A.2}$$

$$Ay = b \tag{A.3}$$

$$x \geq 0 \tag{A.4}$$

$$y \geq 0 \ \text{ and integer,} \tag{A.5}$$

where the complicating y variables take non-negative integer values and, together with non-negative continuous x variables, must satisfy the constraints (A.2)-(A.5). The remaining notations serve as vectors and matrices of coefficients and right-hand sides of the constraints. The objective function (A.1) minimizes the total costs. The MILP can be equivalently rearranged as (A.6) to divide the computation burden,

$$\min_{\overline{y} \in Y} \left\{ f^T \overline{y} + \min_{x \geq 0} \left\{ c^T x : Dx = d - B\overline{y} \right\} \right\}, \tag{A.6}$$

where $\overline{y}$ is a given feasible value for y variables that belong to the set $Y = \{y \in \mathbb{Z}^+ : Ay = b\}$. The inner minimization is a linear program (LP). Dualizing this LP by means of dual variables π associated with the constraint set $Dx = d - B\overline{y}$ yields the dual LP (A.7). The dualized model (A.7) can be interchanged with the inner minimization based on duality theory, resulting in the equivalent formulation (A.8).

$$\max_{\pi} \left\{ \pi^T (d - B\overline{y}) : \pi^T D \leq c \right\} \tag{A.7}$$

$$\min_{\overline{y} \in Y} \left\{ f^T \overline{y} + \max_{\pi} \left\{ \pi^T (d - B\overline{y}) : \pi^T D \leq c \right\} \right\}. \tag{A.8}$$

Remarkably, the feasible space of the inner maximization, i.e., $\Pi = \{\pi : \pi^T D \leq c\}$, is independent of the choice of $\overline{y}$. Unless Π is empty (then the original problem is unbounded), the inner maximization problem is either unbounded or feasible for a fixed $\overline{y}$ value. In the unbounded case, suppose $q \in Q$ is the set of all extreme rays of Π. There exists a direction of unboundedness r_q such that the dual objective becomes unbounded, i.e., $r_q^T(d - B\overline{y}) > 0$ and $r_q^T(d - B\overline{y}) \to \infty$. This indicates the infeasibility of $\overline{y}$ since the inner minimization in (A.6) is rendered infeasible. Hence, we add a cut of the form (A.9) to the outer minimization problem to restrict movement in this direction.

$$r_q^T(d - B\overline{y}) \leq 0 \qquad \forall q \in Q \tag{A.9}$$

In the feasible case, the inner maximization solution is one of its extreme points $e \in E$ where E is the set of extreme points of Π. If all feasibility cuts of the form (A.9) are inserted into the outer minimization problem for each choice of $\overline{y}$, the solution of the inner problem will be one of its extreme points. Therefore, the problem (A.8) is reformulated as (A.10) and (A.11).

$$\min_{\overline{y} \in Y} \quad f^T\overline{y} + \max_{e \in E} \left\{ \pi_e^T(d - B\overline{y}) \right\} \tag{A.10}$$

$$s.t. \quad r_q^T(d - B\overline{y}) \leq 0 \qquad \forall q \in Q \tag{A.11}$$

The non-linear problem (A.10)-(A.11) can be easily linearized by adding a continuous variable η. The resulting linearized problem (A.12)-(A.15) is referred to as the Benders Restricted Master Problem (RMP).

$$\min_{\overline{y} \in Y} \quad f^T\overline{y} + \eta \tag{A.12}$$

$$s.t. \quad r_q^T(d - B\overline{y}) \leq 0 \qquad \forall q \in Q \tag{A.13}$$

$$\pi_e^T(d - B\overline{y}) \leq \eta \qquad \forall e \in E \tag{A.14}$$

$$y \geq 0 \ \text{ and integer.} \tag{A.15}$$

Constraints (A.13) and (A.14) are known as feasibility and optimality cuts, respectively. A complete enumeration of these cuts is impractical. Therefore, Benders (1962) suggested a relaxation of these cuts and an iterative approach instead. At each iteration, the BD solves RMP with a subset of constraints (A.13) and (A.14) to obtain a trial $\overline{y}$. It then solves the subproblem (A.7) given the $\overline{y}$. If the subproblem is unbounded, a feasibility cut of type (A.13) is produced. If the subproblem (A.7) is feasible and bounded, an optimality cut of the form (A.14) is generated. The cuts are inserted into RMP. The procedure alternates between RMP and the dual subproblem (starting from RMP) until an optimal MILP solution is found.

To confirm the BD convergence, an optimality gap can be computed at each iteration. The objective function (A.12) offers a lower bound on the optimal MILP solution since RMP is a relaxation of the original problem. Conversely, if the solution $\overline{y}$ yields a feasible subproblem, then the sum of both $f^T\overline{y}$ and the objective function value of the subproblem (A.7) serves as an upper bound for the objective function value of the original problem (A.1)-(A.5).

Appendix 2.B. Supplementary figures and tables

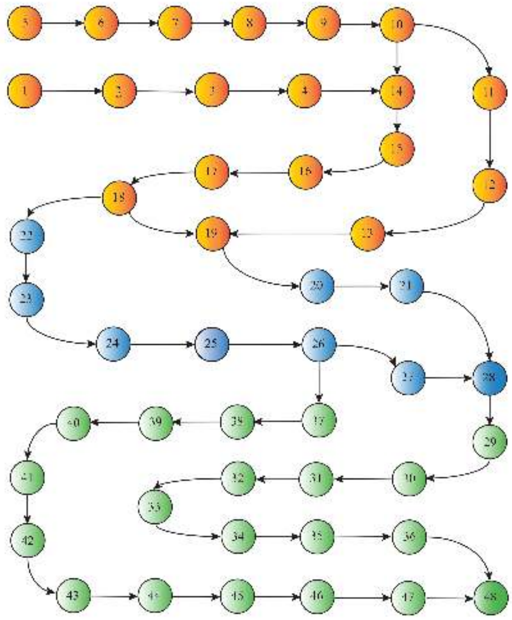

Figure A.1: The network structure corresponding to the Honduras migration crisis. Instances are categorized into small-sized networks $(1, \cdots, 19)$, medium-sized networks $(1, \cdots, 28)$, and large-sized networks $(1, \cdots, 48)$

Table A.1: List of cities and villages constituting the vertices of our migration network in Figure A.1

ID	Name	ID	Name	ID	Name	ID	Name
1	San Pedro Sula	13	Tecpan Guatemala	25	San Cristobal	37	Raudales Malpaso
2	Casa Quemada	14	Chiquimula	26	Tuxtla Gutierrez	38	El Pedregal Moctezuma
3	Copan Ruinas	15	San Esteban	27	Cintalapa	39	Laschoapas
4	Aldea Vado Honda	16	Salama	28	San Pedro Tapanatepec	40	Mina Titlan
5	Tegucigalpa	17	Pachalum	29	Juchitande Zaragoza	41	Hueyapan de Ocampo
6	San Sebastian Comayagua	18	Santacruz Del Quiche	30	Nejapa de Madero	42	Cosamaloapan
7	La Esperanza	19	Quetzaltenango	31	Oaxaca	43	Joachin
8	San Andres	20	Tapachula	32	Asuncion Nochixtlon	44	Cordoba
9	San Markos	21	Pijijiapan	33	Heroica Ciudad	45	Orizaba
10	Esquipulas	22	Huehuetenango	34	San Vicente El Penon	46	Puebla
11	Jalapa	23	La Mesilla	35	Izucar de Matamares	47	San Martin Tex Melucan
12	Guatemala City	24	Comitan	36	Cuautla	48	Mexico City

Table A.2: Structure of the paths associated with different instance sizes of our migration network in Figure A.1

Instances	Paths	Nodes	l_p
Small	P_1	1 2 3 4 14 15 16 17 18 19	10
	P_2	5 6 7 8 9 10 14 15 16 17 18 19	12
	P_3	5 6 7 8 9 10 11 12 13 19	10
Medium	P_1	1 2 3 4 14 15 16 17 18 22 23 24 25 26 27 28	16
	P_2	1 2 3 4 14 15 16 17 18 19 20 21 28	13
	P_3	5 6 7 8 9 10 14 15 16 17 18 22 23 24 25 26 27 28	18
	P_4	5 6 7 8 9 10 14 15 16 17 18 19 20 21 28	15
	P_5	5 6 7 8 9 10 11 12 13 19 20 21 28	13
Large	P_1	1 2 3 4 14 15 16 17 18 22 23 24 25 26 37 38 39 40 41 42 43 44 45 46 47 48	26
	P_2	1 2 3 4 14 15 16 17 18 22 23 24 25 26 27 28 29 30 31 32 33 34 35 36 48	25
	P_3	1 2 3 4 14 15 16 17 18 19 20 21 28 29 30 31 32 33 34 35 36 48	22
	P_4	5 6 7 8 9 10 14 15 16 17 18 22 23 24 25 26 37 38 39 40 41 42 43 44 45 46 47 48	28
	P_5	5 6 7 8 9 10 14 15 16 17 18 22 23 24 25 26 27 28 29 30 31 32 33 34 35 36 48	27
	P_6	5 6 7 8 9 10 14 15 16 17 18 19 20 21 28 29 30 31 32 33 34 35 36 48	24
	P_7	5 6 7 8 9 10 11 12 13 19 20 21 28 29 30 31 32 33 34 35 36 48	22

Appendix 3.A: Linear programming formulation

To evaluate the convergence of the DP framework using Value Iteration (VI), we formulate a Linear programming (LP) equivalent for Eq. (11). The non-negative value functions $\mathcal{V}(s) \in \mathbb{R}^+ \quad \forall s \in \mathcal{S}$ constitute our decision variables. Without loss of generality, we assume that the state-relevance weights $\lambda(s)$, interpreted as the probability distribution of the initial states, sum up to 1. The s' and $\mathcal{S}'(s,x)$ correspond to s_{t+1} and $\mathcal{S}_{t+1}(s_t, x_t)$ that are obtained by Eq. (8).

$$\max \quad \sum_{s \in \mathcal{S}} \lambda(s)\mathcal{V}(s) \tag{A.16}$$

$$\text{s.t.} \quad \mathcal{V}(s) \leq \mathcal{C}(s,x) \ + \ \beta \sum_{s' \in \mathcal{S}'(s,x)} P(s'|s,x)\mathcal{V}(s') \quad \forall s \in \mathcal{S},\ x \in \mathcal{X}(s) \tag{A.17}$$

$$\mathcal{V}(s) \geq 0 \qquad \forall s \in \mathcal{S} \tag{A.18}$$

In a minimization Bellman equation, the objective function of the equivalent LP maximizes the weighted sum of the value functions. Constraints (A.17) establish limits on the value functions for each state and action and serve as a linearization for Eq. (12). Constraints (A.18) define the domain of the value functions. Once the value functions are computed, deriving the optimal policy for each state is translated to identifying the actions that transform constraints (A.17) into equalities.

Appendix 3.B: Table of notations

Table A.3: Glossary of notations

Notation	Description
$t \in \mathcal{T}$	Decision epochs
$s_t \in \mathcal{S}$	State variables
$r \in \mathcal{R} = \{1, \cdots, R\}$	Set of refugee groups
$m \in \mathcal{M} = \{1, \cdots, M\}$	Set of MFs
$\mathcal{J}$	Transient nodes for refugee groups and MFs
$\mathcal{H}$	Terminal nodes for refugee groups
$\mathcal{D}$	Depot sites for MFs
$G^{\mathcal{R}} = (V^{\mathcal{R}}, A^{\mathcal{R}})$	Migration network for refugee groups, where $V^{\mathcal{R}} = \mathcal{J} \cup \mathcal{H}$
$G^{\mathcal{M}} = (V^{\mathcal{M}}, A^{\mathcal{M}})$	Location-relocation network for MFs, where $V^{\mathcal{M}} = \mathcal{J} \cup \mathcal{D}$
τ	SLR parameter
$\mathbf{l}_t = (l_t^r)_{r\in\mathcal{R}}$	Vector of refugee groups' placements in period t, where $l_t^r \in V^{\mathcal{R}}$
$\mathbf{u}_t = (u_t^r)_{r\in\mathcal{R}}$	Vector of refugee groups' SLR status in period t, where where $u_t^r \in \{1, \ldots, \tau\}$
$\mathbf{q}_t = (q_t^m)_{m\in\mathcal{M}}$	Vector of MF placements in period t, where $q_t^m \in \mathcal{D}$
d^r	Population size of refugee group $r \in \mathcal{R}$
b^m	Service act capacity of MF $m \in \mathcal{M}$ in terms of number of refugees per period
$\overline{b}$	Average service act capacity of MFs
$x_t \in \mathcal{X}(s_t)$	Decision variables
y_t^m	1, if MF m provides service act in period t. 0, otherwise
a_t^m	Relocation destination of MF m in period t
L_t	Set of nodes that host refugee groups in period t as service act recipients
L_t^1	Set of nodes that host refugee groups with SLR status 1 in period t
$\omega_{t+1} \in \mathcal{W}_{t+1}$	refugee groups' possible new settlements
$\varphi(s_t, x_t, \omega_{t+1})$	State transition function
$\mathcal{P}_i$	Shortest path emanating from node $i \in \mathcal{J}^{\mathcal{R}}$ to its nearest terminal point
$\mathcal{N}_i$	Adjacent nodes to node $i \in \mathcal{J}^{\mathcal{R}}$
χ_i	Average number of periods to reach an accessible terminal point from node i, where $\chi_j = 0 \forall j \in \mathcal{H}$
σ_{ij}^r	Moving score of refugee group r for transiting from node $i \in V^{\mathcal{R}}$ to $j \in \mathcal{N}_i$
$\overline{\sigma_i}$	Average moving score at node i
$\overline{\overline{\sigma}}$	Average moving score in the network
Υ	Factors influencing the moving score
$w_1, \ldots, w_4$	Weights within the moving score
ϵ	Noise term in the moving score
p_{ij}	Relocation probability for refugee groups from node $i \in V^{\mathcal{R}}$ to $j \in \mathcal{N}_i \cup \{i\}$
$\mathcal{C}(s_t, x_t)$	Immediate cost contribution
c_{ij}^m	Relocation cost for MF m from node $i \in V^{\mathcal{M}}$ to $j \in V^{\mathcal{M}}$
o	Per-kit resupply cost
γ	Deprivation cost per refugee and period
s_t^x	Post-state variable
$\mathcal{V}(.)$	Value function of a given state variable s_t or post-state variable s_t^x
$\overline{\mathcal{V}}(.)$	Approximate value function
$\phi(s_t^x)$	Basis function column vector
Ω_t	Matrix of recorded basis functions
$\hat{C}_t$	Vector of recorded immediate costs
θ	A column vector for the weights of basis functions
$\hat{\theta}$	An estimation of the θ-vector
$\eta_t \in \{1, \cdots, \tau\}$	An variable threshold parameter in period t
$\hat{\mathcal{R}}$	Set of candidate refugee groups to be visited by MFs in VTP
$\mathcal{R}'$	Set of excluded refugee groups from service provision in VTP
π_d	Deterministic service act policy
κ	Refugee group dispersion/cohesion rate
β	MDP discount factor
Δ	VI stopping criterion
N	Number of outer PI iterations
Z	Number of middle PE iterations
I	Number of inner PR iterations
α_n	A polynomial smoothing step-size rule at iteration $n \in N$
μ	Regularization term
δ	Polynomial step-size parameter
N'	Number of VTP simulations
N_{GA}	GA iteration count

Appendix 3.C: Supplementary figures and tables

Table A.4: Distance and MF relocation cost matrix for the illustrative example in Section 5.1

nodes	1	2	3	4	5	6	7	8	9	10	11	12	13	14	15	16	17	18	19
1	0	22	24	40	34	58	53	46	72	57	75	68	77	91	89	97	110	112	125
2	22	0	27	19	21	37	35	43	52	46	58	63	64	76	82	85	97	102	113
3	24	27	0	37	20	53	40	22	61	36	59	44	56	72	66	74	90	89	103
4	40	19	37	0	21	18	21	45	34	39	43	59	54	62	75	75	83	92	101
5	34	21	20	21	0	34	21	25	42	25	42	42	44	58	61	65	77	81	93
6	58	37	53	18	34	0	20	55	18	43	34	63	50	52	75	70	75	88	93
7	53	35	40	21	21	20	0	36	21	23	23	43	33	41	56	54	62	72	80
8	46	43	22	45	25	55	36	0	56	20	47	22	38	56	44	54	71	67	82
9	72	52	61	34	42	18	21	56	0	39	19	57	38	36	64	55	57	73	77
10	57	46	36	39	25	43	23	20	39	0	28	21	21	37	36	40	54	56	68
11	75	58	59	43	42	34	23	47	19	28	0	43	20	19	46	37	41	55	60
12	68	63	44	59	42	63	43	22	57	21	43	0	25	44	22	35	52	45	62
13	77	64	56	54	44	50	33	38	38	21	20	25	0	19	25	21	34	39	49
14	91	76	72	62	58	52	41	56	36	37	19	44	19	0	37	22	22	39	41
15	89	82	66	75	61	75	56	44	64	36	46	22	25	37	0	18	36	24	41
16	97	85	74	75	65	70	54	54	55	40	37	35	21	22	18	0	18	18	28
17	110	97	90	83	77	75	62	71	57	54	41	52	34	22	36	18	0	24	19
18	112	102	89	92	81	88	72	67	73	56	55	45	39	39	24	18	24	0	19
19	125	113	103	101	93	93	80	82	77	68	60	62	49	41	41	28	19	19	0

Table A.5: Experimental base values for the algorithmic factor design of all experiments in Section 5

Description	Algorithmic factor	Value
MDP discount factor	β	0.99
Value iteration stopping criterion	Δ	0.01
Number of outer PI iterations	N	10
Number of middle PE iterations	Z	2,500
Number of inner PR iterations	I	2
Regularization term	μ	10
Polynomial step-size parameter	δ	0.5
Probability steepness coefficient	ζ	5
Number of VTP samples	N'	100
GA population size	pop	$5(R+M)$
GA iteration count	N_{GA}	$4(R+M)$
GA crossover rate	n_c	$1 \times pop$
GA mutation rate	n_m	$0.2 \times pop$

Table A.6: Other parameter settings for the illustrative example in Section 5.1

Description	Algorithmic factor	Value
Node safety factors	$\Upsilon_j^{Safety} \quad j \in \mathcal{J}$	$\begin{cases} 0.7 & \forall j \in \{5,7,10,13,16\} \\ 0.8 & \forall j \in \{1,3,8,12,15,18\} \\ 0.9 & \forall j \in \{2,4,6,9,11,14,17\} \end{cases}$
Road openness factors	$\Upsilon_{ij}^{Openness} \quad (i,j) \in A^{\mathcal{R}}$	$\begin{cases} 0.7 & \forall (i,j) \in \{(3,5),(4,5),(5,7), \\ & (7,10),(7,11),(8,10),(10,13), \\ & (13,16),(15,16),(16,18)\} \\ 0.9 & \text{Otherwise} \end{cases}$
Node pair proximity factors	$\Upsilon_{ij}^{Proximity} \quad (i,j) \in A^{\mathcal{R}}$	$\frac{\max\{\text{road distance}^1\} - \text{Distance(i,j)}}{\max\{\text{road distance}\} - \min\{\text{road distance}\}}$
Weights of move-wait factors	$w_i \quad \forall i \in \{1,2,3,4\}$	$w_1 = 0.4, w_2 = 0.3, w_3 = 0.3, w_4 = 0^2$

[1] Based on road distances reported in Table A.4

[2] To ensure consistent results for comparative analysis, the randomness weight w_4 is set to zero in the illustrative example.

Table A.7: Initial states of the case study instances for which the ADP and VTP results are reported

Instance		**Initial state** $(\mathbf{l}_t, \mathbf{u}_t, \mathbf{q}_t)$
ID	**Title**	
1	R2M2	((1,2),(3,3),(2,14))
2	R2M3	((2,3),(3,3),(2,14,14))
3	R3M3	((1,2,3),(3,3,3),(2,2,14))
4	R3M4	((1,2,3),(3,3,3),(2,14,14,36))
5	R4M3	((1,2,3,13),(3,3,3,3),(14,14,36))
6	R4M4	((1,2,3,11),(3,3,3,3),(14,14,36,51))
7	R4M5	((1,2,3,11),(3,3,3,3),(14,14,36,51,51))
8	R5M5	((1,2,3,5,7),(3,3,3,3,3),(2,14,36,36,36))
9	R5M6	((1,2,3,4,12),(3,3,3,3,3),(2,2,14,36,51,62))
10	R5M7	((1,2,3,4,12),(3,3,3,3,3),(2,2,14,14,36,51,62))
11	R6M7	((1,2,3,9,6,13),(3,3,3,3,3,3),(2,2,14,14,36,51,62))
12	R6M8	((1,2,3,4,5,7),(3,3,3,3,3,3),(2,14,14,36,36,36,51,51))
13	R6M9	((1,2,3,8,5,12),(3,3,3,3,3,3),(2,2,14,14,36,36,51,62,62))
14	R7M9	((1,2,3,8,5,12,18),(3,3,3,3,3,3,3),(2,2,14,14,14,36,36,51,62))
15	R7M10	((1,2,3,9,6,11,12),(3,3,3,3,3,3,3),(2,2,14,14,36,36,51,51,62,62))
16	R7M11	((1,2,3,10,5,7,17),(3,3,3,3,3,3,3),(2,2,14,14,14,36,36,51,51,62,62))
17	R8M11	((1,2,3,4,6,7,11,17),(3,3,3,3,3,3,3,3),(2,2,2,14,14,36,51,51,51,62,62))
18	R8M12	((1,2,3,5,9,12,13,24),(3,3,3,3,3,3,3,3),(2,2,2,14,14,36,36,36,51,51,62,62))
19	R8M13	((1,2,3,5,4,6,12,15),(3,3,3,3,3,3,3,3),(2,2,2,14,14,14,36,36,36,51,51,62,62))
20	R9M13	((1,2,3,5,7,8,11,17,18),(3,3,3,3,3,3,3,3,3),(2,2,14,14,14,36,36,36,51,51,51,62,62))
21	R9M14	((1,2,3,4,6,10,12,15,16),(3,3,3,3,3,3,3,3,3),(2,2,2,14,14,14,36,36,36,51,51,51,62,62))
22	R9M15	((1,2,3,5,7,9,13,15,16),(3,3,3,3,3,3,3,3,3),(2,2,2,14,14,14,36,36,36,51,51,51,62,62,62))
23	R10M16	((1,2,3,5,7,8,11,17,18,20),(3,3,3,3,3,3,3,3,3,3),(2,2,2,14,14,14,36,36,36,36,51,51,51,62,62,62))
24	R10M17	((1,2,3,5,7,8,11,17,18,20),(3,3,3,3,3,3,3,3,3,3),(2,2,2,2,14,14,14,36,36,36,36,51,51,51,62,62,62))
25	R10M18	((1,2,3,5,7,8,11,17,18,20),(3,3,3,3,3,3,3,3,3,3),(2,2,2,2,14,14,14,36,36,36,36,51,51,51,62,62,62,62))

Table A.8: Refugee and MF information within the case study instances

Instance		Refugee groups' population sizes	MF capacities
ID	**Title**		
1	R2M2	(200,300)	(500,400)
2	R2M3	(200,600)	(500,500,400)
3	R3M3	(200,300,400)	(500,500,400)
4	R3M4	(400,500,600)	(500,500,400,400)
5	R4M3	(100,200,300,400)	(500,500,400)
6	R4M4	(200,300,400,500)	(500,500,400,400)
7	R4M5	(300,400,500,700)	(500,500,500,400,400)
8	R5M5	(100,200,300,400,500)	(500,500,500,400,400)
9	R5M6	(200,300,400,500,600)	(500,500,500,400,400,400)
10	R5M7	(300,400,500,600,700)	(500,500,500,500,400,400,400)
11	R6M7	(100,200,300,400,500,600)	(500,500,500,500,400,400,400)
12	R6M8	(200,300,400,500,600,700)	(500,500,500,500,400,400,400,400)
13	R6M9	(300,400,500,600,700,800)	(500,500,500,500,500,400,400,400,400)
14	R7M9	(100,200,300,400,500,600,700)	(500,500,500,500,500,400,400,400,400)
15	R7M10	(200,300,400,500,600,700,800)	(500,500,500,500,500,400,400,400,400,400)
16	R7M11	(300,400,500,600,700,800,900)	(500,500,500,500,500,500,400,400,400,400,400)
17	R8M11	(100,200,300,400,500,600,700,800)	(500,500,500,500,500,500,400,400,400,400,400)
18	R8M12	(200,300,400,500,600,700,800,900)	(500,500,500,500,500,500,400,400,400,400,400,400)
19	R8M13	(300,400,500,600,700,800,900,1000)	(500,500,500,500,500,500,500,400,400,400,400,400,400)
20	R9M13	(100,200,300,400,500,600,700,800,900)	(500,500,500,500,500,500,500,400,400,400,400,400,400)
21	R9M14	(200,300,400,500,600,700,800,900,1000)	(500,500,500,500,500,500,500,400,400,400,400,400,400,400)
22	R9M15	(300,400,500,600,700,800,900,1000,1000)	(500,500,500,500,500,500,500,500,400,400,400,400,400,400,400)
23	R10M16	(100,200,300,400,500,600,700,800,900,1000)	(500,500,500,500,500,500,500,500,400,400,400,400,400,400,400, 400)
24	R10M17	(200,300,400,500,500,600,700,800,900,1000)	(500,500,500,500,500,500,500,500,500,400,400,400,400,400,400, 400,400)
25	R10M18	(200,300,400,500,600,700,800,900,1000,1000)	(500,500,500,500,500,500,500,500,500,400,400,400,400,400,400, 400,400,400)

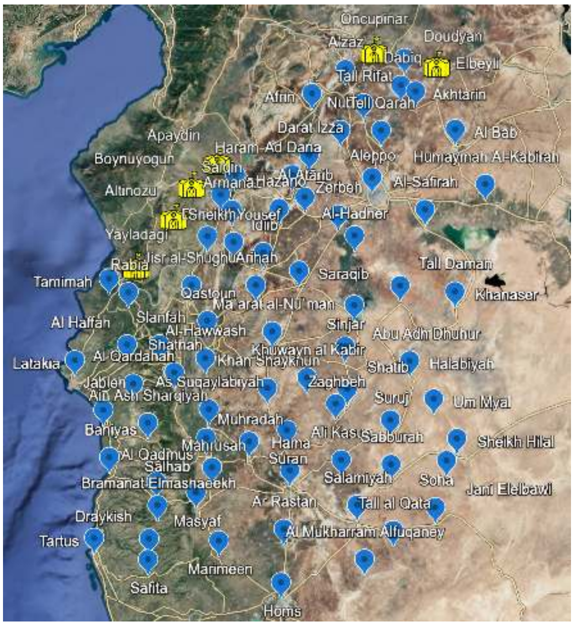

Figure A.2: The network associated with case instances. Blue icons: Transient nodes $\mathcal{J}$ for refugee groups and MFs. Yellow camps: Terminal nodes $\mathcal{H}$ for refugee groups.

Table A.9: List of cities and villages associated with the nodes of the network in Fig. A.2

Node i	Name	Adjacent node(s) $\mathcal{N}_i$	Node i	Name	Adjacent node(s) $\mathcal{N}_i$
1	Safita	{4,5}	41	Maaret Al-Numan	{42,47,50}
2	Homs (Depot site)	{3,6,7}	42	Qastoun	{46,47}
3	Al Mukharram Alfuqaney	{8,10}	43	Abu Adh Dhuhur	{48,50,54}
4	Tartus	{18}	44	Rabia	{45}
5	Draykish	{11}	45	Tamimah	{75}
6	Marimeen	{12}	46	Jisr al-Shughur	{53}
7	Al Rastan	{14}	47	Arihah	{50,51}
8	Tall al Qata	{9,10}	48	Tall Daman	{49}
9	Soha	{16,17}	49	Khanaser	{59}
10	Salamiyah	{14,15,16}	50	Saraqib	{51,55}
11	Bramanat Elmashaeekh	{12,13}	51	Idlib (Depot site)	{52,56}
12	Masyaf	{13,19}	52	Sheikh Yousef	{53,57}
13	Al Qadmus	{18}	53	Darkush	{58,76}
14	Hama (Depot site)	{15,21,23}	54	Al-Hadher	{55}
15	Ali Kasun	{23,24,26}	55	Zerbeh	{61,62}
16	Sabburah	{20,24}	56	Hazano	{61,63,64}
17	Jani Elelbawi	{20}	57	Armanaz	{58}
18	Baniyas	{25,28}	58	Salqin	{64,77}
19	Mahrusah	{21,22}	59	Al Safirah	{60,62}
20	Sheikh Hilal	{27}	60	Humaymah Al-Kabirah	{68}
21	Muhradah	{22,23,29}	61	Al Atarib	{63}
22	Salhab	{25,29}	62	Aleppo (Depot site)	{65,66,67}
23	Suran	{26,32}	63	Ad Dana	{64,65}
24	Suruj	{34}	64	Haram	{78}
25	Ain Ash Sharqiyah	{28,31}	65	Darat Izza	{66,70}
26	Zaghbeh	{30,33}	66	Nubl	{69,70}
27	Um Myal	{34}	67	Tell Qarah	{69}
28	Jableh	{31,36}	68	Al Bab	{71}
29	As Suqaylabiyah	{35,37}	69	Tall Rifat	{73}
30	Shatib	{33,38}	70	Afrin	{73}
31	Al Qardahah	{35,36,39,40}	71	Akhtarin	{72}
32	Khan Shaykhun	{33,41}	72	Dabiq	{74}
33	Khuwayn al Kabir	{38,41}	73	A'zaz	{79}
34	Halabiyah	{38,43,48}	74	Doudyan	{79,80}
35	Shathah	{37,40}	75	Yayladağı (Terminal node)	-
36	Lattakia (Depot site)	{39,44,45}	76	Altınözü (Terminal node)	-
37	Al-Hawwash	{41,42}	77	Boynuyoğun (Terminal node)	-
38	Sinjar	{41,43}	78	Apaydın (Terminal node)	-
39	Al Haffah	{40,44}	79	Öncüpınar (Terminal node)	-
40	Slanfah	{44}	80	Elbeyli (Terminal node)	-